Autoimmunity against oligodendrocyte myelin glycoprotein (OMGP)

Dissertation

zur Erlangung des Doktorgrades der Naturwissenschaften

(Dr. rer. nat.)

an der Fakultät für Biologie

der Ludwig-Maximilians-Universität München

Ramona Nadine Gerhards

München 2020

Diese Dissertation wurde angefertigt
unter der Leitung von Prof. Dr. Edgar Meinl am Institut für Klinische
Neuroimmunologie (Biomedizinisches Centrum, Martinsried)
der Ludwig-Maximilians-Universität München

Erstgutachter: Prof. Dr. Nicolas Gompel
Zweitgutachterin: Prof. Dr. Anja Horn-Bochtler

Tag der Abgabe: 17.03.2020

Tag der mündlichen Prüfung: 09.07.2020

ERKLÄRUNG

Ich versichere hiermit an Eides statt, dass meine Dissertation selbständig und ohne unerlaubte Hilfsmittel angefertigt worden ist. Die vorliegende Dissertation wurde weder ganz, noch teilweise bei einer anderen Prüfungskommission vorgelegt. Ich habe noch zu keinem früheren Zeitpunkt versucht, eine Dissertation einzureichen oder an einer Doktorprüfung teilzunehmen.

München, den 17.03.2020

Ramona Nadine Gerhards

II

ABSTRACT

Background: Multiple sclerosis (MS) and related diseases constitute a spectrum of inflammatory autoimmune diseases of the central nervous system (CNS). The identification of autoantibodies (Abs) targeting myelin oligodendrocyte glycoprotein (MOG) or the water channel protein aquaporin-4 (AQP4), contributed to a better understanding of pathomechanisms in MS, neuromyelitis optica spectrum disorders (NMOSD) and related diseases. However, for most of the patients with MS, the actual target of a misguided autoimmune response is unknown. MS is characterized by both gray and white matter injury. For that reason, a promising novel target could be expressed exclusively in the CNS on neurons and oligodendrocytes. These criteria are fulfilled by the oligodendrocyte myelin glycoprotein (OMGP), which is linked to the membrane via glycosylphosphatidylinositol (GPI) anchor. This study investigates the role and relevance of OMGP Abs and T_{OMGP} cells in an animal model as well as the presence of OMGP autoreactivity in humans.

Materials and Methods: Cell-based (CBAs) and enzyme-linked immunosorbent assays (ELISA) were established for the screening of Abs against OMGP in patients. OMGP was transiently expressed transmembraneously (OMGP-TM) or GPI anchored (OMGP-GPI) on HeLa cells and antibody binding was evaluated using flow cytometry. For the streptavidin-ELISA (STV-ELISA), OMGP was recombinantly produced by HEK293-EBNA cell line, purified and enzymatically biotinylated. Additionally, the recombinant antigen was used for generation of new monoclonal Abs (mAbs), which were evaluated in CBAs and used for immunofluorescence staining of oligodendrocytes and neurons. OMGP-specific T cell lines were generated and injected into Lewis rats, with or without MOG/OMGP Abs. Identification of T_{OMGP} cells in MS patients was carried out by using proliferation assays, ELISA cytokine measurements or bead coupled antigen stimulation and subsequent FluoroSpot analysis of interferon γ (IFNγ), interleukin 22 (IL-22) and IL-17A.

Results: This study identified a few patients who have a clear autoreactivity to OMGP detected with several assays. Using stringent criteria, OMGP autoantibodies were found in patients with MS, pediatric acute disseminated encephalomyelitis (ADEM) and psychosis. Further, patients with NMOSD and limbic encephalitis (LE) were identified with a lower OMGP antibody reactivity. Additionally, features of OMGP Abs could be studied, using affinity purified Abs from a highly reactive patient. This revealed an IgG1 and IgG4 isotype of OMGP Abs and the potential binding of C1q complement to these Abs. By using newly developed mAbs, OMGP expression was successfully evaluated on cortical as well as hippocampal neurons and in spinal cord tissue sections. Moreover, immature O4$^+$ and mature myelin basic protein (MBP) positive

oligodendrocytes, were found to co-express OMGP. T_{OMGP} cells injection into Lewis rats resulted in a novel experimental autoimmune encephalitis (EAE) with inflammation of cortical meninges and the dorsal horn of grey matter of the spinal cord. Since T_{OMGP} cells have the potential to breach the blood-brain barrier (BBB), injected MOG Abs, but not OMGP Abs induced demyelination. Finally, OMGP-specific T cells could also be identified in a few untreated and natalizumab treated MS patients. In summary, this thesis is combining (a) development of three assays to detect autoantibodies to OMGP, (b) screening of a total of 675 sera, (c) detailed analysis of the autoimmunity to OMGP in a highly reactive MS patient by affinity-purifying OMGP-specific ABs, analyzing C1q binding, long term persistence, isotype usage, detection of circulating OMGP-specific B cells and (d) identification of OMGP autoreactive T cells in MS patients. The immunostaining of oligodendrocytes and neurons for OMGP expression as well as determination of the pathogenic potential of OMGP-specific autoimmunity in an animal model, were carried out in collaboration.

Conclusion: This thesis identifies autoimmunity to OMGP in a few percent of patients with inflammatory CNS diseases and shows (in cooperation with NK and HL) that autoimmunity to OMGP is pathogenic in an animal model. These findings have implications for stratification of patients with inflammatory CNS diseases with possible therapeutic consequences.

ZUSAMMENFASSUNG

Hintergrund: Multiple Sklerose (MS) und verwandte Krankheiten bilden ein Spektrum an entzündlicher Autoimmunerkrankungen des zentralen Nervensystems (ZNS). Die Identifikation von Autoantikörpern gegen das Myelin-Oligodendrozyten-Glykoprotein (MOG) oder das Wasserkanalprotein Aquaporin-4 (AQP4) konnten zu einem besseren Verständnis der Pathomechanismen bei MS, Neuromyelitis Optica Spektrum- (NMOSE) und verwandten Erkrankungen beitragen. Für die meisten Patienten mit MS ist das tatsächliche Ziel der fehlgeleiteten Autoimmunreaktion jedoch unbekannt. MS ist charakterisiert durch Entzündungen des ZNS, die sowohl die graue, als auch die weiße Substanz betreffen. Aus diesem Grund könnte sich ein vielversprechendes neues ZNS-spezifisches Ziel auf Neuronen und Oligodendrozyten befinden. Diese Kriterien werden vom Oligodendrozyten-Myelin-Glykoprotein (OMGP) erfüllt, welches über einen Glycosylphosphatidylinositol-Anker (GPI) an der Membran fixiert ist. Diese Arbeit untersucht die Rolle und Relevanz von OMGP Antikörpern (AK) und T_{OMGP} Zellen in einem Tiermodell sowie das Vorhandensein von OMGP-Autoreaktivität beim Menschen.

Material and Methoden: Für das Screening von AK gegen OMGP bei Patienten wurden zellbasierte- (ZBAs) und enzymgebundene Immunosorbent Assays (ELISA) etabliert. OMGP wurde transient entweder transmembran- (OMGP-TM) oder GPI-verankert (OMGP-GPI) auf HeLa-Zellen exprimiert und die AK-Bindung wurde unter Verwendung von Durchflusszytometrie bewertet. Für den Streptavidin-ELISA (STV-ELISA), wurde OMGP rekombinant durch eine HEK293-EBNA-Zelllinie hergestellt, gereinigt und enzymatisch biotinyliert. Zusätzlich wurde das rekombinante Antigen zur Erzeugung neuer monoklonaler AK (mAK) verwendet, die in ZBAs charakterisiert und zu Immunfluoreszenzfärbungen von Oligodendrozyten und Neuronen verwendet wurden. OMGP-spezifische T-Zelllinien wurden etabliert und Lewis Ratten mit oder ohne MOG/OMGP-AK injiziert. Die Identifizierung von T_{OMGP} Zellen bei MS Patienten wurde unter Verwendung von Proliferationsassays, ELISA Zytokin Messungen oder Antigenstimulation durch gekoppelte paramagnetische Kugeln und anschließender FluoroSpot-Analyse von Interferon γ (IFNγ), Interleukin 22 (IL-22) und IL-17A durchgeführt.

Resultate: Diese Studie identifizierte mit mehreren Tests einige Patienten, bei denen eine eindeutige Autoreaktivität gegenüber OMGP nachgewiesen wurde. Unter Verwendung strenger Kriterien wurden OMGP-AK bei Patienten mit MS, pädiatrischer akuter disseminierter Enzephalomyelitis (ADEM) und Psychose gefunden. Ferner wurden Patienten mit NMOSE und limbischer Enzephalitis (LE) mit einer geringeren OMGP-Antikörper Reaktivität identifiziert. Zusätzlich konnten Merkmale von OMGP-AK, unter Verwendung von affinitätsgereinigten AK

eines hochreaktiven Patienten, untersucht werden. Diese ergaben IgG1 und IgG4 als Isotyp von OMGP-AK, sowie zusätzlich die mögliche Bindung des C1q Komplementproteins an diese AK. Unter Verwendung der neu entwickelten mAK wurde die OMGP Expression sowohl an kortikalen, als auch an hippocampalen Neuronen und in Gewebeschnitten des Rückenmarks erfolgreich nachgewiesen. Darüber hinaus wurde festgestellt, dass unreife O4$^+$, sowie reife Oligodendrozyten mit positiver Myelin-Basisprotein (MBP) Färbung, OMGP co-exprimieren. Die Injektion von T$_{OMGP}$ Zellen in Lewis Ratten führte zu einer neuartigen experimentellen Autoimmunenzephalitis (EAE), mit Entzündung der kortikalen Meningen und des dorsalen Horns der grauen Substanz des Rückenmarks. Da T$_{OMGP}$ Zellen das Potenzial haben, die Blut-Hirn-Schranke zu durchbrechen, induzierten verabreichte MOG-AK, jedoch nicht OMGP-AK, eine Demyelinisierung. Schließlich konnten OMGP-spezifische T Zellen auch bei einigen unbehandelten und mit Natalizumab behandelten MS Patienten identifiziert werden. Zusammenfassend kombiniert diese Arbeit (a) die Entwicklung von drei Assays zum Nachweis von Autoantikörpern gegen OMGP, (b) das Screening von insgesamt 675 Seren, (c) die detaillierte Analyse der Autoimmunität gegen OMGP bei einem hochreaktiven MS Patienten durch Affinitätsreinigung von OMGP-spezifischen AK, die Analyse der C1q-Bindung, Langzeitpersistenz, Identifizierung der Isotypen, Nachweis von zirkulierenden OMGP-spezifischen B Zellen und (d) Identifizierung von autoreaktiven OMGP-spezifischen T Zellen bei MS Patienten. Die Immunfärbungen von Oligodendrozyten und Neuronen für die Bewertung der OMGP Expression, sowie die Bestimmung des pathogenen Potentials der OMGP-spezifischen Autoimmunität in einem Tiermodell, wurden in Zusammenarbeit durchgeführt.

Schlussfolgerung: Diese Arbeit identifiziert die Autoimmunität gegen OMGP bei manchen Patienten mit entzündlichen ZNS Erkrankungen und zeigt (in Zusammenarbeit mit NK und HL), dass die Autoimmunität gegen OMGP in einem Tiermodell pathogen ist. Diese Ergebnisse haben Auswirkungen auf die Stratifizierung von Patienten mit entzündlichen ZNS Erkrankungen und zusätzlich mögliche therapeutische Konsequenzen.

Besonders möchte ich mich auch bei allen meinen Freunden bedanken, die mir immer wieder Zuspruch gegeben haben und für mich da waren.

Zuletzt möchte ich den wichtigsten Personen in meinem Leben, meiner Familie und meinem Partner, danken. Ihr wart nicht offensichtlich daran beteiligt, aber im Hintergrund seid ihr der wichtigste Anker in meinem Leben und unterstützt mich schon immer in Allem was ich tue. Danke dafür an meine großartigen Eltern, **Petra** und **Lars** und an meine fantastischen Geschwister **Carina**, **Laura**, **Ian** und **Nils**. Meinem wundervollen Partner **Andreas** bin ich überaus dankbar ihn an meiner Seite zu haben, da er gemeinsam mit mir Höhen und Tiefen durchlebt hat, mich immer wieder ermutigt hat und immer für mich da ist.

TABLE OF CONTENT

X

1. INTRODUCTION

1.1 Autoimmune mediated inflammation of the central nervous system (CNS)

Under healthy conditions the immune system protects the host against diseases. To defend the body, the detection of a broad spectrum of antigens from pathogens is required. If this protective function is disrupted, disorders of the human immune system like immunodeficiency, hypersensitivity or autoimmunity can occur (Theofilopoulos et al., 2017).

The mechanism for preventing autoimmune disease is that immune cells can distinguish own tissue from foreign proteins or non-healthy tissue. If this fails, the immune system will target self-structures and attack the tissue. The susceptibility to autoimmune disease is controlled by environmental and genetic factors (Rosenblum et al., 2015).

Autoimmune diseases have an estimated prevalence of 7.6–9.4 % of the whole world population and occur mainly in younger people (Cooper et al., 2009). They can be on the one hand general like in systemic lupus erythematosus (SLE), where antibodies (Abs) attack nuclear antigens in the whole body or on the other hand organ specific. Typical examples are type 1 diabetes, where insulin producing pancreatic β-cells are destroyed or diseases affecting the CNS (Marrack et al., 2001). Looking at this compartment, patients presenting with psychiatric symptoms and seizures may suffer from autoimmune-mediated limbic encephalitis (LE). These can occur both in a *paraneoplastic* and *non-paraneoplastic* context, with classical autoreactive targets including intracellular antigens or membrane bound antigens like the glutamate receptor NMDAR (Tuzun and Dalmau, 2007). Furthermore, autoantibodies against the glutamic acid decarboxylase (GAD) are also detected in LE patients (Finelli, 2011), other neurological diseases and are therefore named as GAD-Ab–associated neurological disorders (Thaler et al., 2019; Tohid, 2016). These encephalitides can't be completely separated from CNS demyelinating diseases, as it is shown, that they overlap and sequentially show both clinical phenotypes (Titulaer et al., 2014).

Beside LE, a whole spectrum of autoimmune CNS inflammatory and additionally demyelinating diseases exist, including multiple sclerosis (MS), which is discussed in more detail in chapter 1.2, acute disseminated encephalomyelitis (ADEM), optic neuritis (ON) and neuromyelitis optica spectrum disorders (NMOSD). The diagnoses of these clinical heterogeneous groups are challenging, since they can also overlap in cerebrospinal fluid (CSF) and magnetic resonance imaging findings. These groups vary regarding the disease onset, clinical symptoms as well as course and in treatment options.

ON is the inflammation and demyelination of the optic nerve and can occur as an isolated event or relapsing in combination with MS (Ebers, 1985) or NMOSD (Wingerchuk et al., 2007).

Figure 1.1 gives an overview on how the diagnosis of ON can be divided after the first clinical isolated syndrome is diagnosed. If it is recurrent, it can lead to chronic/relapsing inflammatory optic neuropathy (CRION/RION). A subgroup of CRION and NMOSD is further classified by their myelin oligodendrocyte (MOG) or aquaporin-4 (AQP4) autoantibody status (Zabad et al., 2017), which is discussed in detail in section 1.3.
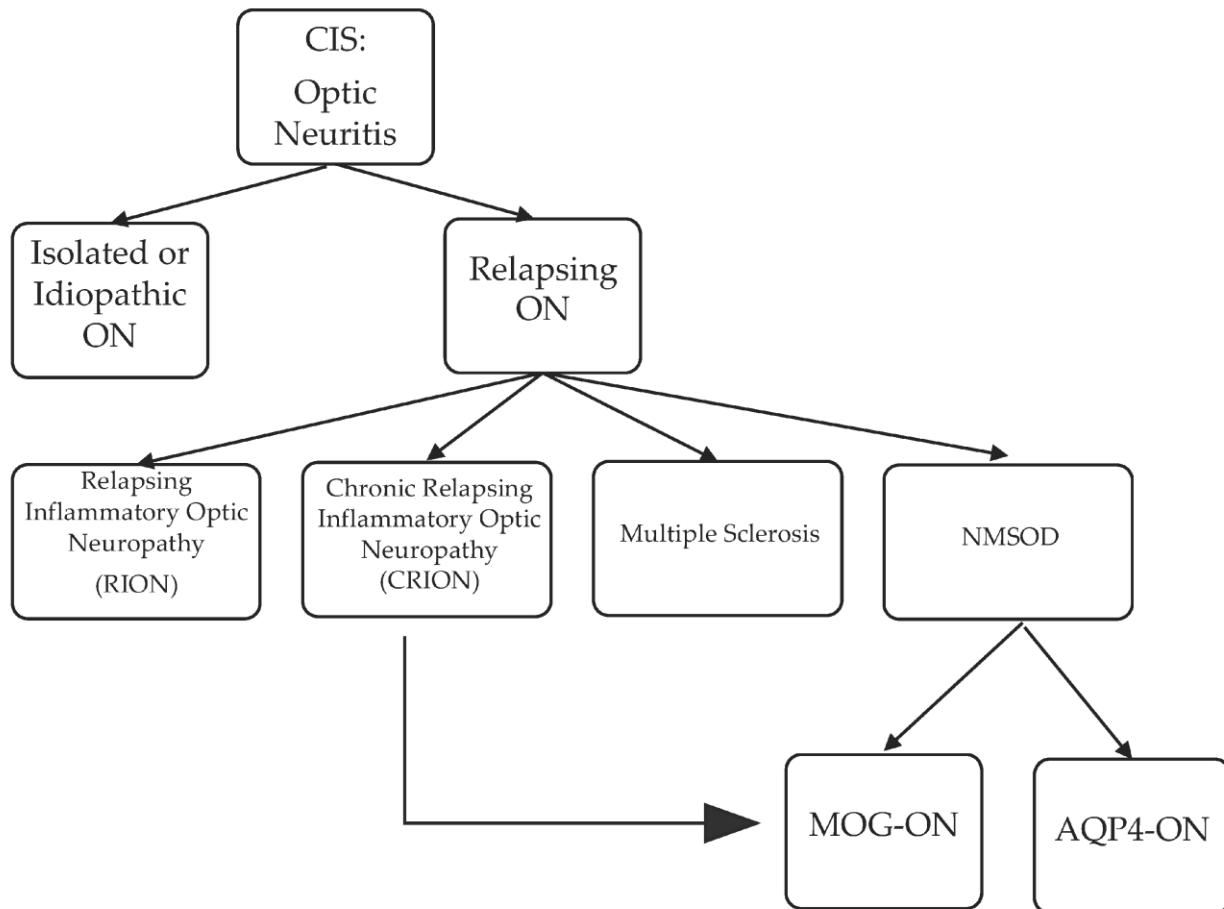
Figure 1.1 Classification of ON in combination with other diseases

The first CIS as ON can be distinguished as an isolated event or as relapsing ON. Patients suffering from recurrent episodes can be diagnosed with RION/CRION, MS or NMOSD. A further stratification of patients by the presence of MOG and AQP4 autoantibodies is possible. (Zabad et al., 2017).

Every year, 5 in 100,000 people are diagnosed with ON (Rodriguez et al., 1995). 70 % of affected people are women and the mean age at onset is 37 years (Langer-Gould et al., 2014). Patients experience unilateral visual loss, which might appear as light flashes or decreased color vision among other symptoms (Hickman et al., 2002). Additionally, patients suffer from ocular or orbital pain, especially while moving their eyes (Foroozan et al., 2002). ON may occur as a first event in developing MS, whereas 38 % may be diagnosed with MS in the next ten years (Beck et al., 2003).

NMOSD patients are diagnosed according to the revised diagnostic criteria (Wingerchuk et al., 2015), considering the presence of serum autoantibodies to AQP4, which were identified in 2005 as novel autoantibodies (Lennon et al., 2005). Patients typically suffer from recurrent ON or longitudinal extensive transverse myelitis (LETM), which can be optionally in association with other CNS autoimmune diseases. In addition to spinal cord (SC) lesions, these patients may have typical NMO brain lesions localized periventricular, in brainstem or hypothalamus (Roemer et al., 2007). Before the discovery of AQP4-IgG as biomarker for NMOSD, the disease was frequently misdiagnosed as MS (Cree et al., 2002). However, NMOSD appears to be more severe since 50 % of patient's lose their walking ability or the functional vison in one eye within five years (Lennon et al., 2004). NMOSD has an incidence of 0.70/100,000 per year analyzed in an Australian cohort (Bukhari et al., 2017), women are nine times more affected than men and the mean age of onset is 39 years (Wingerchuk et al., 2007).

ADEM is an autoimmune demyelination, which predominantly affects children younger than 15 years, with an incidence of 0.64 per 100,000. The diagnostic criteria were updated 2013 and have to include a polyfocal demyelinating event in the CNS and among others, abnormal brain MRI during the acute phase with diffuse large white matter (WM) lesions or optional grey matter lesions (Krupp et al., 2013). ADEM has typically a monophasic disease course and occurs after vaccination or inflammation with a mean age of onset at 5.7 years (Torisu et al., 2010). Long-lasting fever, ataxia, brainstem symptoms and somnolence affect children diagnosed with this disease (Menge et al., 2005). In 40 % of these pediatric cases, autoantibodies to MOG are detected (Brilot et al., 2009).

1.2 Multiple sclerosis

1.2.1 Genetics and epidemiology

MS is a frequent chronic inflammatory demyelinating autoimmune disorder of the CNS and affected in 2002 around 2.5 million people in the world (Compston and Coles, 2002). The prevalence in the USA was in 2010 for women 450.1 and men 159.7 per 100,000. This shows that females are diagnosed 2.8 times more often with MS than males (Wallin et al., 2019), which might be due to sex related differences in the immune system, based on hormones (Greer and McCombe, 2011). The age of disease onset is between 20 and 40 years (Confavreux et al., 1980), but also childhood-onset of MS is described (Renoux et al., 2007).

The cause of MS is multifactorial, since a genetic predisposition and environmental factors appear to contribute to the development of the disease (Sospedra and Martin, 2005b). The life-time risk for first-degree affected relatives is 2-3 % for parents and children, whereas it is 5 % among siblings. With 25 % it is much higher between monozygotic twins (Compston and Coles, 2008). In 1972, the first association with certain alleles of human leukocyte antigen (HLA) was discovered (Jersild et al., 1972) and the highest risk in northern Europeans with the class II gene HLA-DRB1*15 (Hollenbach and Oksenberg, 2015; Olerup and Hillert, 1991). Genome-wide association studies identified several more genes, like mutations in cytokine receptors, which are linked to a higher susceptibility of MS (De Jager et al., 2009; International Multiple Sclerosis Genetics, 2019).

The highest prevalence of MS is seen in North America, South Australia and northern Europe (Noseworthy et al., 2000), but only rarely observed around the equator (Compston and Coles, 2008) as well as in Asians or Africans (Hemmer et al., 2002). Several studies identified less sun exposure, low Vitamin D levels, smoking and certain diets as factors which increase the susceptibility of MS (Reich et al., 2018). Furthermore, through molecular mimicry of antigens, past Epstein-Barr virus (EBV) infections may also contribute to the development of the disease (Goldacre et al., 2004; Nielsen et al., 2007; Sundstrom et al., 2004).

1.2.2 Diagnosis and disease course

The clinical manifestation of MS can be observed in cerebrum, cerebellum, brainstem, spinal cord or optic nerve and therefore leading to various symptoms. Regarding the side of inflammation, patients present with painful color, eventually complete vision loss, weakness, spasms, bladder dysfunction, if the spinal cord is affected or else impaired speech, vertigo, and tremor. Hemisensory or motor dysfunction as well as in rare cases epilepsy, may indicate a cerebellar manifestation (Compston and Coles, 2008). This latter of symptoms among others, show the

complexity of the disease. For the diagnostics, patients need to get a MRI scan to visualize lesions and a lumbar puncture for the evaluation of oligoclonal bands (OCBs) in the CSF. These bands represent intrathecally produced antibodies and are detected by isoelectric focusing (Lowenthal et al., 1959) in 95 % of MS patients (McLean et al., 1990), but are also seen in other neurological diseases (Bourahoui et al., 2004). Regarding the revised McDonald criteria from 2017, after the first CIS, patients must fulfill a combination of characteristics, to be diagnosed with MS. These compose of number of lesions in brain or spinal cord, an attack lasting minimum 24 h and the evaluation of OCBs. The last criteria is optional, if the patient didn't experienced a second relapse. Accordingly, it is possible to show the dissemination in space and time of the disease and diagnose therefore patients with MS (Thompson et al., 2018).

Already before diagnosis, the first event might be seen as radiologically isolated syndrome (RIS) in MRI scans, where white matter lesions appear in the brain without leading to clinical symptoms. Within five years, one-third of RIS patients develop MS (Yamout and Al Khawajah, 2017).

MS starts in 10-20 % with primary progressive MS (PPMS) and in 80-90 % with a relapsing remitting (RRMS) course, with various frequent and severe recurrent attacks without complete remission (Hemmer et al., 2002). Between the relapses, patients experience a stable phase and in a 25 year follow up, 90 % convert into a secondary progressive phase (SPMS), which can be combined with relapses until a continuous worsening level (Hurwitz, 2009). The transition from RIS, CIS, RRMS into SPMS, with an increasing number of lesions, relapses without complete remission and disability, is illustrated in Figure 1.2.

The disability of MS patients is quantified by the expanded disability status scale (EDSS), which is a score in the range from zero, no dysfunction, to ten, which refines death by MS. It is composed of the examination of seven systems, like vision, sensitivity and bladder function among others (Kurtzke, 1983).
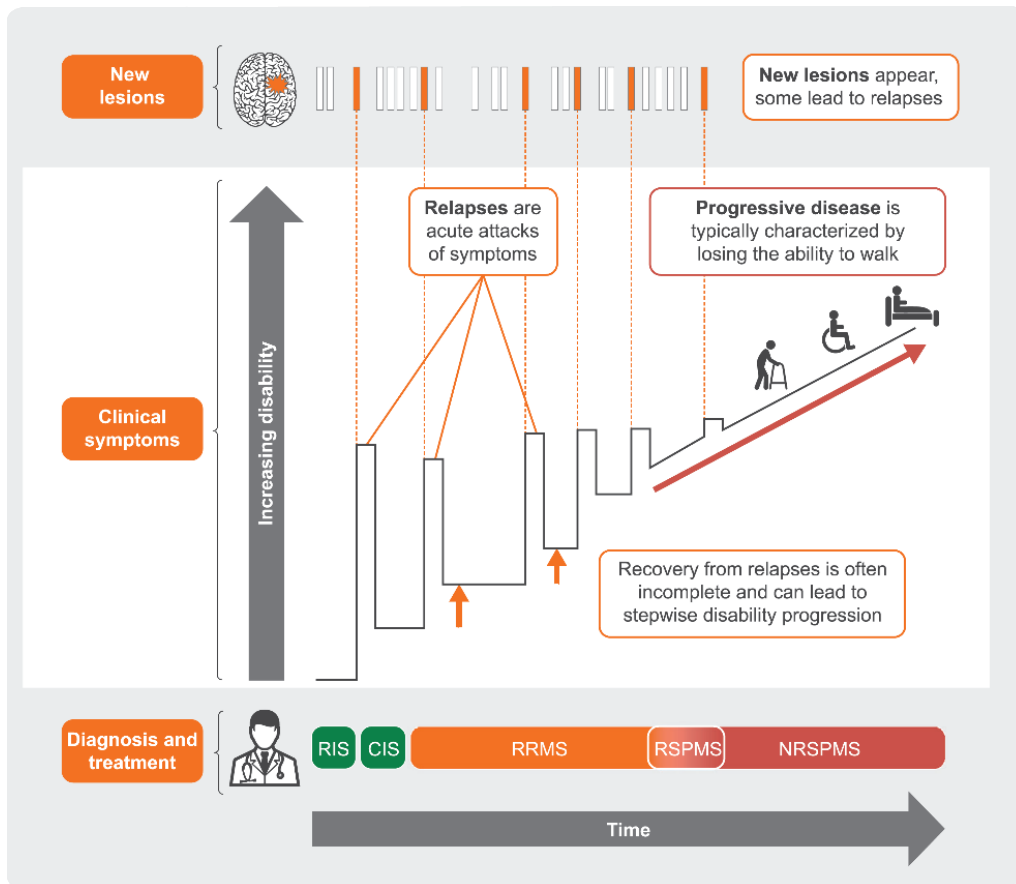
Figure 1.2 Transition from first RIS or CIS event to a relapsing and further progressive MS

Patients with RIS have no clinical symptoms, but lesions in the MRI are visible. CIS is defined as first attack together with MRI findings. From the second relapse on, the diagnose RRMS is made, with several attacks, additional lesions and incomplete remission. The transition phase into non-relapsing secondary progressive MS (NRSPMS) may occur with some relapses (RSPMS), but overall a progression of the disease is observed, until loss of walking ability. Modified from Giovannoni et al. 2016.

Much more occurs in a subclinical state, whereas only the 'tip of the iceberg' (Figure 1.3, A), like the disability progression, the patient-reported outcome and number of relapses, are visible signs (Giovannoni et al., 2016). Besides detectable WM lesions, there might be destruction of the GM, which is currently not sufficiently detectable with standard MRI techniques. A study on postmortem MS brains identified a new myelocortical phenotype, with demyelination in the GM of spinal cord and cerebral cortex. To identify this in living humans, it is necessary to improve the sensitivity of imaging modalities (Trapp et al., 2018). Another postmortem analysis revealed a cortical pathology in progressive MS, distinct from the RRMS pattern. This type of damage is challenging to visualize by MRI, because the destruction occurs in the absence of contrast enhancement, which is used to display lesion activity (Kutzelnigg et al., 2005).
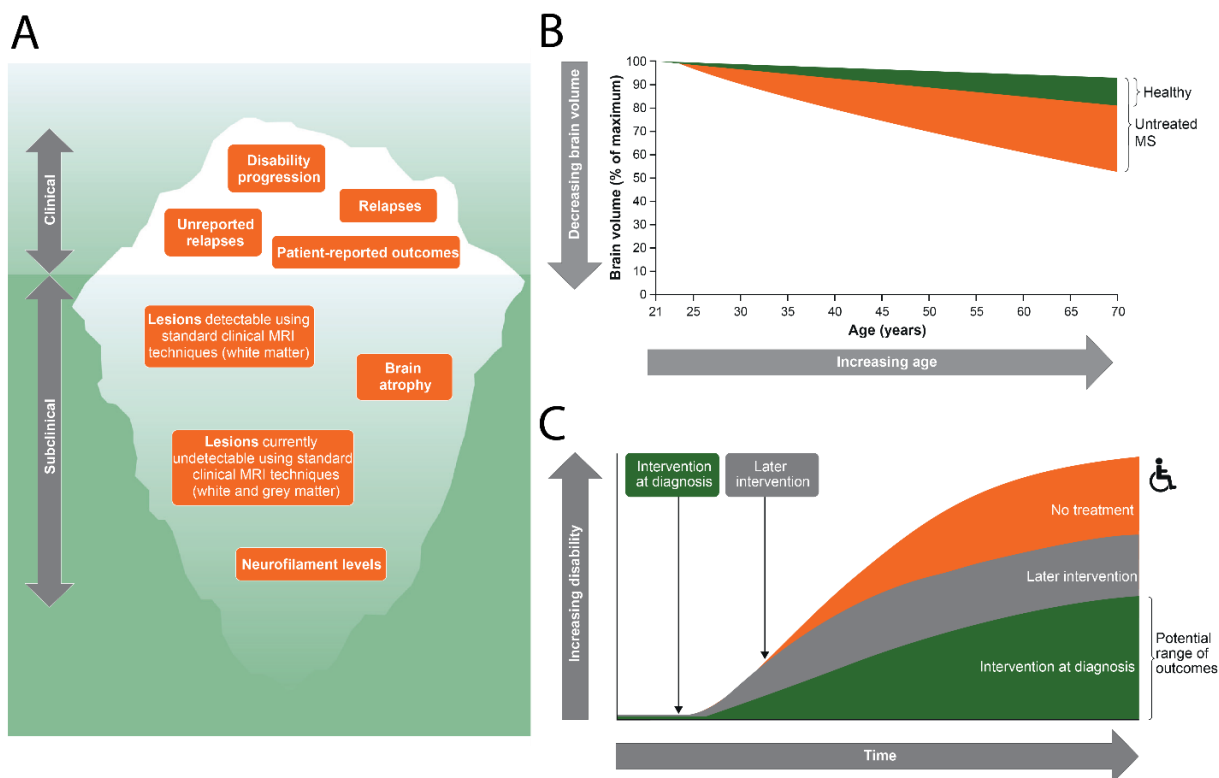
Figure 1.3 Sub-/clinical disease progression of MS accompanied with brain atrophy

(A) Clinical symptoms are only the 'tip of the iceberg' and additionally major signs occur subclinical, like non detectable lesions or brain atrophy. (B) Brain volume loss in MS patients in comparison to healthy controls. (C) The treatment of MS patients should be initiated at the point of diagnosis, to have a lower and slower increase of disability over time, compared to a later time or no treatment. Modified from Giovannoni et al. 2016.

Furthermore, current research projects focus on the identification of useful biomarkers, like neurofilament light chain protein, as indicator for neuronal destruction (Deisenhammer et al., 2019). It was shown, that the reduction of the concentration in CSF, correlates with a lower number of relapses and a decline of new lesion development under treatment (Kuhle et al., 2015).

The loss of brain volume (Figure 1.3, B) is physiologically driven by aging. Healthy individuals loose around 0.1-0.5 % per year, whereas MS patients' brain, especially when untreated, atrophies with a rate of 0.5-1.35 % within a year (De Stefano et al., 2014; Giovannoni et al., 2016). This acceleration in brain atrophy starts early, often before patients are diagnosed with MS. Therefore, it is an interesting aspect to quantify brain atrophy, since it also occurs mainly subclinical and is not assessed in standard MRI. By a meta-analysis study, the treatment effect in RRMS on reduced brain atrophy, resulted in a significant correlation to the lower disability progression (Sormani et al., 2014).

In 2019, another study by Beltran et al. focused on the identification of subclinical neuroinflammation (SCNI) markers in a monozygotic twin cohort. This interesting group composed of pairs, where one twin is diagnosed with MS, whereas the other is healthy or only subclinically affected (SCNI twin). Cells from CSF were analyzed by single-cell RNA sequencing and an early adaptive immune activation of a clonally expanded CD8$^+$ T cell subset was identified. Especially, in the MS group and in SCNI twins, upregulation of activation markers as well as proinflammatory cytokines are detected (Beltran et al., 2019). This is not seen in the healthy twins and may determine to diagnose the subclinical affected twin with prodromal MS (Wijnands et al., 2017).

In summary, the disability in MS patients increase over time by relapses, number of lesions and brain atrophy among others, which might not be obviously seen, since many events happen subclinical. This leads to the recommendation to start therapeutic intervention already at the time point of diagnosis (Figure 1.3, C). Consequently, it is possible to slow down and lower disease progression and finally cause a better outcome of the patients' disability (Giovannoni et al., 2016).

1.2.3 Immunopathogenesis - Role of B and T cells in MS

MS is induced through misguided tolerance of the immune system, where the main key players in this disease are CD4$^+$, CD8$^+$ T cells, B cells and autoantibodies (Hohlfeld et al., 2016a; Hohlfeld et al., 2016b; Sospedra and Martin, 2005b). Furthermore, CNS damage is localized to white and grey matter (Kutzelnigg et al., 2005).

The animal model experimental autoimmune encephalitis (EAE) allows to study the pathogenesis as an MS like disease with similarities. As initial step of EAE, myelin derived peptides like proteolipid protein (PLP), MOG and MBP were used to induce encephalitis (Anderson et al., 2000; Zamvil and Steinman, 1990). The final proof of the relevance of CD4$^+$ T cell was given through passive adoptive transfer of MBP or MOG-specific CD4$^+$ T cells into a healthy recipient (Gold et al., 2006; Hohlfeld and Wekerle, 2004). Both, CD4$^+$ in active and CD8$^+$ T cells in a greater number in chronic MS lesions, are found in patients (Chitnis, 2007; Lassmann, 2014). CD8$^+$ T cells also play a role in early subclinical MS, as proinflammatory markers are upregulated in a subclinical patient cohort, found by CSF single-RNA sequencing in a clonally expanded T cell subset (Beltran et al., 2019). Further, CD8$^+$ T cells are also expanded at the site of lesions (Lassmann and van Horssen, 2011). The search for new autoreactive targets of T cells in MS remains to be an interesting field (Hohlfeld et al., 2016a).

B cells and autoantibodies are important key players in EAE and MS (Hohlfeld et al., 2016b). First, the CSF of patients with MS harbors, beside clonally expanded CD8$^+$ T cells, also expanded plasma cells, producing intrathecal antibodies, which then can be detected as OCBs (von Budingen et al., 2010). Additionally, it was possible to isolate the antibodies, coming from OCBs and analysis of the self-antigens resulted in intracellular non-brain tissue specific targets, which is a hint for the mechanism of molecular mimicry (Brandle et al., 2016; Obermeier et al., 2008).
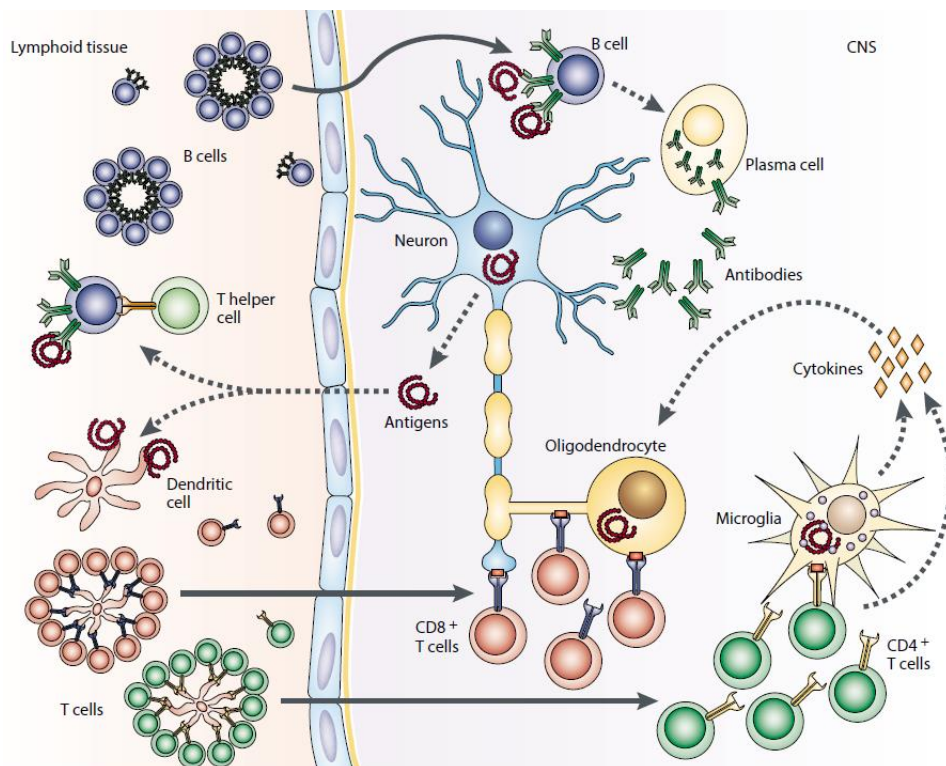
Figure 1.4 Interplay of B and T cells in the immunopathogenesis of MS

B and T cells get primed outside the CNS by recognizing self-antigens, which are released upon destruction or through molecular mimicry and get clonally expanded. CD4+ T cells re-enter the CNS and induce with cytokines a proinflammatory environment. Expanded B cell clones mature in the CNS to antibody secreting plasma cells. (Hemmer et al., 2002).

The putative complex interplay of B and T cells in MS pathology is illustrated in Figure 1.4, where B cells have several functions. Inside the CNS and in the periphery, B and T cells recognize autoantigens which might have been released by the brain tissue or are detected upon molecular mimicry (Sospedra and Martin, 2005b). After priming, clonally expanded B and T cells re-enter the CNS and target the structures on neurons or oligodendrocytes, where T cells secrete cytokines and produce a proinflammatory milieu, which is harmful for the brain tissue itself. B cells maturate to autoantibody secreting plasma cells (Hemmer et al., 2002). These can bind their targets and

mediate, as brain reactive antibodies, cytotoxicity by induction of the complement cascade and formation of the membrane attack complex (Brimberg et al., 2015). It was shown, that MOG-specific antibodies augment the disease severity (Linington et al., 1988). Furthermore, in an animal model it is demonstrated, that the antigen presentation by B cells enhances neuroinflammation, through expansion of antigen specific B cells and therefore amplify the interaction between B and T cells (Parker Harp et al., 2015).

A strong evidence is the presence of antibodies and complement deposition in lesions of some MS patients, which is classified as MS-Type-II pattern (Lucchinetti et al., 2000). These patients benefit from plasmaexchange leading to immunoglobulin (Ig) removal (Keegan et al., 2005). By administration of anti-CD20 B cell depleting antibodies, they have less change to mature to Ig releasing plasma cells, which is a concept in treatment of MS and leads to a reduction of the relapse rate (Hoffmann and Meinl, 2014; Krumbholz and Meinl, 2014). This is a further prove of the importance of B cells in MS and shows the relevance for ongoing research on the identification of new autoantigens, which may help for stratification and treatment of the heterogeneous disorder MS (Hohlfeld et al., 2016b).

1.2.4 Treatment

Looking at B cells, as highly relevant mediators of MS immunopathogenesis, many therapies among others are directed against those, and ameliorate the disease (von Budingen et al., 2015).

Some of the treatment possibilities, like anti-CD20, anti-BAFF, anti-C5 complement, anti-IL-6-R and the corresponding affected B cell function are exemplary illustrated in Figure 1.5. Anti-CD20 treatment is frequently used for B cell depletion up to the plasmablast stage (Krumbholz and Meinl, 2014) and targets additionally the small subpopulation of CD3$^+$/CD20$^+$ T cells, as it was later shown (Schuh et al., 2016). Among those, the chimeric antibody rituximab and the humanized ocrelizumab are used for RRMS treatment (Sellebjerg et al., 2020; von Budingen et al., 2015). Other antibodies, like anti-IL-6-R prevent the spread of the proinflammatory cytokine signal, aquaporumab and anti-C5 complement factor used in clinical trials in NMOSD. The antibodies directed against BAFF affect the survival of the B cells.
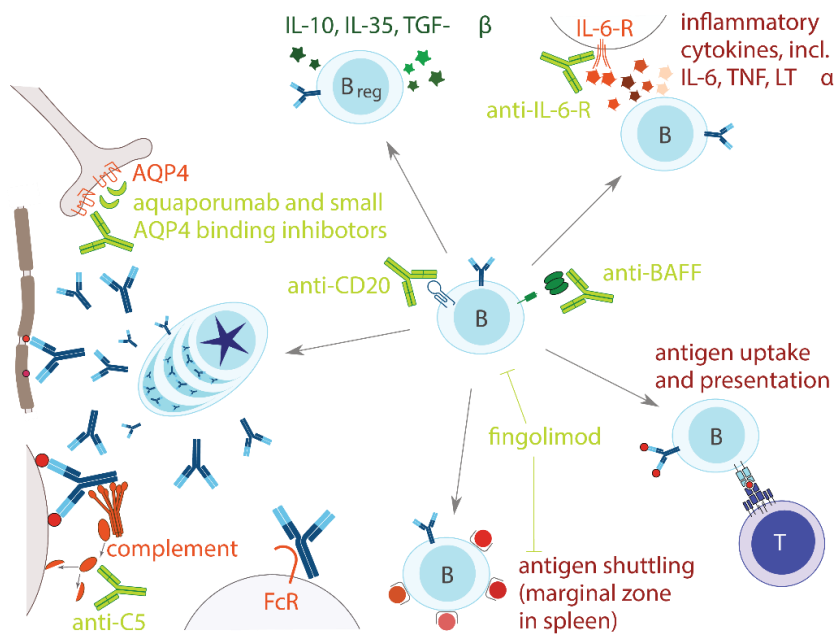
Figure 1.5 Effector functions of B cells and treating possibilities

The centered B cell can maturate into a plasma cell and produce antibodies, e.g. Anti-AQP4. Further they function as antigen presenting cells, shuttling antigens or produce proinflammatory cytokines (IL-6, TNF) and IL-10/IL-35, as regulatory B cells. Each function can be blocked by intervention of antibodies, anti-CD20, anti-BAFF, anti-C5, anti-IL-6-R or other substances, like fingolimod. (Krumbholz and Meinl, 2014).

Beside the named agents, there are two further antibodies which target not exclusively B cells. Natalizumab binds the cell adhesion molecule VLA4 and retains the leucocytes in the blood stream and alemtuzumab binds CD52 on B and T cells. Substances like fingolimod prevents lymphocytes to exit from lymph nodes and cladribine blocks DNA synthesis and therefore prevents the proliferation of B and T cells (Dendrou and Fugger, 2017; Krumbholz et al., 2012). In addition there is the possibility of an autologous hematopoietic stem-cell transplantation, which is an extreme intervention and should therefore be considered well (Dendrou and Fugger, 2017).

The overall aim in MS therapy would be to restore the dysbalance in autoimmunity and bring back the physiological self-tolerance (Sospedra and Martin, 2005a). To implement this, antigen specific therapies are necessary. A study by Lutterotti et al. tried this approach, by coupling myelin peptides to red blood cells and reinfuse these back into patients. The outcome looks promising due to reduced autoreactive T cells, but the treatment still remains in an early experimental phase (Lutterotti et al., 2013; Lutterotti and Martin, 2014).

1.3 Stratification of patients with MS and related disorders

Due to the described heterogeneous disease course and the pathogenesis, which involves many parts of the immune system, diagnosis and treatment of MS, NMOSD and related diseases remains challenging. Therefore, the individual stratification of patients by their presence of autoantibodies or autoreactive T cells, supports this process.

1.3.1 Autoantibodies

Serology is an essential diagnostic tool and gives additional information for the assessment of autoimmune diseases. In the past 30 years, several groups studied the role of MOG autoantibodies in MS and related neurological disorders. In 1991 these autoantibodies were identified for the first time by enzyme-linked immunosorbent assay (ELISA) and Western blot (WB) in CSF of MS patients (Xiao et al., 1991). Other studies followed and proofed by using tetramers of conformational intact MOG in radio immune assay, the presence of circulating MOG autoantibodies in some ADEM and a few MS patients (O'Connor et al., 2007). Further methods developed and MOG autoantibodies are analyzed by cell-based assays (CBAs), where cells are transfected with the antigen and analyzed by flow cytometry (Brilot et al., 2009; Probstel et al., 2011; Spadaro and Meinl, 2016). Live CBA are the gold standard (Yeh and Nakashima, 2019), but they differ in their technical implementation, as some laboratories use beside flow cytometer the immunofluorescence evaluation of titers determined by microscopy (Mader et al., 2011) or IgG1 specific detection antibodies (Waters et al., 2015).

Some assays identify beside MS patients also other neurological disease and healthy donors with autoantibodies to MOG (O'Connor et al., 2007; Spadaro, 2017). This leads to the current view, that MOG associated disease is a separate entity of disorders (Wynford-Thomas et al., 2019). The diagnoses of MOG seropositive patients are summarized in Figure 1.6. The affected patients range from children with recurrent ON (Rostasy et al., 2012), pediatrics MS (McLaughlin et al., 2009) or ADEM (Brilot et al., 2009) to adults. These MOG seropositive patients are diagnosed with NMOSD (Mader et al., 2011), bilateral recurrent ON (Ramanathan et al., 2016) or MS with NMOSD-like clinical phenotype (Spadaro et al., 2016). More recent studies identified MOG Abs in patients with cortical encephalitis and epileptic seizures (Ogawa et al., 2017; Wang et al., 2019). The pathogenicity of monoclonal MOG antibodies is shown in rats (Brunner et al., 1989; Linington et al., 1988) and furthermore transfer of human MOG autoantibodies induces lesions in mouse brain (Saadoun et al., 2014) as well as in Lewis rats (Spadaro et al., 2018).

MOG-antibody disease at onset
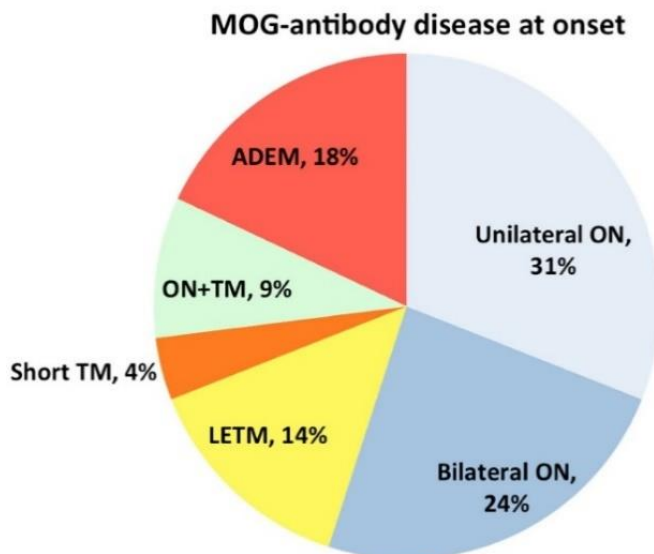
Figure 1.6 First diagnose of patients presenting with MOG autoantibodies

Patients having MOG Abs are diagnosed with various diseases, from uni-/bilateral ON to ADEM, LETM or combination of both ON and transverse myelitis. The minority with 4 % of seropositive patients have short transverse myelitis (TM). (Jurynczyk et al., 2019).

NMO specific autoantibodies, as another serological biomarker, were identified in 2004 in patients (Lennon et al., 2004) and one year later the target water channel protein AQP4 was described (Lennon et al., 2005). The autoantibodies are identified either by indirect immunofluorescence or CBA, the latter having the higher sensitivity (Waters and Vincent, 2008). The pathogenicity of one patient was shown by recombinant production of the AQP4 specific autoantibodies from CSF cells and the antibody was transferred into EAE rats. There they induced a NMOSD like pathology with complement and Ig deposition and perivascular astrocyte destruction (Bennett et al., 2009). As it is already described above with MOG Abs, the patients having AQP4-Abs show a clinically diverse pattern and often overlap in some criteria like LETM, or severe ON with MS pattern (Roemer et al., 2007).

Regarding this heterogeneity, these biomarkers like MOG or AQP4 autoantibodies help, to separate the diseases and support a better diagnosis. The dependency and relation of these Abs to different diseases is illustrated in Figure 1.7, whereas MOG Abs positive patients can suffer from ON, ADEM, myelitis or other encephalitides.
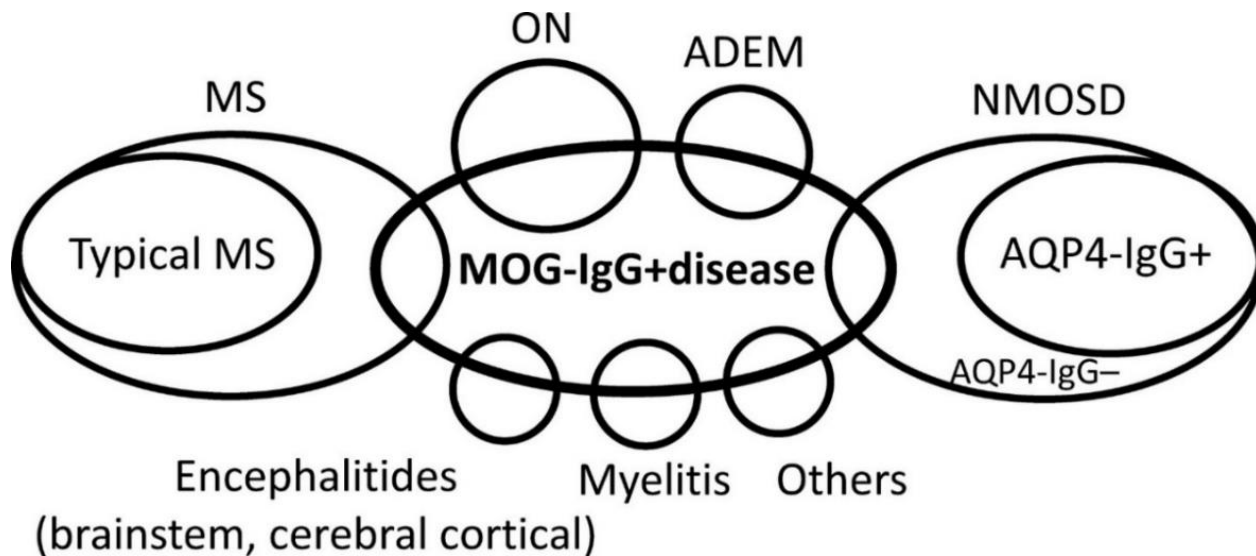
Figure 1.7 Overview of MOG and AQP4 autoantibodies related to the diseases

MOG immunoglobulin disease overlaps with MS, NMOSD, ON, ADEM, myelitis and other encephalitides. AQP4-IgG only appear in NMOSD. (Fujihara et al., 2018).

64.7-80 % of adult patients with typical NMOSD and LETM have AQP4 autoantibodies and in the seronegative group, 3-7.4 % are positive for MOG autoantibodies (Akaishi et al., 2017; Sato et al., 2014). MOG Abs are more commonly found in children, with 40 % in an ADEM cohort (Brilot et al., 2009), compared to 4.8 % in adults in a preselected MS cohort. This group fulfills the McDonald criteria but has clinical features of NMOSD, like severe recurrent ON, myelitis and brainstem involvement (Spadaro et al., 2016). Patients with MOG Abs have compared to AQP4-IgG seropositive cases a better visual and motor outcome and respond quicker to first line treatments (Reindl et al., 2017). There are only rare cases (1/43) describing recurrent ON patients having both MOG and AQP4 autoantibodies (Peng et al., 2018).

The differences between these serological MOG and AQP4 antibody markers are, that patients with AQP4 Abs are mainly non-Caucasian and have rarely brain involvement with specific lesions. The MOG seropositive patients have no specific ethnic origin but frequent brain involvement with unspecific lesions (de Seze, 2017). Coexistence of other autoantibodies in NMOSD, like NMDAR-Abs are rarely seen in MOG[+]-Abs patients, but more common in AQP4^{+}-Abs patients (Titulaer et al., 2014).

Searching for other autoimmune targets in MS, neurofascin (NF) was identified by a proteomic approach (Mathey et al., 2007). This antigen is shared between central and peripheral nervous system and exists as isoform NF155 paranodal on myelin or NF186 as neuronal protein on myelinated axons at the node of Ranvier (Sherman et al., 2005). The distribution of these isoforms

is displayed in Figure 1.8. A further detailed analysis, including cell-based assays and ELISA, revealed that a subset of patients with chronic inflammatory demyelinating polyneuropathy (CIDP) had Abs to NF155 isoform (Ng et al., 2012). This was confirmed in subsequent studies by many other labs (Vural et al., 2018).

Contactin-1 and Caspr-1 autoantibodies are identified in CIDP patients by ELISA and CBA (Cortese et al., 2020; Doppler et al., 2016) and target these proteins at the paranode (Figure 1.8). Contactin-2, localized at the juxtaparanode, was identified 2009 by ELISA as target for autoantibodies in MS patients (Derfuss et al., 2009). Caspr-2 as associated protein in the same region, is also recognized as autoantigen in patients with LE, epilepsy or Morvan syndrome (Irani et al., 2010; van Sonderen et al., 2016). Patients suffering from this syndrome have insomnia, fatigue, muscle weakness, spontaneous hyperexcitability of muscles and cramps (Lee et al., 1998).
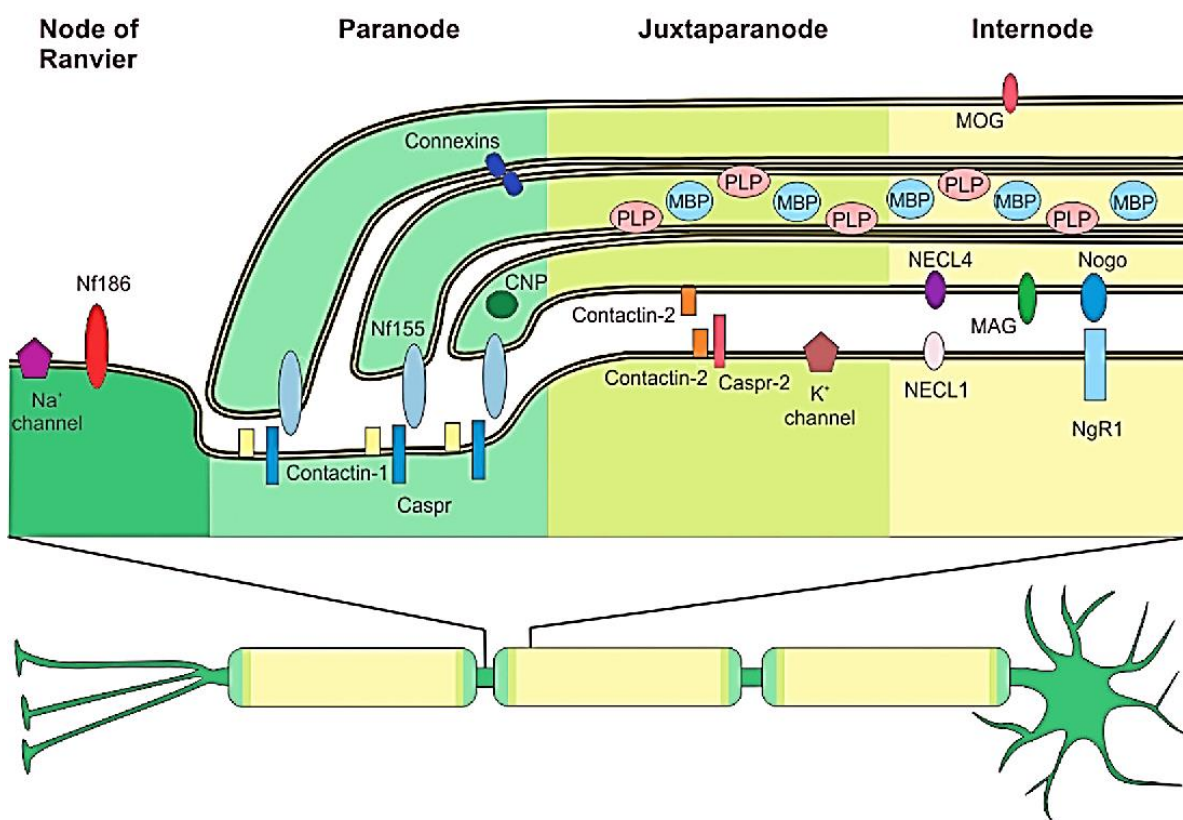
Figure 1.8 Localization of myelin related and neuronal autoantigens

Autoreactive targets can be clustered into four groups: internodal, juxtaparanodal, paranodal or located at the node of Ranvier, which contains the neurofascin186 isoform (NF). Nf155 isoform, Contactin-1, Contactin associated protein 1 (Caspr) and cyclic-nucleotide-phosphodiesterase (CNP) are found paranodal. Contactin-2 and Caspr-2 are juxtaparanodal, whereas myelin basic protein (MBP), proteolipid protein (PLP) are juxtapara-/internodal. MOG, myelin-associated glycoprotein (MAG), neurite outgrowth inhibitor (Nogo) and its receptor (NgR1) are localized internodal. (Mayer and Meinl, 2012).

In 2016 a new autoreactive target, chloride channel anoctamin 2 (ANO2), in MS patients was identified by a bead based protein array (Ayoglu et al., 2016). This target shares similarity in the amino acid sequence with EBV nuclear antigen 1 (EBNA) and autoantibodies may be developed due to molecular mimicry (Tengvall et al., 2019).

The group of Vanda Lennon, who already in 2005 identified AQP4 on astrocytes as target of autoantibodies in NMOSD (Lennon et al., 2005), discovered glial fibrillary acidic protein (GFAP) as autoreactive target in 2016. In a cohort of 103 patients, 16 have autoantibodies against GFAP analyzed by CBA. These seropositive patients suffer from meningoencephalitis and 38 % developed neoplasia within the next three years from the time point of neurological disease onset (Fang et al., 2016).

The progress in research over the last decades contributed enormously to a better understanding of neurological autoimmune diseases. Due to the identification of several novel autoantigens, there was an improvement in diagnosis and stratification of patients with putative similar disorders.

1.3.2 Autoreactive T cells

Beside the analysis of autoantibodies, also the evaluation of autoreactive T cells may be important for various diseases. The first reactivity of MS patients' CSF derived T cells reactive to MBP, was reported in 1983 (Richert et al., 1983). In 1990, peripheral blood of MS patients reacted upon MBP peptide stimulation and could be used for generation of MBP specific T cell lines (Ota et al., 1990; Pette et al., 1990). Furthermore, PLP is also an autoreactive target for T cells in MS patients. In this study they used radioactive DNA thymidine incorporation assays to study the T cell proliferation upon stimulation (Trotter et al., 1991).

Another technique for the identification of antigen specific T cells is by enzyme-linked immune absorbent spot assay (ELISPOT). Hereby, peripheral blood mononuclear cells (PBMCs) from MS patients, which were stimulated with Contactin-2, resulted in secretion of Interleukin-17 (IL-17) and Interferon γ (IFNγ) by T cells using an ELISPOT assay (Derfuss et al., 2009). The same assay led to the identification of MOG-specific T cells in MS patients by analyzing the IL-17A, IL-22 and IFNγ response. Interestingly, in this study antigens were bound to paramagnetic beads and used for purification reasons within the antigen production (Bronge et al., 2019b).

Using thymidine incorporation assay and carboxyfluoresceinsuccinimidylester (CFSE) staining of proliferating cells, AQP4 specific T cells in NMO patients could be detected upon peptide stimulation. Additionally, this study showed that some AQP4 specific T cells of patients are cross reactive to peptides of adenosine triphosphate-binding cassette transporter permease protein

from *Clostridium perfringens* (Varrin-Doyer et al., 2012). The cross reactivity or molecular mimicry might be a potential mechanism in the development of autoimmune diseases (Fujinami and Oldstone, 1985).

In 2018 a research group in Berlin analyzed autoreactive T cells against NF186/155, myelin protein zero (P0) as well as MBP in CIDP, multifocal acquired demyelinating sensory and motor polyneuropathy (MADSAM) patients. Regarding this IFNγ ELISPOT analysis, the patient cohort could be stratified into groups of NF186 autoreactive T cells, which are more present in MADSAM, whereas higher MBP and P0 protein autoreactivity is found in CIDP patients (Diederich et al., 2018).

Recently, as a new neuronal autoreactive target, α- and β-synuclein specific T cells were identified in MS patients. Especially the SPMS cohort has a significant higher rate of CD4 positive T cell proliferation upon antigen stimulation, analyzed in CFSE assay. In the same study, a new EAE animal model in Lewis rats was developed by injection of β-synuclein specific T cells, directed against grey matter. This induces destruction of neurons and further develops brain atrophy (Lodygin et al., 2019).

In summary, patients are more often stratified by using autoantibodies as biomarkers. For technical reasons, it is difficult to use the rarely occurring autoreactive T cells for this purpose. So far it is only applied in diagnostics for cytomegalovirus (CMV) or tuberculosis (Schmidt et al., 2014) and for difficult diagnosis of invasive mold infections (Bacher et al., 2015).

For most of the patients the autoantigen is unknown, but the past identification of autoimmune targets in MS, NMOSD and other related disorders helped for a better understanding of the diseases and stratification of patients. Therefore, screening and evaluation of new neuronal and oligodendrocyte expressed proteins, like the subsequently discussed oligodendrocyte myelin glycoprotein, is of great relevance in neuroimmunolgy research.

1.4 Oligodendrocyte myelin glycoprotein (OMGP)

1.4.1 Structure and localization of OMGP

The OMGP protein was identified as glycoprotein, first only in in the WM of human CNS (Mikol et al., 1988), but later also in GM (Habib et al., 1998). The 120 kDa protein was detected by binding to the lectin peanut agglutinin and released by phosphatidylinositol specific phospholipase C (PI-PLC) from its glycosylphosphatidylinositol (GPI) -anchor (Mikol et al., 1988). The remaining 105 kDa protein is highly glycosylated with twelve predicted (UNIPROT) N-linked glycosylation

sites, with a weight of 25 kDa and additional 30 kDa of O-linked sugars (Mikol and Stefansson, 1988). This anchor provides a high mobility, it can be quickly removed by PLC from the membrane (Mikol and Stefansson, 1988; Wang et al., 2002b) and leaving diacylglycerol as signaling mediator (Ferguson and Williams, 1988). GPI anchored proteins often cluster in lipid rafts, as it was also shown for OMGP (Boyanapalli et al., 2005).

The 433 amino acid (aa) long protein, located in the neurofibromin-1 gene on chromosome 17 (Viskochil et al., 1991), consists of 32 aa long cysteine rich motif, 172 aa long leucine rich repeats as well as 197 aa of serine and threonine rich domain (Mikol et al., 1990a). Additionally, a portion of the isolated OMGP from human brain, contains the carbohydrate epitope "human natural killer-1" (HNK-1) and might therefore be a hint for developmental and regional variation (Mikol et al., 1990b). In an earlier study, where only WM fraction was analyzed, the HNK-1 epitope was not detected (Mikol and Stefansson, 1988). This carbohydrate is involved in synaptic plasticity (Yamamoto et al., 2002) and mediates cell adhesion (Kunemund et al., 1988).

OMGP is found to be present on the outermost surface of compact myelin and is not responsible for the nodal architecture (Chang et al., 2010). A study focused on traumatic spinal cord injury in mice, detected elevated OMGP levels after the impact. By immunofluorescence, physiological intact tissue was tested in advance and OMGP is also expressed on oligodendrocytes in WM of the spinal cord and on neurons in the GM, but not on astrocytes. It is further detected by WB in cerebrum and cerebellum (Dou et al., 2009). The expression pattern on neurons varies throughout brain development in mice, with an increase of OMGP from embryo to adults, detected by WB. Furthermore, it is shown that hippocampal and cortical neurons express OMGP. For the hippocampal neurons, OMGP co-localizes with synapses (Gil et al., 2010).

So far, the ocular expression of OMGP is not studied as extensively as for the MOG protein, where a high expression in the Müller cells of the retina (Quesada et al., 2011) as well as in the optic nerve is detected (Renner et al., 2017). This plays a role for the pathogenesis of MOG associated diseases, since in the MOG induced animal model (Bettelli et al., 2003; Horstmann et al., 2013) and in humans, an inflammation of the optic nerve occurs (Ramanathan et al., 2016; Rostasy et al., 2012). The OMGP protein is only found to be low expressed in the inner plexiform layer of the retina (Liao et al., 2011) and further on the optic nerve (Chang et al., 2010).

1.4.2 Function of OMGP

The initial inhibitory neurite outgrowth function of OMGP together with Nogo-A and MAG was detected in 2002 (Kottis et al., 2002). Through binding to Nogo receptor (NgR1) the growth cone collapse is induced (Lee and Petratos, 2013; Wang et al., 2002b). Besides OMGP, MAG and Nogo bind to the GPI anchored NgR, which needs the co-receptor p75/TROY/LINGO-1 for signal transduction (Figure 1.9) and the activated RhoA GTPase induces the collapse of the growth cone (Lee and Petratos, 2013; Wang et al., 2002a).
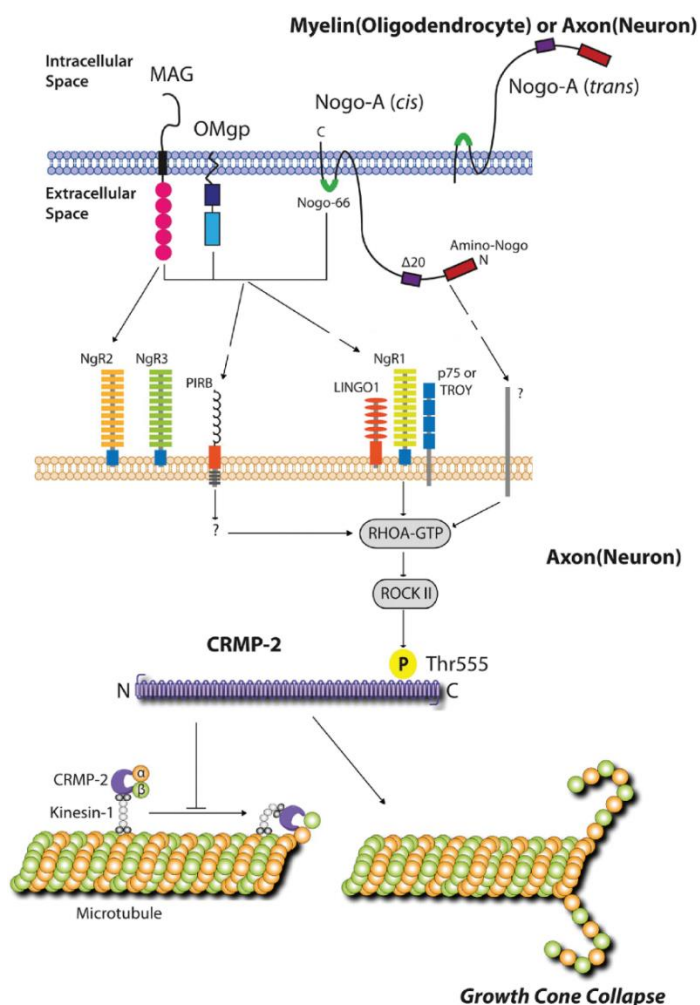
Figure 1.9 NgR and PirB signaling upon binding of its ligands

The scheme illustrates the interactions of NgR, PirB and its ligands MAG, OMGP and Nogo-A. NgR is like OMGP a GPI anchored protein and binds p75/TROY and LINGO-1 as co-receptor, to induce signal transduction. The downstream RhoA-GTPase induces via collapsin response mediator protein 2 (CRMP-2) growth cone collapse in the neuron. Modified from Lee and Petratos, 2013.

Another receptor, paired immunoglobulin-like receptor B (PirB), which also induces growth cone collapse, was found to bind OMGP, Nogo and MAG too (Figure 1.9). This receptor was first described on immune cells, but now additionally found in cerebellum and dorsal root ganglia. The discovery of PirB is an important step, as in this study by blocking both receptors NgR and PirB the inhibition of neurite outgrowth by OMGP, Nogo and MAG could be abrogated (Atwal et al., 2008).

OMGP can be shed through exogenously added PLC and could therefore also act as soluble ligand on the NgR (Mikol and Stefansson, 1988; Wang et al., 2002b). If the protein is soluble or substrate bound, seems to play a role in its function, as it was shown that substrate bound OMGP and Nogo is not effective in neurite outgrowth inhibition. In contrast, the substrate bound OMGP and Nogo bind to NgR and induce growth cone collapse (Chivatakarn et al., 2007).

Analysis OMGP-deficient mice revealed several findings. First, in the MAG-Nogo-OMGP system of inhibition of axonal outgrowth, there is redundancy and OMGP deficiency does not have a strong effect on regulating axonal outgrowth (Cafferty et al., 2010). Second, OMGP is a negative regulator of activity-dependent synaptic plasticity (Raiker et al., 2010). Third, OMGP knock out mice showed altered distribution of thalamo-cortical axons in cortical layer IV (Gil et al., 2010) and mice fell more often from the rotating wheel in the locomotion test, than WT animals (Lee et al., 2010). Furthermore, OMGP deficient mice are hypomyelinated and show an enhanced sensitivity to MOG induced EAE (Lee et al., 2011).

In summary, OMGP inhibits axonal outgrowth like Nogo and MAG via NGR and PirB. These effects have been described for membrane-bound OMGP as a component of myelin and for soluble OMGP, as it is GPI anchored and can be shed by exogenously added PLC. OMGP-deficient mice revealed hypomyelination and altered distribution of thalamo-cortical axons. Additionally, this protein is exclusively expressed in CNS in white as well as grey matter and makes it therefore as an interesting target for further investigations in neurological autoimmune mediated diseases.

1.5 Objectives

This study address the evaluation of OMGP as novel autoreactive target for B and T cells in MS and related disorders. OMGP was selected, since the autoantigen is expressed CNS specific in WM and GM. The following points were the main aims of this study:

- Development of three assays for autoantibody screening, including GPI and transmembrane anchored OMGP cell-based assays as well as streptavidin ELISA with recombinant produced antigen.

- Testing patient cohorts with MS, pediatric ADEM, limbic encephalitis with GAD antibodies and other neurological/inflammatory diseases (OND/OIND) for OMGP Abs.

- Affinity purification of OMGP Abs from highly reactive patient for studying features of these autoantibodies.

- Identification of OMGP-specific T cells in treated and untreated MS patients, by using recombinant produced OMGP in proliferation assays or FluoroSpot analysis.

- Evaluation of the pathogenic relevance of OMGP autoimmunity in an animal model (in collaboration with Dr. Naoto Kawakami and Prof. Hans Lassmann)

2. MATERIALS AND METHODS

2.1 Materials

2.1.1 Patient material

Sera, PBMCs and CSF were obtained from Prof. Dr. Tania Kümpfel of the MS outpatient clinic at the Institute of Clinical Neuroimmunology of the Klinikum Großhadern (Munich, Germany). Additional samples were provided by Prof. Dr. Tomas Olsson and Dr. Mohsen Khademi from the Karolinska institute in Stockholm and the Canadian Pediatric Study Group (Prof. Dr. Amit Bar-Or and Prof. Dr. Brenda Banwell).

The original stocks were stored at -80 °C, whereas the working aliquots were stored at -20 °C. PBMCs were obtained from EDTA blood by ficoll density gradient as described in section 2.5.2 and stored in liquid nitrogen.

2.1.2 Reagents and buffers

Table 2-1 List of generally used Buffers and media

Name	Use	Composition
PBS pH 7.4	ELISA, WB, protein purification	130 mM NaCl 3.5 mM Na_2HPO_4 1.5 mM NaH_2PO_4 x H_2O
PBST	ELISA	0.05 % Tween in PBS
Trypan blue	cell counting	0.05 % trypan blue in PBS
LB agar plate	cloning	5 g Bacto tryptone 2.5 g Bacto yeast extract 7.5 g Bacto agar 5 g NaCl 500 ml H_2O
LB medium	retransformation, cloning	5 g Bacto tryptone 2.5 g Bacto yeast extract 5 g NaCl 500 ml H_2O
Carbonate coating buffer pH 9.5	ELISA	15 mM Na_2CO_3 35 mM $NaHCO_3$ 3 mM NaN_3
Blocking buffer	ELISA	3 % BSA in PBST
Incubation buffer	ELISA	0.5 % BSA in PBST
Milk blocking solution	WB	5 % milk powder in PBST (0.05 % Tween)
Ammonium sulfate solution pH 7.4	Ab purification	4.1 M $(NH_4)_2SO_4$

RIPA buffer pH 8	cell lysis	150 mM NaCl 1 % NP40 0,5 % Na-Deoxycholat 50 mM Tris 0.1 % SDS in 50 ml H_2O add freshly 1 tbl. Protease inhibitor
Blocking buffer IF	IF	5 % Saccharose, 10 % FCS
FACS buffer	FACS	1 % FCS in PBS
DMEM	cell culture	1 % Pen Strep 10 % FCS
RPMI complete	cell culture	10 % FCS 1 % Pen Strep 1% non-essential amino acid solution 1 % sodim pyruvate 1 % L-glutamine
Cryoprotection buffer	IF	30 % sucrose
Sodium citrate pH 8.5	antigen retrieval	10 mm Sodium citrate
Blocking free floating	IF	10 % goat serum 0.5 % Triton in PBS
Stop solution	ELISA	1 M H_2SO_4
TAE buffer	gel electrophoresis	484 g Trizma base 114.2 ml Acetic acid 50 mM EDTA in 2 l of H_2O
Freezing medium	cell culture	FCS 10 % DMSO
HEK293-EBNA medium	cell culture	Freestyle medium 0.1 % Pluronic 25 µg/ml Geneticin
Dialysis buffer pH 7.5	protein purification	20 mM Na_2HPO_4 x 2 H_2O 0.5 M NaCl 10 mM Imidazole
Elution buffer pH 7.5	protein purification	20 mM Na_2HPO_4 x 2 H_2O 0.5 M NaCl 1 M Imidazole
Coomassie Stain	SDS gelelectrophoresis	0.1 % Brilliant Blue G250 50 % Methanol 7 % Acetic acid in H_2O
Coomassie destainer	SDS gelelectrophoresis	50 % Methanol 7 % Acetic acid in H_2O
SDS Gel fixation	SDS gelelectrophoresis	7 % Acetic acid in H_2O
Stripping buffer	SDS gelelectrophoresis	0.9 g glycine 0.06 g SDS in 60 ml H_2O

Solubilization buffer pH 7.4	patients Ab purification	150 mM NaCl 6 mM Tris-base 3 mM Tris-HCl in 500 ml H_2O add freshly 1% octyl-beta-glucoside
Antibody acidic elution buffer pH 3	patients Ab purification	0.1 M glycine/HCl
Antibody neutralization buffer pH 8	patients Ab purification	1 M Tris-HCl

Table 2-2 List of commercial kits

Name	Use	Source
BirA Kit	biotinylation of OMGP	Avidity
Biotinylation Kit	biotinylation of antibodies	Abcam, ab201795
Human IFN-gamma DuoSet ELISA	T cell proliferation assay	R&D, DY285-05
Human IFN-γ/IL-22/IL-17A FluoroSpot	bead-based antigen stimulation of T cells	Mabtech, FSP-011803-10
Human IgG ELISA	determination of IgG in plasma/sera/cell culture supernatants	Mabtech, 3850-1AD-6
Click-it-plus-EdU staining	T cell proliferation assay	Invitrogen, C10632
HiSpeed Plasmid Mini	cloning	Qiagen, 27106
HiSpeed Plasmid Midi	cloning	Qiagen, 12643
HiSpeed Plasmid Maxi	cloning	Qiagen, 12663
RNeasy Mini Kit	cloning	Qiagen, 74106
QIAshredder	cloning	Qiagen, 79656
DNA Clean & Concentrator	cloning	Zymo Research, D4013
PCR purification	cloning	Qiagen, 28004
MinElute Gel Extraction Kit	cloning	Qiagen, 28604
Pierce BCA Protein Assay Kit	protein concentration	Thermo Scientific, 23227
Mouse IgG ELISA	determination of IgG in hybridoma supernatants	eBioscience, 88-50400-88
Rat IgG ELISA	determination of IgG in hybridoma supernatants	eBioscience, 88-50490-88

Table 2-3 List of reagents

Name	Use	Source
HiTrap streptavidin columns	antibody purification	GE Healthcare, GE17-5112-01
HisTrap HP	protein purification	GE Healthcare, GE17-5247-01
Rabbit complement	neuronal complement assay	Cedarlane, CL3111
CFSE - Cell Labeling Kit	T cell proliferation assay	Abcam, ab113853

Concanavalin A	T cell proliferation assay	Sigma, C5275
Measles	T cell proliferation assay	MyBioSource, MBS239121
Tetanus toxin	T cell proliferation assay	Sigma, T3194-25UG
DAPI	IF	Thermo Scientific, 62248
Propidium iodide	flow cytometry	P4864-1ML
Complement component C1q	complement assay	Sigma, C1740
Human complement	complement assay	Sigma, S1764
X-Vivo 15	T cell proliferation assay	Lonza, BE02-060Q
VECTASHIELD Mounting Medium	IF	Biozol, VEC-H-1000
Fluoromount-G	IF	Thermo Scientific, 00-4958-02
T4 DNA Ligase	cloning	NEB, M0202T
ECL Western Blotting System	WB	GE Healthcare, RPN2109
ECL Prime Western Blotting System	WB	GE Healthcare, RPN2232
Human AB-Serum	T cell proliferation assay	Sigma, H4522-100ML
IvIg	rat transfer	Kedrion
dNTPs	cloning	Thermo Scientific, R0181
Phusion High-Fidelity DNA Polymerase	PCR	NEB, M0530S
Optipro medium	HEK293-EBNA	Gibco, 12309-019
Lactalbumin	HEK293-EBNA	BD Biosciences, 259962
PEI	HEK293-EBNA	Polysciences, 23966-2
Lipofectamine 2000	transfection HeLa, HeK293T	Invitrogen, 11668-019
Optimem	transfection HeLa, HeK293T	Gibco, 31985-062
Milk powder	WB	Spinnrad
PNGase F	Deglycosylation	NEB, P0704S
NP-40	patients' Ab purification	Sigma, I-3021
Octyl-beta-Glucopyranoside	patients' Ab purification	Sigma, 08001-25G
Triton-X-100		Roche, 789704
Tween20	ELISA, WB	Biorad, 170-6531
DMEM	cell culture	Sigma, D5796-500ML
RPMI	cell culture	Sigma, R0883-500ML
Pen/Strep	cell culture	Gibco, 15140-122
MEM non-essential amino acid solution 100x	cell culture	Sigma, M7145
FBS Superior	cell culture	Millipore, S0615
Sodium pyruvate 100 mM (100x)	cell culture	Gibco, 11360-039

L-Glutamin	cell culture	Sigma, G7513
Trypsin – EDTA	cell culture	Sigma, 59417C-100ML
Tissue freezing medium	embedding of tissue	Leica, 0.201.08926
A&B detection ELISA R&D		R&D, DY999
SuperScript™ II Reverse Transcriptase	cloning of mAbs	Invitrogen, 18064-014
Recombinant ribonuclease inhibitor	cloning of mAbs	Takara, 2313A
RNase-Free DNase Set	cloning of mAbs	Qiagen, 79254
Bovine Albumin Fraction V	ELISA	Serva, 11945.03
TMB	ELISA	Sigma, T8665-100ML
pNPP	ELISA	Sigma, P7998-100ML
Novex Sharp Pre-stained Protein Standard	SDS-PAGE, WB	Invitrogen, LC5800
NuPAGE MOPS SDS Running Buffer (20X)	SDS-PAGE	Invitrogen, NP0001
NuPAGE LDS Sample Buffer (4X)	SDS-PAGE	Invitrogen, NP0007
NuPAGE Sample Reducing Agent (10X)	SDS-PAGE	Invitrogen, NP0004
Gel Loading Dye, Purple (6X)	agarose gel	NEB, B7024S
1 kb Plus DNA Ladder	agarose gel	NEB, N3200L
Agarose	agarose gel	Biozym, 840004
Ampicillin	cloning	Sigma, A9518-25G
Kanamycin	cloning	Sigma, K1377-5G
R848	PBMC stimulation	Sigma
IL2	PBMC stimulation	R&D
Dephosphorylation CIAP	cloning	Fermentas, EF0341
Freestyle medium	HEK293-EBNA	Gibco, 12338-018
Geneticin	HEK293-EBNA	Gibco, 10131-035
10% Pluronic F68	HEK293-EBNA	Gibco, 24040-032
Imidazole	IMAC	Merck, 1.04716.0250
Pancoll	PBMC density gradient	Pan Biotech, P04-60500
Peq green	agarose gel	Peqlab, 37-5010
Soc medium	cloning	NEB, B9020S
DMSO	freezing medium	Sigma, D8418-500ML

Table 2-4 List of materials

Name	Use	Source
PVDF membrane	WB	GE Healthcare, 10600023
NuPage 4-12 % Bis-Tris Gel	SDS-PAGE	Invitrogen, NP0321

96 well FACS plates	cell-based assay	Thermo Scientific
F96 MaxiSorp Nunc immunoplate	ELISA, BCA	Thermo Scientific, 442404
Nunc Immobilizer streptavidin F96	ELISA	Thermo Scientific, 436014
Amicon Ultra 0.5 ml 50K	protein purification	Merck Millipore, UFC505096
Amicon Ultra 0.5 ml 3K	protein purification	Merck Millipore, UFC500396
Amicon Ultra 15 ml 50K	protein purification	Merck Millipore, UFC905024
Amicon Ultra 15 ml 30K	protein purification	Merck Millipore, UFC903024
D-Tube Dialyzer Maxi 12-14 kDa	protein purification	Millipore, 71510-3
Spectra Por7 Dialysis Membrane 50 kDa	protein purification	Spectrum, 132130

2.1.3 Primer

The following primers were all synthesized at Metabion (Martinsried) and delivered as lyophilized product. The primers were diluted in ddH$_2$O to a stock concentration of 100 µM. For the PCRs or sequencing a working concentration of 100 mM was used.

Table 2-5 List of primers

Name	Sequence 5'-3'
sequencing	
ratOMGP-GPI sequ-3	CCTCTCTGAAGGAACAGA
pEGFP-N1_rev	CGACTGCAGAATTCGAAGCTT
CMV_fwd	CGCAAATGGGCGGTAGGCGTG
pEGFP-N1_rev_2	GCAGCTTGCCGGTGGTGCAGATGAAC
pTT5-forw	GGGGTGAGTACTCCCTCTCAAAAGC
pTT5-rev	GGGGCAGAGATGTCGTAGTCAGG
rOMGP-seq-Fwd	CATATTGTGGACCTGTC
GFP sequencing-1	GGAGTACAACTACAACAG
hOMGP sequencing-2	CTGGAAAGTCTTCCCGC
hOMGP-GPI sequ-3	AATTCTCTGAGCGTAGTG
pTT5-sequ-FWD	CTTTCTCTCCACAGGTGTCCAC
ratOMGP sequencing-2	TTCAAACAACAGGCTTG
cloning of soluble rOMGP	
rOMGP-sol_FWD	ATAGGTACCATTTGTCCTCTCCAATGTATATGCACAG
rOMGP-sol_REV	ATAGCTAGCGGAAGGTGGCTGAGTCTTTACATTT

cloning of hOMGP-GPI-T2A-EGFP	
BsrGI_T2A-hOMGP_Fwd	GCTGTACAAGGGTTCTGGTGAGGGCAGAGGAAGTCTTCTAAC ATGCGGTGACGTGGAGGAGAATCCCGGCCCTATGGAATATCA GATCC
NotI-GPI-hOMGP_Rev	tcgcggccgcTCAGACAGCCAGCATGACCACAACATTGAGCAATA AGAGAAATGAAGCATTTACTTTCCAAGCATTTGCCACGGAAG GCAGAGGAGTC
cloning of rOMGP-GPI-T2A-EGFP	
BsrGI_T2A-hOMGP_Fwd	GCTGTACAAGGGTTCTGGTGAGGGCAGAGGAAGTCTTCTAAC ATGCGGTGACGTGGAGGAGAATCCCGGCCCTATGGAATATCA GATCC
NotI-GPI-ratOMGP_Rev	TCGCGGCCGCTCAGACAGCCAGCATGACCACAACATTGAGC AATAAGAGAAATGAAGCATTTACTTTCCAAGCATTTGCCACGG AAGGTGGCTGAG
rOMGP insertion-rev	CGGTACCGTCGACTGCCAGAATTCC
cloning 22H6 rIgG2A antibody into hIgG1-pTT5	
HC_mG1/2a_rG1/2a/2b_r	CTCAATTTTCTTGTCCACCTTGGTGC
HC_mG2b_r	CTCAAGTTTTTTGTCCACCGTGGTGC
LC-kappa_m/r_r	CTCATTCCTGTTGAAGCTCTTGAC
LC-lambda_m-1-4/r-1_r	ACACTCAGCACGGGACAAACTCTTCTC
LC-lambda_m-2-3/r-2_r	ACACTCTGCAGGAGACAGACTCTTTC
CHeavy_rev_uni_SalI	GTGCCCCCAGAGGTCGACTTGGAGGAGGGTGCCAGGGGGA AGACCGATGGGCCCTTGG
CHeavy_ SacII_for_22H6	GTTTCCGCGGTGGGTCCTGTCCCAGGTTACTCTGAAAGAGTC TGGC
CHeavy_rev_22H6	AGACCGATGGGCCCTTGGTGGAGGCTGAGGAGACAGTGACT GAAGTTC
lamda_BssHII_for_22H6	AACGGGCGCGCGATGAGCTATGAGCTGATCCAACCAC
L-to-ka_ KasI_r_22H6	AGATGGCGCCGCCACAGTTCGTAGGACAGTGAGCTTGGTTC C
L_BssHII_FWD-ORF22H6	AACGGGCGCGCGATGTAGCTATGAGCTGATCCAACCAC
TSO_PCR	AAG CAG TGG TAT CAA CGC AG
TSO-FWD_E. Beltran	AAGCAGTGGTATCAACGCAGAGTACATrGrG+G

2.1.4 Plasmids

Table 2-6 List of plasmids

Vector	Resistance	Expression	Size [kb]	Plasmid number	Source
T2A-mOMGP-hGPI_pMA-T	Ampicillin	surface, GPI-anchor	3.8	60	Geneart
rOMGP-CD80_pMK-RQ-Bs	Kanamycin	surface, transmembrane	1.5	33	Geneart

secr_hOMGP_Avi_His_pMK-RQ	Kanamycin	soluble	3.7	35	Geneart
pEGFP	Kanamycin	cytoplasm	4.7	65	CLONTECH Laboratories
pEGFP-hOMGP-CD80	Kanamycin	surface, transmembrane	6.2	28	Institute (AG Meinl)
pEGFP-hOMGP-T2A-GPI	Kanamycin	surface, GPI-anchor	6.1	48	Institute (AG Meinl)
pEGFP-rOMGP-T2A-GPI	Kanamycin	surface, GPI-anchor	6.1	51	Institute (AG Meinl)
pEGFP-mOMGP-T2A-GPI	Kanamycin	surface, GPI-anchor	6.1	61	Institute (AG Meinl)
pTT5	Ampicillin	/	4.4	37	Dr. Jenne (Perera et al., 2013)
pTT5-hOMGP-Avi-His	Ampicillin	soluble	5.7	40	Institute (AG Meinl)
pTT5-rOMGP-Avi-His	Ampicillin	soluble	5.7	101	Institute (AG Meinl)
pTT5-hIgG1-heavy-22H6	Ampicillin	soluble	5.8	102	Institute (AG Meinl)
pTT5-hIgG1-kappa-22H6	Ampicillin	soluble	5.1	103	Institute (AG Meinl)
pTT5-hIgG1-heavy-HK3	Ampicillin	soluble			Institute (AG Dornmair)
pTT5-hIgG1-kappa-HK3	Ampicillin	soluble			Institute (AG Dornmair)

2.1.5 Restriction enzymes for digestion

Table 2-7 Used endonucleases

Name	Source
Avr II, BssH I, BamH I, BsrG I, EcoR I-HF, Hind III, Kas I, Kpn I, Nhe I, Not I, Sac I, Sac II-HF, Sal I-HF, Xho I	NEB

2.1.6 Cell lines

Table 2-8 Cells for cell culture

Name	Use	Source
HeLa	cell-based assay	Institute (AG Meinl)
HEK293T	cell-based assay	Institute (AG Meinl)
HEK293-EBNA	human embryonic kidney cell line, G418-resistence	Dr. Jenne (Perera et al., 2013)
HEK-293S-GnT1-/-	test reduction of glycosylation on antigen	ATCC

2.1.7   Proteins and Peptides

Table 2-9 List of proteins and peptides

Name	Description	Expression system	Source
hOMGP	Human oligodendrocyte myelin glycoprotein	HEK293-EBNA	Institute (AG Meinl)
rOMGP	Rat oligodendrocyte myelin glycoprotein	HEK293-EBNA	Institute (AG Meinl)
mOMGP	Mouse oligodendrocyte myelin glycoprotein	Mouse myeloma cell line	R&D (1674-MG-025)
rOMGP-peptide	BIOT-SP-ETTANVKTQPPS-HHHHHH	synthesized	Peps4LS
Avi-His_CTR	ASGSGMGMGMGMMGLND IFEAQKIEWHEPRSGGSGH HHHHH	synthesized	Thermo Fisher Scientific
22H6-hIgG1	monoclonal OMGP antibody	HEK293-EBNA	Institute (AG Meinl)
HK3-hIgG1	monoclonal neuroborreliosis antibody	HEK293-EBNA	Institute (AG Dornmair)

2.1.8   Antibodies

Table 2-10 Primary antibodies

Antibody specificity	Use	Dilution/final concentration	Conjugate	Host	Source
C1q-HRP	ELISA	1:200	HRP	sheep	LifeSpan Biosciences, LS-C41845
His-tag-HRP	WB	1:1000	HRP	mouse	Sigma- Aldrich, A7058
Biotin-HRP	ELISA WB	1:2000	HRP	goat	Cell signaling, 7075
GFP-HRP	WB	1:1000	HRP	goat	GeneTex, GTX26663
human-CD3	FACS	1:15	APC	mouse	BD Pharmingen, 555342
human-CD4	FACS	1:60	PerCP	mouse	eBioscience, 12-0048-42
human-CD8	FACS	1:60	efluor450	mouse	eBioscience, 48-0088-42
HNK-1	FACS ELISA WB	1:1000 1:100	-	mouse IgM	Sigma, C0678
mAb-OMGP	FACS WB ELISA	1-10 µg/ml 1 µg/ml	-	rat IgG1	R&D MAB1674
pAb-OMGP	FACS WB ELISA IF	1-10 µg/ml 0.4 µg/ml 1 µg/ml 5 µg/ml	-	polyclonal goat IgG	R&D AF1674
β-III-tubulin	IF	1:200	-	rabbit IgG	Cell signaling, D7169

22H6	FACS ELISA IF	1-10 µg/ml 1-10 µg/ml 20 µg/ml	-	rat IgG2A	Helmholtz Zentrum München (AG Feederle)
31A4	FACS ELISA IF	1-10 µg/ml 1-10 µg/ml 20 µg/ml	-	mouse IgG2B	Helmholtz Zentrum München (AG Feederle)
14A9	FACS ELISA IF	1-10 µg/ml 1-10 µg/ml 20 µg/ml	-	rat IgG 2B	Helmholtz Zentrum München (AG Feederle)
human-IgG1	FACS	1:50	-	sheep	The binding site, AU006
human-IgG4	FACS	1:50	-	sheep	The binding site, AU009

Table 2-11 Secondary antibodies

Antibody specificity	Use	Dilution/final concentration	Conjugate	Host	Source
HRP	FACS	1:100/1:2000	647	goat	Jackson, 123-605-021
rat-IgG	WB ELISA	1:2500 1:7000	HRP	goat	Jackson, 112-036-003
	IF	10 µg/ml	594	goat	Invitrogen, A-11007
	IF	10 µg/ml	488	donkey	Invitrogen, A-21208
	FACS	1:500	647	mouse	Jackson, 212-605-082
	FACS	1:500	biotin	goat	Jackson, 112-065-062
goat-IgG	IF	10 µg/ml	488	donkey	Invitrogen, A-11055
	IF	10 µg/ml	594	donkey	Invitrogen, A-11058
	ELISA	1:7000	HRP	rabbit	abcam, ab6741
	FACS	1:500	biotin	donkey	Jackson, 705-065-003
mouse-IgG	ELISA	1:7000	HRP	goat	Jackson, 115-036-072
	IF	10 µg/ml	488	donkey	Invitrogen, A-21202
	FACS	1:500	647	rat	Jackson, 415-605-166
	FACS	1:500	biotin	goat	Jackson, 115-067-020
mouse-IgM	FACS	1:500	biotin	goat	Jackson, 115-067-020
	ELISA	1:7000	HRP	goat	Jackson, 115-035-075
sheep-IgG	FACS	1:100	647	donkey	Jackson, 713-606-147

rabbit-IgG	IF	10 µg/ml	488	goat	Invitrogen, A-11008
	IF	1:500	594	donkey	Invitrogen, A-21207
human-IgM	ELISA FACS	1:500 1:50	HRP	mouse	Zymed, 05-4920
	FACS	1:20	APC	mouse	eBioscience, 17-9998-42
human-IgE	ELISA FACS	1:500 1:50	HRP	mouse	Zymed, 05-4720
	FACS	1:100	APC	mouse	Pharmingen, 34612D
human-IgA-RPE	FACS	1:50	RPE	goat	Jackson, 109-115-011
human-IgG	IF	10 µg/ml	550	rabbit	Invitrogen, SA5-10111
	IF	10 µg/ml	555	goat	Invitrogen, A-21433
	FACS	1:50	RPE	goat	Jackson, 109-116-098
	FACS	1:500	biotin	goat	Jackson, 109-066-098
	WB ELISA	1:2500 1:5000/1:7000	HRP	goat	Jackson, 109-036-003
	FACS	1:150/1:500/ 1:1000	alexa647	goat	Invitrogen, A21445
human-IgG1	ELISA FACS	1:500 1:50	HRP	mouse	Zymed, 05-3320
	FACS	1:500/1:1000	biotin	mouse	Invitrogen, MH1515
	FACS	1:50	RPE	mouse	abcam, ab99776
	FACS	1:50	BIMA	mouse	Southern Biotech, 9054-28
	FACS	1:50/1:500	biotin	mouse	Southern Biotech, 9052-08
	FACS	1:50/1:100	PE	mouse	Southern Biotech, 9052-09
	FACS	5 µl/5x10^{4}cells	APC	mouse	R&D, FAB110A
human-IgG2	FACS	1:50	RPE	mouse	abcam, ab99781
	FACS	1:100	PE	mouse	Southern Biotech, 9060-09
	ELISA FACS	1:500 1:50	HRP	mouse	Zymed, 05-0520
	FACS	1:50/1:500	biotin	mouse	Southern Biotech, 9060-08
human-IgG3	FACS	1:50	RPE	mouse	abcam, ab99831
	ELISA FACS	1:500 1:50	HRP	mouse	Zymed, 05-3620
	FACS	1:50	PE	mouse	Southern Biotech, 9210-09
	FACS	1:50/1:500	biotin	mouse	Southern Biotech, 9210-08

human-IgG4	FACS	1:50	PE	mouse	Southern Biotech, 9200-09
	FACS	1:50	RPE	mouse	abcam, ab99819
	ELISA FACS	1:500 1:50	HRP	mouse	Zymed, 05-3820
	FACS	1:50/1:500	biotin	mouse	Southern Biotech, 9200-08

Table 2-12 Streptavidin conjugated dyes

Name	Use	Dilution	Conjugate	Source
streptavidin-alexa647	FACS	1:2000	alexa647	Jackson, 016-600-084
streptavidin-peroxidase	WB ELISA	1:100.000	HRP	Jackson, 016-030-084
streptavidin-HRP	ELISA	1:10-1:200	HRP	R&D, DY998

Table 2-13 Isotype controls

Name	Use	Source
mIgG2B	ELISA, IF, rat transfer	BD Pharmingen, 559530
mIgG2A	ELISA, IF, rat transfer	BD Pharmingen, 554645
rIgG2B	ELISA, IF, rat transfer	BD Pharmingen, 556968
rIgG2A	ELISA, IF, rat transfer	BD Pharmingen, 553926
rIgG polyclonal	IF	Abcam, ab27478
rat IgG1	IF	R&D, MAB005
goat IgG	IF	R&D, AB-108-C

2.2   Molecular cloning

For the production of expression vectors, the following section describes how the plasmids were amplified, cloned, processed and expanded. Applying these techniques, the vectors were used for the production of target proteins.

2.2.1   Polymerase chain reaction (PCR)

To amplify or modify DNA fragments and plasmids, the PCR technique with the following reaction mixture (Table 2-14) was used in a total volume of 50 µl. The parameters for the PCR program are listed in Table 2-15.The elongation time was adjusted to the length of the amplified product, whereas in 60 sec 1000 bp can be elongated.

Table 2-14 Reaction mixture for PCR

component	µl	final concentration in 50 µl
Phusion buffer 5x	10	1x
dNTPs 10 mM	1	0.2 µM
Primer forward 10 µM	2.5	0.5 µM
Primer reverse 10 µM	2.5	0.5 µM
DNA template 50 ng/µl	1	10 ng/ml
Phusion polymerase	0.5	
ddH$_2$O	32.5	

Table 2-15 PCR program

function	temperature	time	cycles
initial denaturation	98 °C	30 sec	1
denaturation	98 °C	20 sec	
hybridization	60 °C	20 sec	30
elongation	72 °C	60 sec/1000 bp	
final elongation	72 °C	10 min	1
cooling	4 °C	∞	

2.2.2 RNA extraction

Hybridoma cell pellets of the 22H6/14A9/31A4 OMGP antibodies were frozen at -80 °C. The RNA of 5×10^6 cells was extracted by RNeasy Mini Kit from Qiagen. The protocol was carried according to the manufacturer's protocol.
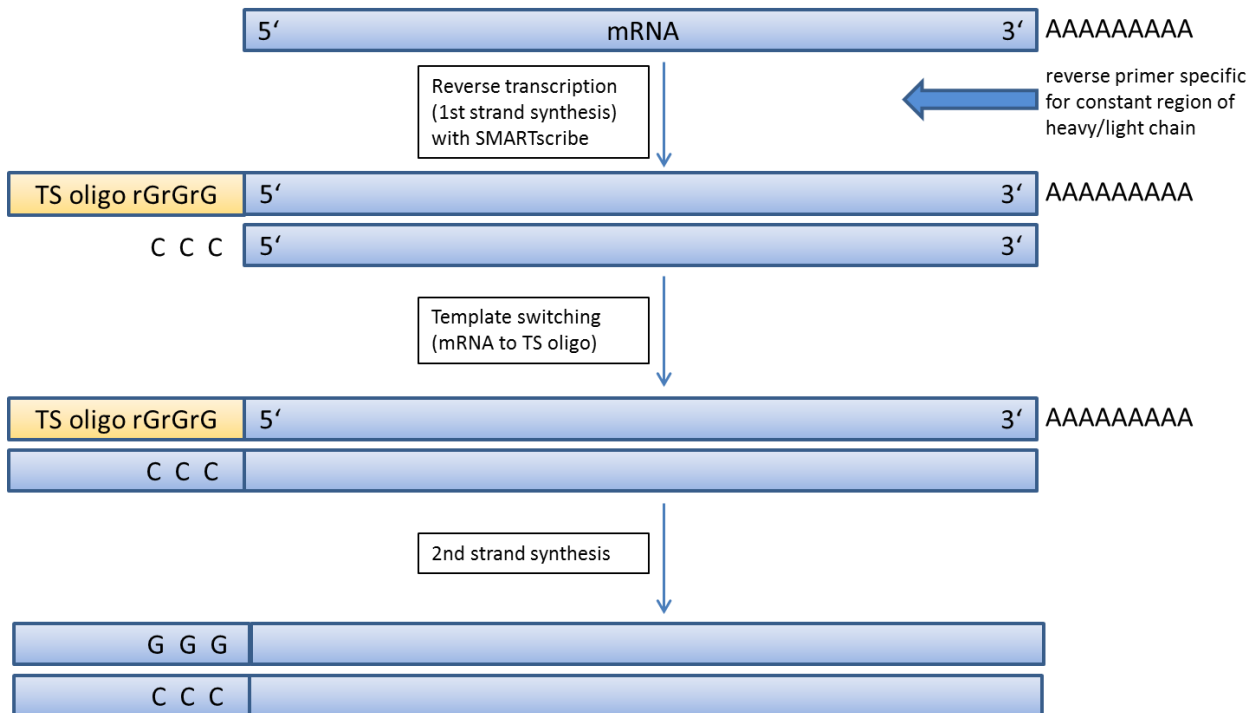
2.2.3 Reverse transcription (RT) and template switch PCR

The purified RNA serves as template for the generation of complementary DNA (cDNA). For this process the sequence of 5' end and the 3' end of the mRNA is important. The reverse primer "HC_mG1/2a_rG1/2a/2b_r" for the cDNA synthesis (Table 2-5) of the constant heavy region can be used for the amplification of mouse IgG1/IgG2A and rat IgG1/IgG2A/IgG2B, whereas for the constant heavy region of mouse IgG2B there is a separate primer. For the kappa and lambda light chain other primers were used (Table 2-5).

The sequences of the antibodies, coming from the hybridoma cells, are unknown. Therefore, we used the described reverse primers flanking the constant region (Kontermann and Dübel, 2010)

and the SMARTscribe reverse transcriptase together with 5'-template-switching oligonucleotide (TSO) primer (Figure 2.1).

Figure 2.1 SMARTscribe acting as reverse transcriptase

The figure shows the mRNA template with an unknown 5' end. After SMARTscribe reaches the 5' end, additional deoxycytidine are added and allows the template switching oligonucleotide (TSO) primer to bind with it complementary guanosines.

This SMART (switching mechanism at the 5' end of RNA template) enzyme is a modified version of the moloney murine leukemia virus (MMLV)-RT and it adds upon reaching the 5' end of the RNA template additional deoxycytidine. The TSO forward primer carries three riboguanosines (rGrGrG) at its 3' end and the complementary to this 3' deoxycytidine extension of the cDNA molecule allows the subsequent template switching (Picelli et al., 2014).

All reagents listed in Table 2-16 were mixed and the tube was incubated for 3 min at 72 °C, followed by 2 min at 42 °C.

Table 2-16 cDNA synthesis (first step)

component	µl
H-chain_RT reverse primer 10 µM	1
L-chain_RT reverse primer 10 µM	1
dNTPs 10 mM	1
RNA (max. 2 µg)	2

After the preincubation with the reverse primer, the 5.25 µl of Table 2-17 were added and the PCR run was continued for 1 h at 42 °C and a final step for 10 min at 70 °C. The synthesized cDNA was purified using DNA Clean & Concentrator™-5 (ZYMO RESEARCH) and eluted in 8 µl of elution buffer.

Table 2-17 cDNA synthesis (second step)

component	µl
buffer 5x	2
DTT 20 mM	1
TSO 10 µM	1
SMARTscribe 100 U/µl	1
RNase inhibitor 40 U/µl	0.25

2.2.4   Isolation of Plasmid DNA

Bacterial cultures were grown at 37 °C overnight in LB medium with 100 µg/ml Ampicillin or 50 µg/ml Kanamycin. For Miniprep *E. coli* were cultured in 2ml and in 200-300 ml for Mini-/Maxiprep. Cells were harvested and processed regarding the manufacturers protocol. The plasmid concentration was determined by Nanodrop.

2.2.5   Agarose Gelelectrophoresis

DNA constructs were loaded on an agarose gel. Therefore, 1 % agarose was dissolved in TAE buffer and supplemented with 5 µl of Peq green in a total volume of 50 ml. 10 µl of DNA ladder 1 kb from NEB was loaded and 110 V were applied for 45-60 min. If DNA was cut out of the gel, the bands of interest were cut out and purified using the Qiagen MinElute Gel Extraction kit.

2.2.6 Digest of DNA

The different endonucleases used in this study are listed in Table 2-7. All restriction digests were carried out in a total volume of 25 µl in the buffer as recommended by the manufacturer, using the appropriate amount of enzyme units. The optimal temperatures for the enzyme were used for 1 h to digest the construct.

2.2.7 DNA Ligation

T4 DNA ligase was used to ligate the insert into the cut vector. Molar ligation ratios of 1:3 and 1:7 vector (100 ng) to insert together with a negative control (vector only) were incubated in 20 µl at 16 °C overnight. On the next day 5 µl of the ligation mixture were pipetted to the chemical competent *E. coli.*

2.2.8 Transformation of chemically competent *E. coli*

E. coli DH5α (NEB, C2987H) were thawed on ice. 1 µl of DNA was added and gently mixed by squiring the pipet tip. After an incubation of 20 min on ice a heat shock pulse for 90 sec at 42 °C followed. The tubes were chilled for 5 min on ice and cells recovered for 60 min shaking at 37 °C in SOC medium. For expanding the bacteria 50 µl of the bacteria were grown in 200-300 ml LB medium with required antibiotics. If the *E. coli* were transformed after ligation, 100 µl of bacteria were spread on an ampicillin or kanamycin agar plate and transferred to a 37 °C incubator overnight.

2.2.9 DNA Sequencing

Cloning was proofed by using the Sanger sequencing method of the sequencing service from the LMU faculty of biology. The listed primers (Table 2-5) were used for it and data was analyzed using "Chromas Lite" software.

2.2.10 Cloning of OMGP-TM and OMGP-GPI (human/rat/mouse) for cell-based assay

The cell-based assay was conducted using antigens expressed in the pEGFP-N1 vector (Figure 2.2). For studying the autoantibody binding *in vitro,* the OMGP antigen was expressed on HeLa cells in two versions.
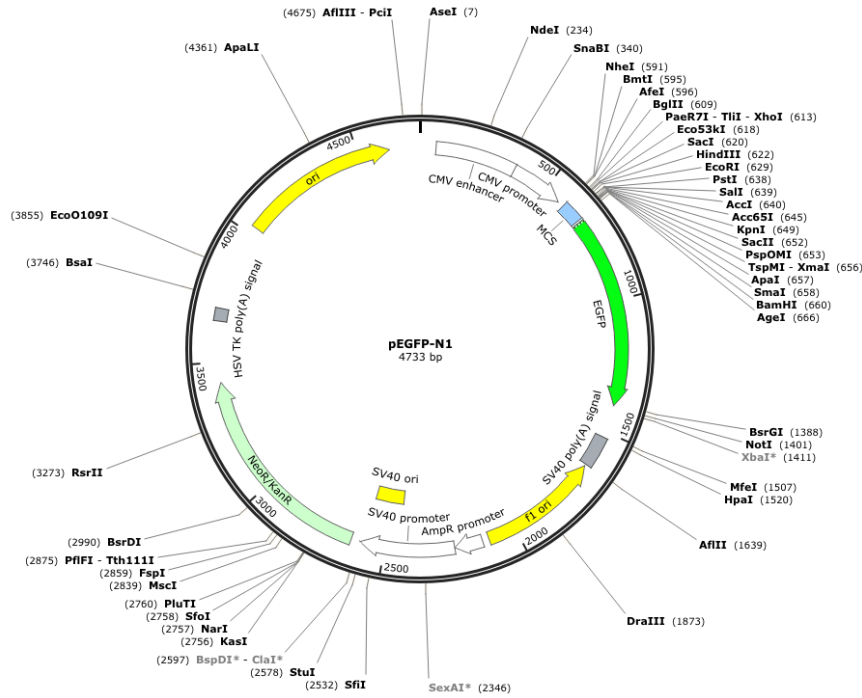
Figure 2.2 Plasmid map of pEGFP-N1

The vector consists of a multiple cloning site (MSC), where OMGP constructs are inserted and driven by CMV promoter. Kanamycin resistance gene is used in this vector.

In the first construct, the human OMGP (Uniprot P23515) was fused to the transmembrane part of CD80 (murine B lymphocyte activation antigen CD80 (Uniprot, Q549R2) P237 to end, stop codon deleted). Therefore, the physiological occurring GPI-anchor signal peptide V418-V440 was deleted, replaced by CD80 and further fused to EGFP in the vector. This hOMGP-TM construct was introduced into pEGFP-N1 by the endonuclease XhoI and HindIII. It was developed for having a stable anchored protein in the membrane (Figure 2.3, A).
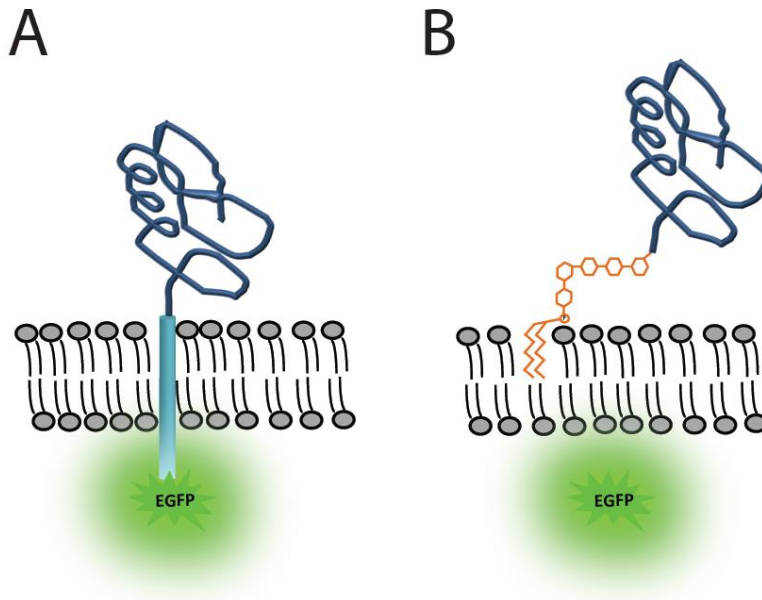
Figure 2.3 Anchoring of OMGP to the membrane

The two anchoring methods of the OMGP protein expression systems are displayed. (A) OMGP-TM, where it is fused to the CD80 transmembrane part and further to EGFP or (B) as second variant where OMGP is anchored via GPI in the cell membrane like *in vivo*. In this construct EGFP is separated from the protein.

The second variant was cloned with a GPI-anchor (Figure 2.3, B), like the protein is expressed *in vivo*. To guarantee the recognition of the signal peptide on the N-terminus, the antigen was introduced into pEGFP-N1 with BsrGI and NotI. Thereby the stop codon of EGFP was removed and a T2A (thosea asigna virus 2A) ribosome sequence (GSGEGRGSLLTCGDVEENPGP) was cloned in between. Due to sterically hindrance, the ribosome skips during the translation (Kim et al., 2011) at the glycyl-prolyl peptide bond (Figure 2.4), which results in cleavage between the EGFP and the downstream OMGP. Two further constructs were generated in the same way: mOMGP-GPI (UNIPROT, Q63912) and rOMGP-GPI (UNIPROT, Q7TQ25). For these two rodent specific antigens, the human specific GPI signal peptide was used, since the protein expression efficiency in HeLa cells was very little using the rodent specific signal sequence.
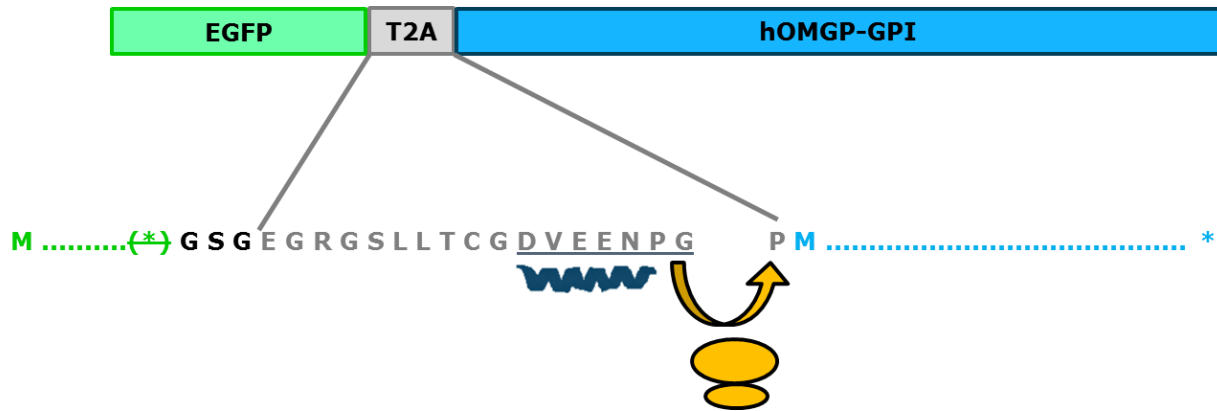
Figure 2.4 Schematic ribosome skipping between EGFP and OMGP-GPI

The pEGFP-T2A-hOMGP-GPI plasmid induces the transcription of one mRNA (green EGFP, gray T2A sequence and blue hOMGP-GPI). During translation the ribosome (yellow) skips between glycine and proline, resulting in two separated proteins.

2.2.11 Cloning of human/rat OMGP for protein expression

In house proteins were produced using the mammalian HEK293-EBNA expression system as described later in chapter 2.3.1. Therefore, the human (Uniprot P23515) or rat (Uniprot Q7TQ25) OMGP was cloned into pTT5 expression vector (Figure 2.5) using EcoRI and BamHI restriction sites.
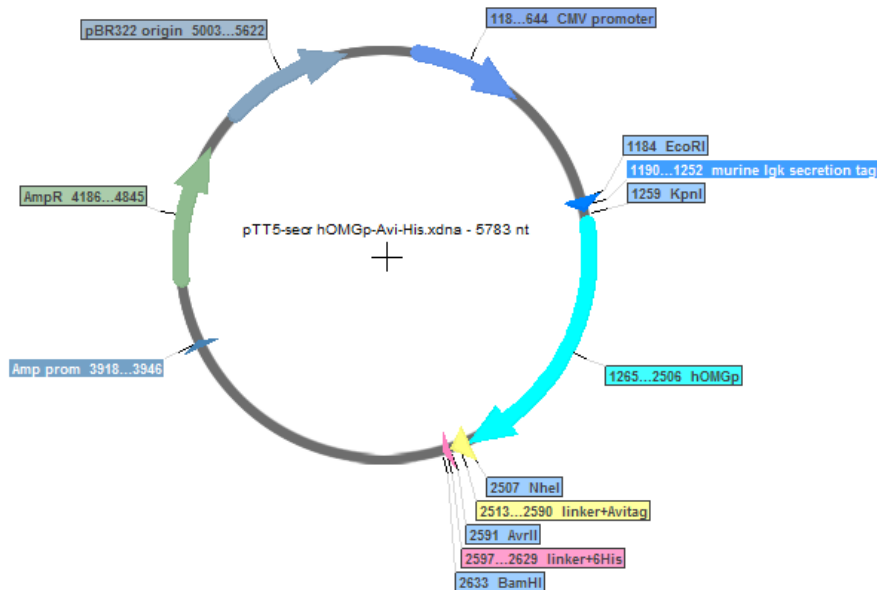
Figure 2.5 Plasmid map of pTT5

The human OMGP in the pTT5 protein expression vector with an N-terminal murine Ig kappa secretion tag and a C-terminal Avi- and His-tag. The construct is driven by the CMV promoter.

The construct harbors N-terminal murine Ig κ secretion tag for the protein production into the supernatant, followed by the OMGP sequence without the GPI signal peptide. The C-terminus of the protein was designed with a flexible 11–amino acid linker (GSGMGMGMGMM) (O'Connor et al., 2007) for the following Avi-tag sequence (GLNDIFEAQKIEWHE), used for site-specific biotinylation (Fairhead and Howarth, 2015) and a poly-His-tag sequence for IMAC purification (section 2.3.2).

2.2.12 Cloning of recombinant antibody

To clone the OMGP-specific antibody 22H6-rIgG2A, which was produced by the Helmholtz Center, with a human IgG1 Fc part, the RNA and cDNA was processed as described in section 2.2.2 and 2.2.3. The amplified antibody DNA fragments were sent for sequencing (section 2.2.9) and aligned to the IMGT database to determine leader, variable and constant regions. Afterwards the variable antibody sequences were cloned into pTT5-hIgG1 heavy and pTT5-light-kappa chain vectors, which were provided by AG Dornmair. The heavy chain was introduced with SacII and SalI restriction sites, whereas the light chain with BssHI and KasI endonucleases.

2.3   Recombinant protein production

Studying antigens and also antibodies, the proteins are required in big amounts. Therefore, they were produced in house by a mammalian cell line, where it is secreted into the supernatant and followed by an ion metal affinity chromatography (IMAC) purification.

2.3.1   Eukaryotic expression system of HEK293-EBNA

The cell line is related to the HEK293 cells and stably transfected with the Epstein-Barr virus nuclear antigen-1 (EBNA1), which is under antibiotic selection to Geneticin G-418 (Geisse and Kocher, 1999). Cells are grown as suspension culture in Freestyle media without serum and supplemented with 25 µg/ml Geneticin and 0.1 % Pluronic F68 for reduction of foam formation. Multitron shaker was used for shaking cells at 37 °C, 8 % CO2, 70 % humidity and 90 rpm.

For optimal growth and survival, cells were maintained at concentrations of 0.2-3 x 10^6 cells and therefore splitted two to three times per week. Live and dead cells were distinguished using 0.05 % trypan blue in a 1:10 dilution and 10 µl were pipetted in a Neubauer counting chamber.

Large amounts of proteins could be produced by transfecting the HEK293-EBNA cells with pTT5 vector constructs (section 2.2.11). This vector allows due to its oriP and improved cytomegalovirus (CMV) expression cassette a three- to tenfold increase in protein expression compared to pcDNA3.1 and pCEP4 vectors (Durocher et al., 2002).

To produce recombinant proteins, cells were transfected at a final concentration of 1×10^6 cells/ml in a total volume of 100-1000 ml. 1 µg of DNA (for antibodies 500 ng heavy and 500 ng light chain) and 2 µg of the transfection reagent polyethylenimine was used per 1 ml of culture. Therefore, two tubes were prepared, whereas in tube A the respective amount of DNA was diluted into OptiPro with a volume of 1/20 of the total cell suspension and in tube B the required PEI also into OptiPro (1/20 of total volume). After mixing the tubes and incubation for 30 min at RT, the solution was added slowly dropwise on the culture. 24 h after transfection 0.5 % lactalbumin was added. Cells were incubated for four days until the supernatant was harvested by centrifugation for 15 min at 2500 rpm and subsequently sterile filtered with 0.22 µm.

2.3.2   Ion metal affinity chromatography

Supernatant containing the secreted antigen/antibody was dialyzed in 50 kDa tubes in dialysis buffer (500 mM NaCl, 20 mM Na_2HPO_4, 10 mM Imidazole, pH 7.5) overnight. On the next day the solution was filtered again (0.22 µm) and the HisTrap column was equilibrated using the ÄKTA-START machine with 10-15 column volumes (CV) of dialyzing buffer and 1 ml/min. Afterwards sample was loaded with 0.5 ml/min and column was washed with 10-15 CV dialyzing buffer. To elute the His-tagged protein, an increasing gradient from 0.01-1 M Imidazole was applied. The wavelength was measured at 280 nm for tracking the fractions containing the eluted protein. All samples, load, flow-through, wash and elution fractions were applied on SDS gel (section 2.4.1) to check the size and purity of the recombinant protein. Pooled elution fractions were concentrated using 50 kDa Amicon tubes, dialyzed against PBS and protein concentration was determined by BCA assay (section 2.4.3).

2.3.3   Enzymatic biotinylation

Proteins having an Avi-tag can be enzymatically biotinylated using the BirA ligase. This enzyme recognizes the 15 amino acid long motif (GLNDIFEAQKIEWHE) and site specifically adds the biotin to the lysine of the sequence. 10 nmol of protein were incubated with 10 x biotin mix A and biotin mix B as well as 2.5 µg of the BirA ligase of the company Avidity at 30 °C overnight. On the next day the mixture is dialyzed in an Amicon 50 kDa to remove the excess biotin and the BirA

ligase with a size of 33.5 kDa. The success of biotinylation is proofed by using an ELISA or Western Blot and detection by streptavidin-HRP. Biotinylated OMGP was used in this study for the affinity purification of patient derived OMGP-specific antibodies, for screening of patients by ELISA and for C1q binding assay.

2.4 Protein analysis

Assessment of quality and concentration of the in house produced proteins is important prior to usage in various assays.

2.4.1 Sodium dodecyl sulfate polyacrylamide gel electrophoresis (SDS-PAGE)

Using SDS-PAGE allows the separation of proteins regarding their molecular weight in an electric field. Samples are incubated with the anionic detergent SDS and migrate therefore to the positive cathode.

Precasted ten or twelve well 4-12 % Bis-Tris gels (Invitrogen) were inserted in Xcell Mini Cell electrophoresis chamber and filled with NuPAGE MOPS SDS running buffer. Sample preparation could be conducted either under reducing or non-reducing conditions to keep disulfide bonds connected. In both cases, samples were diluted 1:4 with NuPAGE LDS sample buffer and only for dissolving these bonds, NuPAGE sample reducing agent containing 50 mM dithiothreitol (DTT) was added 1:10 and samples were boiled at 95 °C for 5 min. As protein marker next to the samples, 10 µl of Novex Sharp pre-stained protein standard were loaded. For 90 min an electric field of 130 V was applied.

To visualize the proteins, gels were soaked with Coomassie staining solution for 15 min at RT, followed by three rounds of 10 min with Coomassie destainer solution. Afterwards gels were transferred into 7 % acetic acid overnight to reduce unspecific background staining. Gels were imaged with digital systems Odyssey Fc from Leica.

2.4.2 Mass spectrometry

The mass spectrometry was carried out by the technician Reinhard Mentele from the Dornmair lab at the LMU. Therefore, the band on a SDS gel of patients' purified antibodies at the height of 150 kDa was cut out from the gel and transferred into 100 µl water. The subsequent steps and analysis were all carried out in the mass spec facility of the LMU.

2.4.3 Bicinchoninic acid assay (BCA)

This assay allows the quantification of purified proteins (BCA kit, Pierce). The photometric test is based on the formation of Cu^{2+} complexes with the peptide bonds and the reduction of it to Cu^+ in an alkaline environment. The assay was carried out according the manufacturer's instruction. The samples were incubated with the reaction mixture at 37 °C for 30 min and subsequently measured at 540 nm. Total protein concentration was calculated by using a bovine serum albumin (BSA) protein standard curve 2000-25 µg/ml.

2.4.4 Endotoxin quantification in protein preparations by LAL assay

The endotoxin/lipopolysaccharide (LPS) quantification was carried out by the technician Heike Rübsamen using limulus amebocyte lysate assay (LAL), regarding the manufacturer's instructions (Pierce Chromogenic Endotoxin Quant Kit). The samples were analyzed in a 96 well plate at 37 °C.

2.4.5 Affinity purification of patient derived OMGP-specific antibodies

The plasma of patients with OMGP-specific antibodies was thawed on a magnet stirrer and slowly an equal volume of saturated ammonium sulfate solution was added until the solution became cloudy. After stirring 1 h at RT the mixture was centrifuged at 4 °C, 8000 g for 30 min. The pellet, containing the precipitated immunoglobulin was dissolved in 30-50 ml PBS and dialyzed in 50 KDa tubes in PBS at 4 °C overnight without stirring. On the next day, PBS was replaced by fresh PBS and the dialysis continued for 48 h with stirring. Subsequently, the material from the tubes was centrifuged at 4 °C, 8000 g for 1 h, filtered with a 0.45 µm filter and diluted 1:10 in solubilization buffer. Meanwhile, 1 ml HiTrap streptavidin HP column (GE Healthcare) was equilibrated with 10 CV of solubilization buffer, followed by the load of 1 mg biotinylated OMGP (section 2.3.3) diluted in the same buffer. Then, the previously prepared immunoglobulin solution was loaded at 4 °C with a flow rate of 0.5 ml/min in rotation overnight onto the column. Afterwards, the column was washed again with 10 CV of solubilization buffer and the OMGP-specific antibodies were eluted with 0.1 M glycine/HCl (pH 3) and immediately neutralized with 1/10 of volume with 1 M Tris/HCl (pH 8). Concentration of eluted antibodies was carried out using 50 KDa Amicons. Then, the purified patient's derived OMGP-specific antibodies were dialyzed against PBS at 4 °C overnight, followed by binding test to OMGP in cell-based assay and ELISA.

2.5 Cell culture

Immortalized cell lines are useful for *in vitro* assays and can be produced in endless amounts using the required conditions. Beside these lines also primary cells from humans, PBMCs, were cultured for this study.

2.5.1 Culturing of immortalized cell lines

HEK293T cells and HeLa cells were cultured in T75/T175 flasks in DMEM supplemented with 10 % FCS and 1 % Penicillin/Streptomycin at 37 °C and 5 % CO_2. Cells were passaged every two days in a ratio of 1:10. First media was removed and cells were washed with PBS, followed by 5 min incubation with 4 ml of Trypsin at 37 °C. Reaction was stopped by adding 6 ml medium and cells were split into a new flask.

For seeding cells in 10, 6 or 3 cm dish, number of living cells was determined by diluting cells 1:10 in 0.05 % trypan blue and count 10 µl in a Neubauer counting chamber. Four big squares were counted and multiplied by the dilution factor as well as 10^4 to get the cell number per 1 ml. Cells were seeded on a plate at a concentration of 2-2.5 x 10^5 cells/ml.

2.5.2 PBMC isolation

Lymphocytes are purified out of human peripheral blood by separating PBMCs from red blood cells and granulocytes. Peripheral blood was withdrawn in EDTA tubes and subsequently diluted 1:2 in PBS in a 50 ml falcon. 15 ml of Pancoll was filled into a new 50 ml falcon and the diluted blood was carefully layered above. This Pancoll gradient medium with a density of 1.077 g/ml allows the separation of a low density population, upper fraction of PBMCs and a higher density fraction, red blood cells and granulocytes, which sink down to the bottom of the tube. Therefore, the gradient was centrifuged for 30 min at 400 g without break of the centrifuge. Afterwards, plasma (yellow most upper fraction) and white PBMCs clumps were collected. Cells were washed thrice in PBS, centrifuged at 400 g for 10 min, counted as described in section 2.5.1 and either directly used in RPMI complete medium or frozen in FCS with 10 % DMSO at -80 °C. In average, 1 x 10^6 PBMCs per 1 ml of blood were obtained. For long term storage PBMCs were transferred into liquid nitrogen. To thaw PBMCs, cells were quickly put in 15 ml of warm RPMI and washed twice with RPMI by centrifugation for 10 min at 400 g. Cells were counted in a Neubauer counting chamber as described in section 2.5.1.

2.6 Immunological methods

2.6.1 Enzyme-linked immunosorbent assay (ELISA)

ELISAs were carried out for testing different hypothesis. The target protein was directly coated on the plates. For testing IgG concentrations the MaxiSorp-ELISA was used, whereas for patients screening for autoantibodies the streptavidin (STV)-ELISA was applied.

a) MaxiSorp-ELISA

For an OMGP ELISA, the protein was directly coated with 1 µg/ml in PBS and 100 µl per 96 well. As control protein BSA was diluted to the same concentration. After incubation at 4 °C overnight on a shaker, the plate was washed four times with 250 µl PBST (0.05 % Tween). The next step, blocking with 200 µl of 3 % BSA in PBST was carried out at RT for 2 h. Plate was washed as mentioned above and incubated with sera 1:100 or primary anti-OMGP with 10 µg/ml for 2h at RT. Afterwards, the secondary antibody, either directly labeled with HRP or biotinylated, was added in 0.5 % BSA in PBST for 1 h at RT. After 4x of additional washing, the plate was incubated for around 15 min with 100 µl TMB substrate. In the meanwhile TMB was oxidized to a blue complex. The reaction was halted by adding 50 µl H_2SO_4 which turns the complex into yellow. The OD was measured at 450 nm and 540 nm for the correction of the plate background.

b) STV-ELISA

The biotinylated OMGP was coated with 1 µg/ml in PBST (0.05 %) in 100 µl per 96 well and incubated for 2 h at RT. The plate was washed four times with 250 µl PBST and sera were diluted 1:100 in PBST and added overnight at 4 °C on a shaker. As positive control, commercial available polyclonal or monoclonal OMGP antibodies were used with 1 µg/ml. On the following day, the plate was washed again as mentioned above and an anti-human-IgG-HRP conjugated antibody was diluted 1:7000 in PBST. Plate was incubated for 1 h at RT, washed again and developed for approx. 10 min with 100 µl of A&B-ELISA detection solution (R&D). Color formation was stopped by adding 50 µl H_2SO_4. The OD was measure at 450 nm and 540 nm.

c) C1q-ELISA

For testing the ability of antibodies activating the complement cascade, a C1q-binding ELISA was carried out. Therefore, a STV plate was coated for 2 h at RT with 1 µg/ml of biotinylated OMGP. The plate was washed four times with 250 µl PBST (0.05%) and sera were diluted 1:100, mAb with 1-10 µg/ml, and incubated overnight at 4 °C on the plate. On the next day, the plate was washed as mentioned above and 5-10 µg of C1q complement was added for 2 h at RT. After an additional washing step, the binding was detected by an anti-C1q-HRP antibody, diluted 1:200 for

30 min at RT. 100 µl TMB substrate were added to the plate after washing again and then the reaction was stopped after 10-15 min by 50 µl H_2SO_4. The OD was measured at 450 nm and 540 nm.

d) IFNγ ELISA upon T cell stimulation

Due to activation of T cells by an antigen binding to their T cell receptor (TCR), they secrete IFNγ into the supernatant. Therefore, 2×10^5 PBMCs were seeded in each 96 well in a volume of 200 µl and stimulated with ConA, tetanus toxoid, measles antigen and OMGP as mentioned above. After seven days of incubation at 37 °C with 5 % CO_2, the supernatant was analyzed using an IFNγ sandwich ELISA.

2.6.2   Western Blot

Prior to the blotting, proteins are separated by size through SDS-PAGE as described in section 2.4.1. For the subsequent detection of proteins by an antibody, they are transferred on a polyvinylidene difluoride (PVDF) membrane. The membrane was activated in methanol and then together with Whatman paper soaked in transfer buffer containing 10 % methanol. The activated membrane was placed on three layers of filter paper and above was the gel from the SDS-PAGE, followed by three more layers of soaked filter paper. Throughout the horizontal blotting for 90 min with 60 mA, the negatively charged proteins migrate to the anode to the membrane. Afterwards the membrane was blocked by incubating 1 h at RT in 5 % milk in PBST (0.05%). Directly labeled antibodies were incubated for 1 h in 5 % milk in PBST, whereas unlabeled primary antibodies at 4 °C overnight. On the next day, the membrane was washed three times for 10 min in PBST and incubated for 1 h at RT with the secondary HRP labeled antibody diluted in 5 % milk in PBST. After washing three times 10 min with PBST, the enhanced chemiluminescence substrate solution (ECL/ECL prime for higher sensitivity) was mixed (50 % solution A + 50 % solution B) and dropped onto the blot. Signals were captured using the digital imaging systems Odyssey Fc from Leica.

2.6.3   Immunofluorescence

For studying the OMGP antigen expression, murine spinal cord and primary hippocampal/cortical neuronal cultures were stained. Furthermore immunofluorescence was carried out to visualize the binding of OMGP autoantibodies to OMGP transfected HeLa cells.

a) Staining of free floating tissue

Spinal cord of C57BL/6J mice was stained for OMGP expression. Surgery and paraformaldehyde fixation was carried out by Aleksandra Mezydlo (lab of Prof. Martin Kerschensteiner). Tissue was transferred for two days in 30 % sucrose for cryoprotection and then spinal cord was cut between Th12-L2. The embedded tissue was sliced sagittal at the cryostat with 55 µm, transferred into 24 well plates and remaining embedding medium was removed by washing three times 10 min in PBS at RT with shaking. Therefore, the wells were filled with PBS and the tissue was carefully transferred with a brush from one well to the other.

To break the methylene bridges, that were formed during PFA fixation and to allow antibodies to bind to antigenic sites, the sections were incubated for 20 min at 80 °C in 10 mM sodium citrate pH 8.5. The tissue was washed as mentioned above and blocked for 1 h at RT in 10 % goat serum in 0.5 % Triton-PBS. After an additional washing procedure, tissue was incubated overnight at 4 °C in a 48 well plate with 300 µl primary antibody diluted in 1 % goat serum in 0.5 % Triton/PBS. On the next day, sections were washed again incubated overnight at 4 °C in a 48 well plate with 300 µl secondary antibody diluted 1:1000 in 1 % goat serum in 0.5 % Triton/PBS. Then the tissue was washed as previously and the nucleus was stained using DAPI 1:10.000 in PBS for 10 min. After washing, sections were mounted with vectashield on slides and sealed with nail polish. Spinal cord was imaged using confocal microscopy.

b) Staining of murine primary hippocampal and cortical neurons

Preparation of neurons was carried out by Dr. Hung-En Hsia (lab of Prof. Stefan Lichtenthaler). Methanol fixed cells on cover slips were blocked for 1 h at RT in PBS containing 5 % sucrose and 10 % FCS. After one night incubation with the primary antibodies, diluted in the blocking buffer, cover slips were washed three times with 200 µl PBS. Secondary antibodies were diluted in blocking buffer and incubated for 1 h at RT and then washed as mentioned previously. The nucleus was stained with DAPI 1:10.000 for 10 min and neurons were washed again with H_2O before they were mounted and sealed on slides. Neurons were imaged using the Leica DFC 300 G microscope.

2.6.4 Cell-based assay – Flow cytometry

Antigens can be detected by fluorescence labeled antibodies in a flow cytometer. For the detection of OMGP autoantibodies, patients' sera and CSF were screened in a cell-based assay and subsequently analyzed with FACSVerse instrument from BD. Therefore, on the first day 2-2.8 x10^6 HeLa cells were seeded in the afternoon in a 10 cm dish. Next morning, HeLa cells were

transfected with 14 µg of pEGFP, pEGFP-OMGP-TM, or pEGFP-OMGP-GPI using 68 µl of Lipofectamine 2000 according to the manufacturer's protocol. After 22-26 h of incubation the transiently transfected cells were removed by washing the plate with ice cold PBS. Cells were counted as described (section 2.5.1) and 5×10^4 cells were transferred in each 96 well (v-bottom shape). From there on, all steps were carried out on ice. Whereas in the entire screening always living non-fixed cells were used, in one experiment cells were fixed for 20 min at RT in 4 % PFA and washed afterwards. To spin down the cells, the plate was centrifuged at 400 g for 5 min at 4 °C and supernatant was removed by quickly inverting the plate. Three rounds of washing were carried out where the cells were resuspended in 150 µl of FACS buffer (1 % FCS in PBS) and centrifuged. Sera were screened 1:50, plasmapheresis material 1:25 and CSF 1:2 diluted in FACS buffer in 100 µl per 96 well for 45 min at 4 °C on a shaker. For verification of the OMGP expression, commercial monoclonal/polyclonal OMGP antibodies were used. After three washing steps as mentioned above, the secondary anti-human-IgG biotinylated antibody was diluted 1:500 in FACS buffer and incubated with 50 µl per 96 well for 30 min at 4 °C shaking. Before streptavidin-alexa647 was added 1:2000 with 50 µl per 96 well for 30 min at 4 °C shaking, the cells were washed again. Death cells were excluded from the analysis by propidium iodide (PI). Therefore, HeLa cells were washed again and resuspended in 100 µl PI diluted 1:2000 in PBS and transferred in small FACS tubes. After analysis at the FACSVerse, data was analyzed using FlowJo software.

The isotype testing of OMGP Abs was carried out as described above, but using 1:50 dilution of secondary Abs: anti-human-IgG1 or anti-human-IgG4 and detected with 1:100 diluted anti-sheep-IgG-alexa647. More subclasses were evaluated by using 1:50 diluted: anti-human-IgG1-4-HRP, or anti-human-IgM-HRP, followed by detection with 1:100 diluted anti-HRP-alexa647.

2.6.5 Stimulation of human peripheral B cells for immunoglobulin secretion

6×10^5 PBMCs of patients were cultured in 24 well plate in RPMI complete medium supplemented with 1000 U/ml IL2 and 2.5 µg/ml of the toll-like receptor (TLR) 7/8-ligand resiquimod (R848) at 37 °C and 5 % CO_2. With this condition it is possible to stimulate 30–40 % of memory B cells secreting approximately 200 ng IgG (Pinna et al., 2009). After eleven days, supernatants were harvested and tested for specific antibody production in cell-based assay and IgG concentration was measured by human IgG ELISA from Mabtech.

2.6.6   Stimulation of human peripheral T cells

Activation of T cells in the presence of an antigen was measured by T cell proliferation or IFNγ cytokine secretion into cell culture supernatant. Therefore, PBMCs of healthy donors and patients were cultured in RPMI complete with FCS/human AB serum or in X-VIVO15 medium.

a) Carboxyfluoresceinsuccinimidylester (CFSE) staining for T cell proliferation analysis

Proliferating cells will take up the CFSE dye and due to cell division the dye is reduced. The more proliferation, the less dye will be seen afterwards in the flow cytometry analysis. 1×10^6 PBMCs/ml were stained with 0.1 µM CFSE for 15 min at 37 °C by diluting 2×10^6 PBMCs 1:2 into the warm 0.2 µM CFSE-PBS staining solution. Staining was quenched to remove unincorporated CFSE by adding same volume of warm media for 5 min at RT. Cells were washed with media and centrifuged for 10 min at 400 g. For stimulation, 1×10^6 stained PBMCs were seeded into 24 well plate and the following antigens were added to different wells: 5 µg/ml ConA, 5 µg/ml tetanus toxoid, 20 µg/ml measles antigen, 50 µg/ml OMGP, and medium only as background control. After an incubation of 3 or 7 days at 37 °C with 5 % CO_2, cells were analyzed by flow cytometry.

b) 5-Ethynyl-2´-deoxyuridine (EdU) staining for T cell proliferation analysis

PBMCs were stimulated without CFSE staining with the conditions mention above and stained (d3/d6) with 10 µM EdU 24 h prior flow cytometry analysis, which was on fourth and seventh day. The intracellular staining procedure on the day of analysis was carried out regarding the manufacturer's protocol. Due to high proliferation, cells will incorporate more dye into the DNA and can be distinguished thereby from non-activated or less responsive cells.

2.6.7   FluoroSpot assay

The coupling of the antigen to the beads and the LPS removal by NaOH washing, was carried out by Mattias Bronge (lab of Prof. Hans Grönlund), as described previously by their group (Bronge et al., 2019b).

Precoated 96 well FluoroSpot plates (FSP-011803, Mabtech) were washed three times with 200 µl sterile PBS and blocked for 2 h at RT with 200 µl RPMI complete. 2.5×10^5 PBMCs in 100 µl were seeded in each well and stimulated in duplicates with CMV-beads, which are coated with antigenic peptides from cytomegalovirus (Bronge et al., 2019a), negative empty control beads, Avi-His-tag coupled beads or OMGP beads. These beads were either washed with 0.01 M or 0.1 M NaOH before. For CD3 stimulation wells only 1.25×10^5 PBMCs in 100 µl were seeded and stimulated with 10 ng/ml with anti-CD3 from the kit.

The bead preparation was carried out in a master plate where stocks were diluted in RPMI to reduce the possibility of beads sticking to plastic. These diluted beads were then transferred to the cells, to have a final concentration of around 10 beads/cell. Wells were filled with 100 µl RPMI to a total volume of 200 µl. Plates were incubated for 44 h at 37 °C with 5% of CO_2.

FluoroSpot assay was developed according the manufacturer's protocol and spot forming units (SFUs) of plates were analyzed by IRIS reader (Mabtech).

2.7 Animal experiments

Dr. Naoto Kawakami performed the experiments in a Lewis rat model. OMGP-specific T cell lines were generated by injecting the in house produced hOMGP. T_{OMGP}/T_{MBP}/ T_{OVA} cells were expanded and maintained by Dr. Kawakami. For the experimental autoimmune encephalitis (EAE) model, 10 x 10^6 T_{OMGP}, 15 x 10^6 T_{OVA} or 1.1 x 10^6 T_{MBP} cells were injected intravenously (i.v.) in the tail of the rats (Figure 2.6).
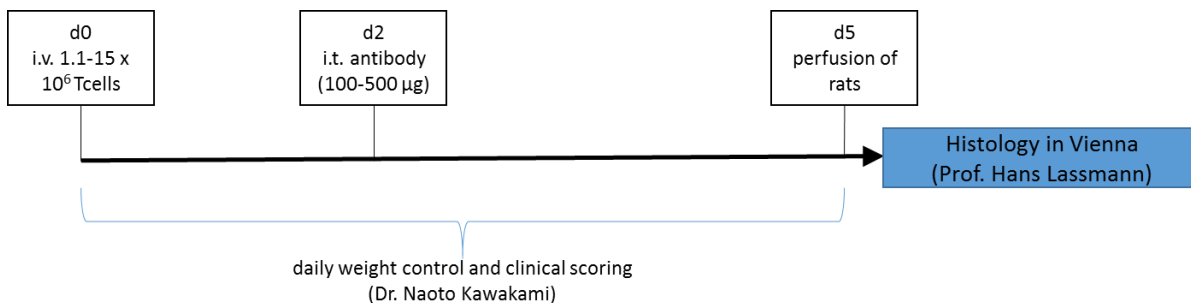
Figure 2.6 Scheme for EAE animal experiments in Lewis rats

The figure illustrates the procedure for the T cell transfer experiments. On day zero the intravenous (i.v.) injection of T cells into the tail vein, day two the intrathecal (i.t.) injection of antibodies and on day five rats were sacrificed, perfused and sent for histological analysis to Vienna.

Every day the body weights and the clinical score of the animals were evaluated (

Table 2-18). Two days after the injection of the T cells, 500 µg of the following antibodies were injected intrathecal (i.t.): 14A9-rIgG2B, 31A4-mIgG2B, 22H6-rIgG2A, 22H6-hIgG1, 8-18C5-hIgG1, IvIg and isotype controls respectively. Three days after antibody injection, rats were sacrificed and perfused with 4 % PFA in PBS. The brain and spinal cord were then postfixed with 4 % PFA in PBS at 4 °C. For neuropathological analysis the material was sent to Prof. Hans Lassmann to the medical university of Vienna.

Table 2-18 Scoring scale for EAE

Score	Clinical symptoms
0	no detectable signs
0.5	loss of tail tonus
1	tail paralysis
2	gait disturbance
3	hind-limb paralysis
4	fore-limb paralysis
5	death

2.8   Statistical analysis

Prism software from GraphPad was used for statistical analysis. For the identification of statistical differences, spearman correlation analysis were carried out. The data is represented as mean ± standard deviation (SD) or standard error of the mean (SEM). P-values ≤0.05 were considered significant (* p≤0.05; ** p≤0.01; *** p≤0.001).

3. RESULTS

3.1 Detection of autoantibodies by cell-based assays

In the laboratory of Prof. Edgar Meinl, autoantibodies in the serum and CSF of patients are screened by using cell-based assays. These assays were already established for other autoantigens of the CNS like MOG CBA (Spadaro and Meinl, 2016), neurofascin CBA (Ng et al., 2012), aquaporin-4 (AQP-4) IF assay (Mader et al., 2010) and others, but not for OMGP so far.

3.1.1 Development of OMGP-TM and OMGP-GPI cell-based assays

The first aim of this study was to develop an assay where patients' sera can be screened for autoantibodies against the OMGP protein. Therefore, the transient transfection efficiency of HeLa and HEK293T cells was compared. By using Lipofectamine 2000 the best transfection rate could be obtained with the HeLa cell line (Figure 3.1), where 19.1 % of the cells expressed the human OMGP-TM-EGFP (transmembrane anchored variant, which is explained later) fusion protein on the surface and 80.9 % of the cells were EGFP negative. The transfection of HEK293T cells resulted only in a portion of 7.92 % OMGP positive cells, which is around 60 % less effective than with HeLa cells.
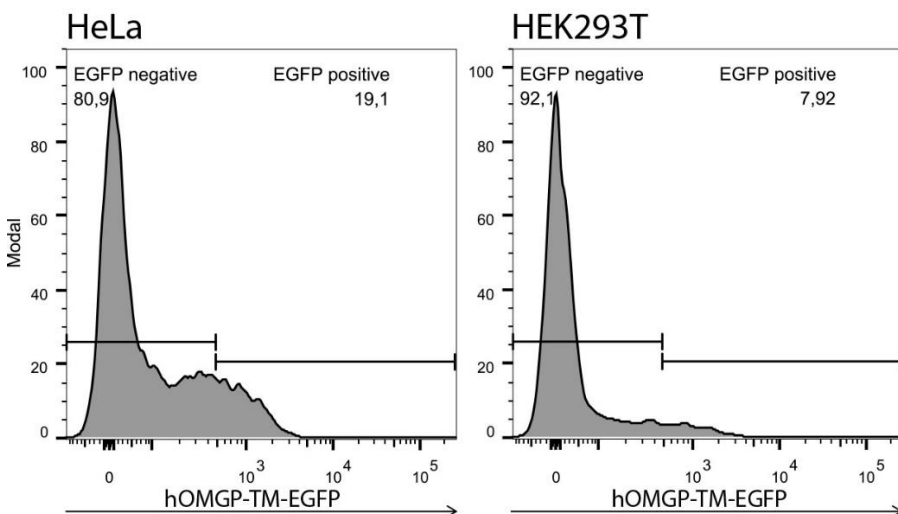

Figure 3.1 Comparison of transfection efficiencies between HeLa and HEK293T cell lines

The x-axis indicates the EGFP fluorescence intensity. In the left graph HeLa cells were transfected with hOMGP-TM-EGFP, whereas on the right side HEK293T cells are displayed. EGFP positive cells are above the fluorescence intensity of 500 and <500 the cells are EGFP negative.

As threshold for positive transfection, the gate is set on cells with fluorescence intensity >500. Regarding this result the screening for autoantibodies against OMGP in patients (chapter 3.2) was conducted with transient transfected HeLa cells. Due to the transient transfection, the efficiency of OMGP-EGFP positive cells can vary from 15-40 %. In this thesis, the term OMGP-TM and OMGP-GPI always describes the human variant of the protein. If the mouse variant is used it is indicated as mOMGP, whereas for the rat as rOMGP.

To detect autoantibodies in the serum of patients, two cell-based assays were established. In the first OMGP was transiently expressed as transmembrane variant by fusing OMGP to the membrane spanning part of CD80 (OMGP-TM) and also fused to EGFP. In the second assay OMGP was expressed like *in vivo* with a GPI-anchor (OMGP-GPI) on the cell membrane and not fused to EGFP, since the construct harbors the ribosome skipping element T2A (Figure 2.4). With this, out of one mRNA two proteins, OMGP-GPI and cytosolic EGFP are translated which was verified by Western blot (Figure 3.2). OMGP-TM and OMGP-GPI were detected by monoclonal anti-OMGP (Figure 3.2, A) in transiently transfected cell lines HEK293T and HEK293S. The HEK293S is a special variant by having a knock out in the gene of N-acetylglucosaminyltransferase I (GnT1). This leads to less glycosylation of proteins which is detectable in the visible size shift in the blot. OMGP has around 105 kDa (Mikol et al., 1990a) and is larger in the OMGP-TM variant because it is fused to EGFP. OMGP-GPI band in HEK293T is at 105 kDa, since the EGFP is cut due to the successful ribosome skipping.

The detection of the OMGP proteins with an anti-GFP mAb (Figure 3.2, B) is still visible in the OMGP-TM variant due to the direct fusion to EGFP. Several bands appear, which represents incomplete produced protein fragments. For the OMGP-GPI construct the antibody detected only EGFP with 30 kDa because of the separation of the two proteins. Recombinant OMGP was not fused to EGFP and therefore is not detected by the antibody.
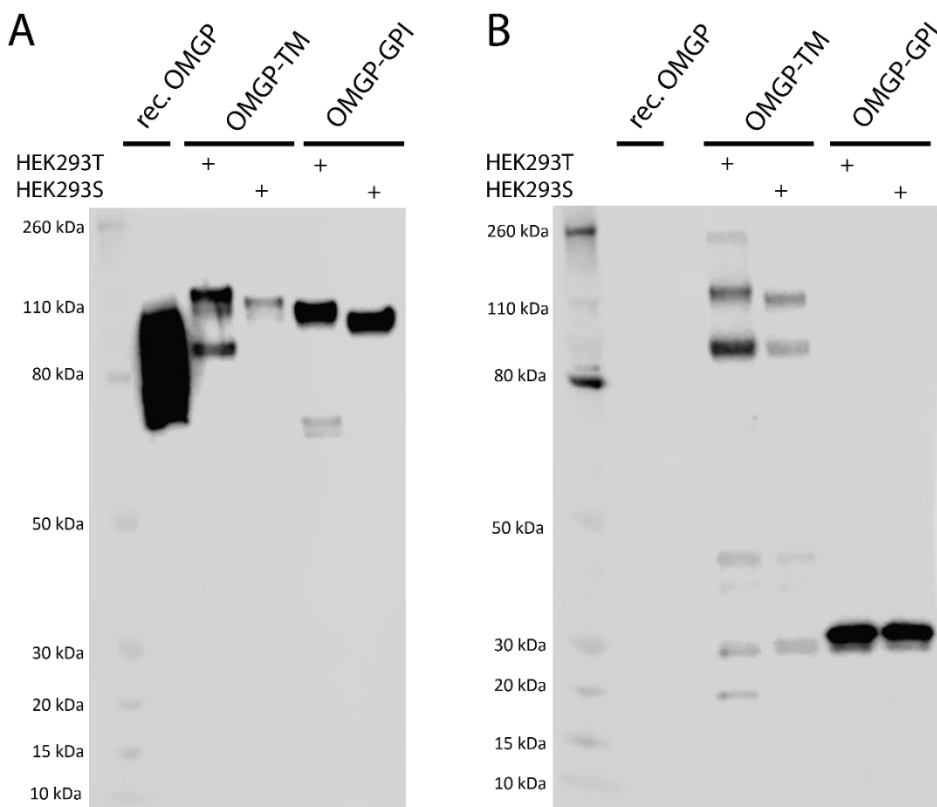
Figure 3.2 WB of OMGP-TM and OMGP-GPI constructs expressed in two HEK cell lines

HEK293T or HEK293S (with N-acetylglucosaminyltransferase I (GnT1) knock out) transfected cell lysates were loaded on SDS gel and Western blot was developed with mAb anti-OMGP (A) or anti-GFP (B). As positive control for anti-OMGP detection, recombinantly produced OMGP was loaded in the first lane next to the standard.

In the next step, the correct expression of OMGP on the surface of the cells was verified by using a commercial monoclonal and polyclonal antibody (Figure 3.3). In the dot blot, grey represents the antibody binding on EGFP-, blue on OMGP-TM-EGFP and orange on EGFP-OMGP-GPI-transfected cells. Two different methods were used for the evaluation of antibody binding. For the OMGP-TM mean fluorescence intensity ratio is calculated by dividing mean fluorescence intensity (MFI) from cells above the EGFP fluorescence intensity >500. Therefore for MAB1674 antibody the MFI of 911 of OMGP-TM is divided by the background MFI of 1.9 of EGFP cells. This results in a MFI ratio of 479.47 (Figure 3.3, upper row). The analysis for antibodies binding to the OMGP-GPI construct is evaluated by ΔMFI values and for this purpose the horizontal line is adjusted to the background control (grey blot, EGFP control cells). To calculate the binding of MAB1674, the percentage of cells in the Q2 gate of EGFP (0.63 %) is subtracted from the number in Q2 gate of OMGP-GPI cells (orange dot plot, 23.6 %) resulting in ΔQ2 of 22.97 %. In the same way it is done for the polyclonal antibody AF1674 (Figure 3.3 , lower row). The OMGP-TM MFI ratio results in 1390/68.8 = 20.2, whereas ΔQ2 for OMGP-GPI is 26.3-2.28 % = 24.02 %.
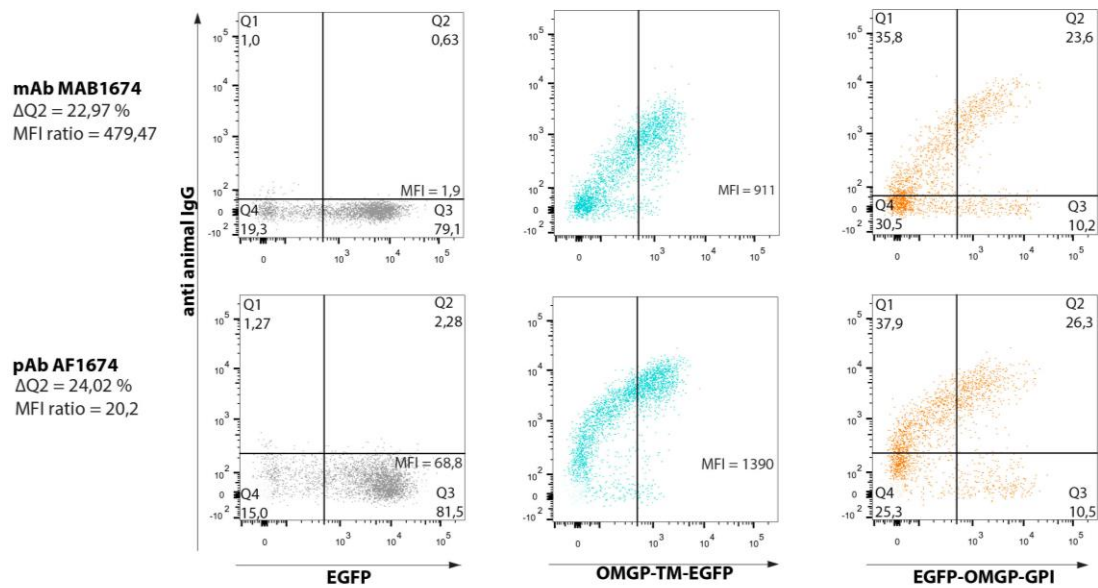
Figure 3.3 Detection of OMGP by mAb MAB1674 and pAb AF1674

Hela cells were transiently transfected with the constructs indicated on the x-axis and then stained with two OMGP-specific Abs. Dot plots represent the evaluation of commercial available monoclonal MAB1674 and polyclonal AF1674 antibody on EGFP (grey), OMGP-TM-EGFP (blue), EFGP-OMGP-GPI (orange) transfected cells. Vertical line is set to fluorescence intensity 500 and MFI values are calculated >500. For OMGP-TM, the MFI ratio by dividing the OMGP-TM MFI by EGFP MFI is calculated. For OMGP-GPI, the ΔQ2 is calculated by subtraction of EGFP from OMGP-GPI Q2 percentage. Therefore, the horizontal line is adjusted to the background control (EGFP, grey blot).

By using these commercial antibodies which result in high MFI ratios for OMGP-TM (479.47 for MAB1674, 20.2 for AF1674) and high ΔQ2 values for OMGP-GPI (22.97 % for MAB1674, 24.02 % for AF1674) it was proofed, that these cells express OMGP on their surface. Therefore, these assays could be used for autoantibody screening in the sera and CSF of patients. The following chapter describes how this CBA was optimized and the sensitivity of antibody detection could be increased.

3.1.2 Optimization of CBA

For MOG CBA established in the lab of Prof. Edgar Meinl, the HeLa cells are removed for the screening of autoantibodies by a short trypsin digest. This method on OMGP transfected cells cut quickly a lot of transfected protein from the surface, since OMGP has 33 predicted recognition sites (Table 3-1) for the trypsin enzyme (ExPASy PeptideCutter tool).

Table 3-1 Position and number of Trypsin cleavage sites within OMGP

Name of enzyme	No. of cleavages	Positions of cleavage sites
Trypsin	33	**7** (100%) **35** (100%) **37** (100%) **44** (100%) **81** (100%) **89** (100%) **99** (100%) **112** (100%) **116** (100%) **126** (100%) **132** (100%) **137** (95.7%) **142** (89.7%) **146** (100%) **157** (95.3%) **168** (100%) **202** (91.4%) **226** (100%) **232** (100%) **240** (100%) **246** (100%) **262** (92.8%) **299** (100%) **302** (100%) **305** (64.2%) **308** (100%) **310** (90.9%) **320** (86.7%) **329** (92.8%) **372** (100%) **404** (100%) **412** (100%) **423** (100%)

An alternative method for removing adherent cells is by incubating them instead of trypsin in EDTA solution. This was done for OMGP and EGFP transfected cells in comparison of 10 min, 6 min trypsin digest and 0.5 mM EDTA (Figure 3.4). It was demonstrated that trypsin cuts within 6-10 min high levels of OMGP from the surface, since with serum of a patient having OMGP antibodies (2492) the detection signal diminished (MFI ratio 2.1 for 10 min and 1.9 for 6 min). If the transfected HeLa cells were removed by 0.5 mM EDTA, no OMGP was shed from the surface and the higher MFI ratio of five is measured. The same effect was also noticeable by detecting OMGP with the commercial MAB1674. This antibody is a purified monoclonal and still detected the small amounts of OMGP on the surface, no matter if cells were incubated 6 min or 10 min with trypsin, the MFI ratio of 27.8 is comparable to 32.5. But the MFI ratio of 151.2 is much higher when the EDTA removal was used, which shows again that there is much more OMGP available on the surface. This effect was seen to a greater extend for the detection of the OMGP autoantibodies within patients' sera, because the concentration and the affinity of these antibodies is much less than the commercial antibody. In this way the CBA could be improved by using an alternative cell removal with 0.5 mM EDTA or then furthermore cold PBS removal was developed. By flushing down the cells with cold PBS the outcome was the same and it is even less manipulation on the cells.
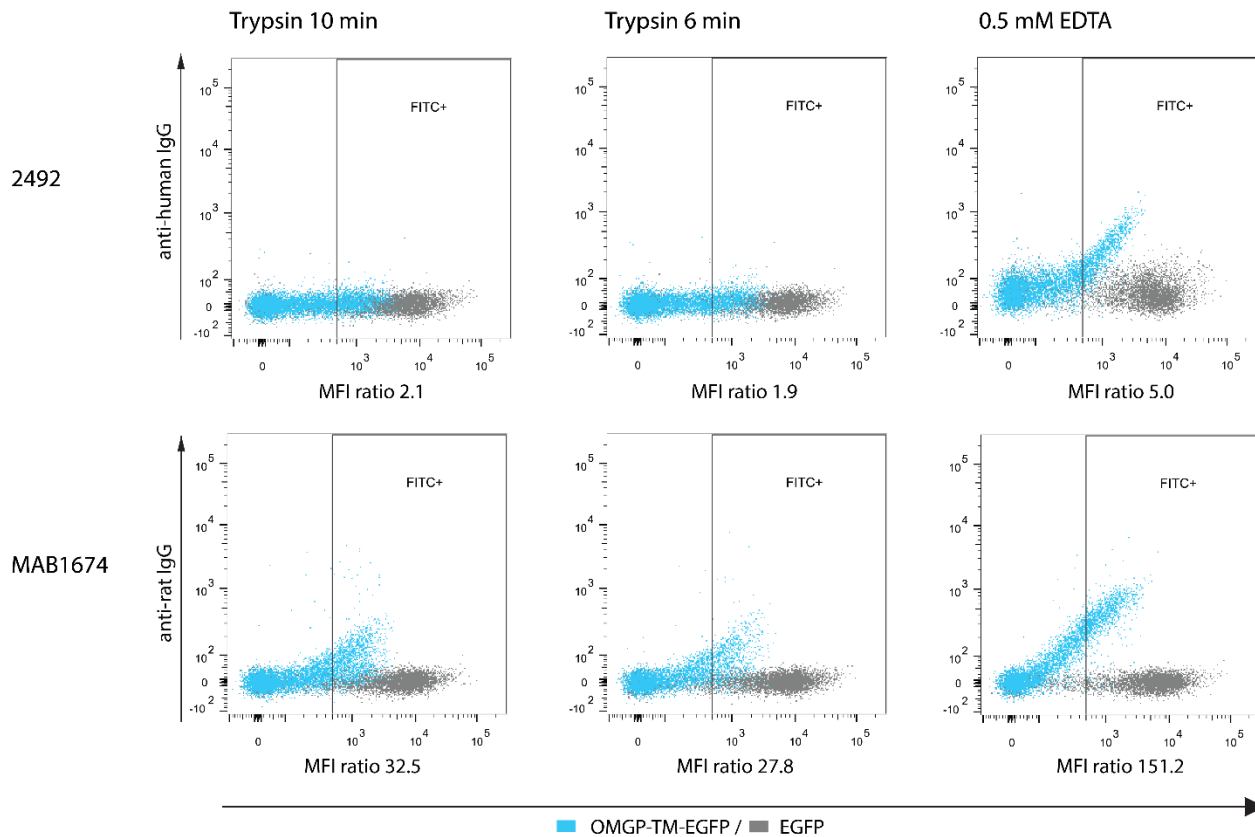
Figure 3.4 Effect of trypsin or EDTA treatment on OMGP transfected HeLa cells

HeLa cells were transfected either with EGFP (grey) or OMGP-TM-EGFP (blue) and the surface expression of OMGP was detected by a patient having OMGP autoantibodies (2492) or the commercial monoclonal antibody (MAB1674). The variation of the detection was compared by using 10 min, 6 min of trypsin digest or 0.5 mM EDTA for removal of the transfected adherent HeLa cells. MFI ratios are indicated below each dot plot.

Additionally, the sensitivity of rare autoantibody detection in patients' sera could be improved by using a biotinylated secondary antibody followed by incubation with streptavidin-alexa647 dye. This amplification of the signal in Figure 3.5 was compared to an anti-human-IgG antibody directly labeled with alexa647. Patient PPH035 had a MFI ratio of 2.7 for the detection with a directly labeled one, whereas by amplification of the signal with the biotin-streptavidin system the MFI ratio increased to 20.3. Additionally, the same effect but less imposing was seen with the serum of patient 1913, where the MFI ratio increased from 3.7 with the directly labeled antibody to 3.9 by using the biotinylated secondary antibody. Moreover, the incubation time of the staining can be carried out on a shaker in the cold room and not only in standing tubes on ice. This lead also to an improvement of detection, which was seen in the increase of the MFI ratio from 3.9 to 10.8 in patient 1913. For patient PPH035 shaking during incubation time didn't had this effect since the MFI ratio of 11.4 was even a bit lower, than in the non-shaking condition with 20.3.
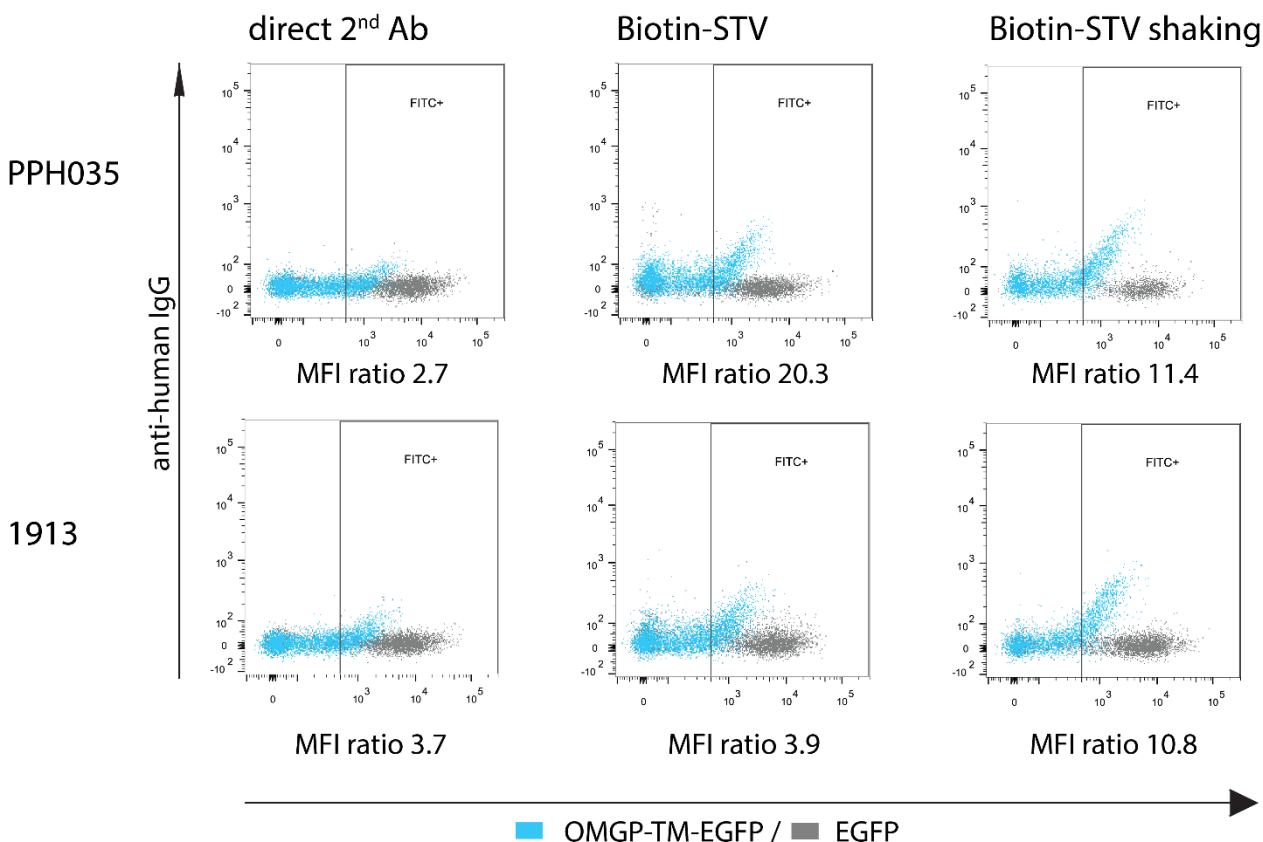
Figure 3.5 Increased sensitivity of autoantibody detection in CBA by using Biotin-STV system

Two different patients with autoantibodies against OMGP were compared for the detection using a directly labeled (direct 2nd Ab) or a biotinylated secondary antibody followed by incubation with a streptavidin coupled fluorophore (Biotin-STV). In the last column (Biotin-STV shaking), the staining was carried out on a shaker in the cold room during the incubation time, whereas for the other conditions it was done in a usual non-shaking condition on ice. The patient PPH035 displays plasmapheresis material, while patient 1913 is a serum sample. MFI ratios are indicated under each single dot plot.

The CBA for MOG autoantibody screening is conducted with living HeLa cells and therefore the OMGP cell-based assay was also tested for using living or fixed cells. Figure 3.6 illustrates the effect of autoantibody binding from two patients (1913, 2492) and two commercial antibodies (AF1674, MAB1674) to paraformaldehyde fixed or non-fixed cells expressing OMGP on their surface. If the cells were fixed, the autoantibody binding to OMGP was completely abolished in patient 1913 with a MFI ratio of 1.0 compared to non-fixed with 4.7. For patient 2492 it decreased similarly from a MFI ratio of 7.8 in living cells to 1.1 in fixed cells.
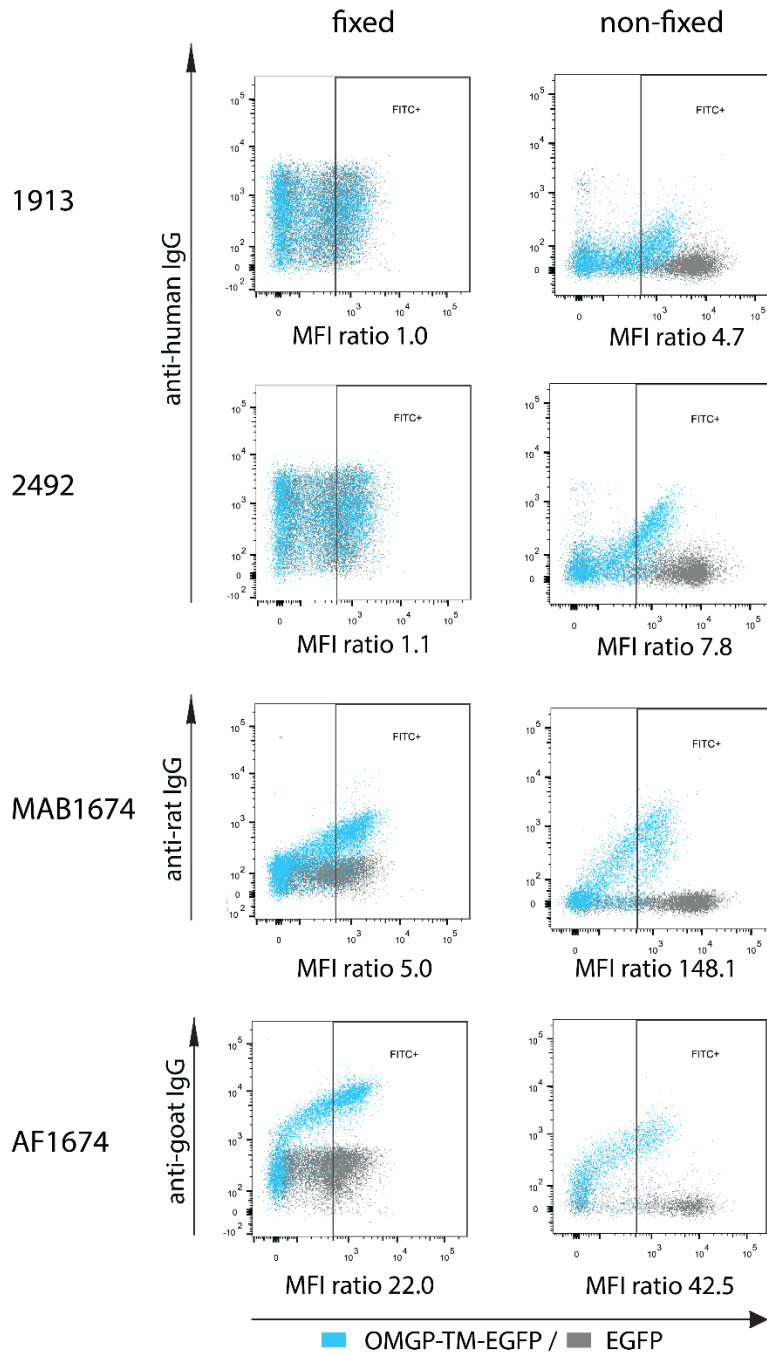
Figure 3.6 Effect of fixation on transfected HeLa cells for screening of autoantibodies in CBA

The dot plots illustrate the antibody binding of two commercial antibodies (MAB1674, AF1674) and two autoantibody positive patients' sera (1913, 2492) to OMGP-TM-EGFP (blue) and EGFP (grey) transfected cells. The right column demonstrates the antibody binding to living non-fixed HeLa cells and the left column to PFA fixed HeLa cells.

Also the binding of the monoclonal antibody MAB1674 to OMGP was decreased due to fixation from a ratio of 148.1 in non-fixed cells to 5.0 in the fixed condition. The least affected polyclonal antibody AF1674 showed the same trend also with a higher MFI ratio of 42.5 in non-fixed

compared to 22.0 in fixed cells. All sera with autoantibodies and commercial antibodies showed that due to fixation the antigen can no longer be recognized as good as on living cells, since the epitopes got destructed. Therefore, the CBA was carried out on non-fixed living HeLa cells expressing OMGP on their surface.

The CBA for OMGP autoantibody screening was established similar to the MOG assay, where sera are screened on living HeLa cells expressing the antigen transiently expressed on their surface (Spadaro and Meinl, 2016). Furthermore, the sensitivity of detection could be increased, by using the biotin-streptavidin amplified signal and an incubation of the staining on a shaker. While in the MOG assay, cells are removed by a short trypsin treatment, in OMGP CBA cells were flushed down with cold PBS.

3.2 CBA screening for autoantibodies against OMGP-TM and OMGP-GPI

In total 675 samples, coming from three different centers, were analyzed for OMGP autoantibodies. The pediatric ADEM cohort is kindly provided by Prof. Amit Bar-Or (currently University of Pennsylvania), MS and OND/OIND cohort from Prof. Tomas Olsson (Karolinska Institute in Stockholm), patients with GAD Abs, MS/CIS and MS twin cohorts from the Institute of Clinical Neuroimmunology LMU (Prof. Tania Kümpfel and colleagues).

The raw data of the screening of 675 sera and 14 plasmapheresis samples are demonstrated in Figure 3.7. The quantification of the data was carried out as described in Figure 3.3.
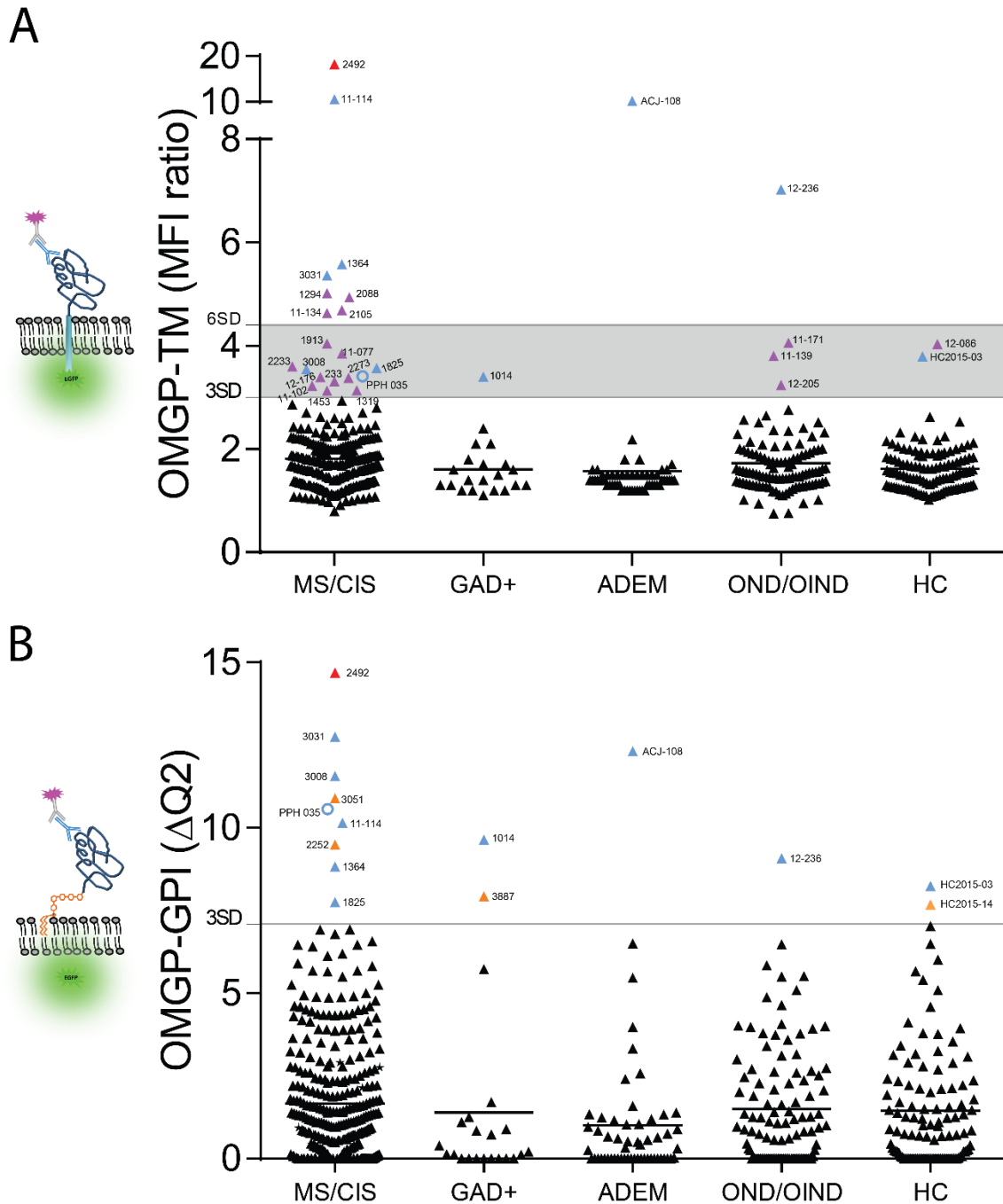
Figure 3.7 CBAs for OMGP autoantibody screening

The graphs show the results of the autoantibody screening for two different OMGP anchored constructs. (A) For OMGP-TM, six cohorts were tested: MC/CIS (n=376), patients having glutamic acid decarboxylase autoantibodies (GAD+, n=22), children with acute disseminated encephalomyelitis (ADEM, n=56), other neurological diseases (OND) or other inflammatory neurological diseases (OIND, n=107), healthy controls (HC, n=114) and 37 twin pairs, discordant for MS. (B) OMGP-GPI was analyzed within the same cohorts, except the MS twins. Red triangle marks highest positive index patient (mean value of 30 measurements as daily control in each assay), blue symbols are subjects positive for OMGP-TM[+] and OMGP-GPI[+], purple for OMGP-TM[+]/OMGP-GPI[-], orange for OMGP-TM[-]/OMGP-GPI[+]. Beside sera, this figure also includes measurements of 14 plasmapheresis samples (open circle), whereas only one above the cutoff is visible. The horizontal lines indicate the thresholds in each graph and are calculated by mean value of HCs plus three/six times SDs (OMGP-TM lower cutoff 3.0, higher cutoff 4.4 and OMGP-GPI cutoff 7.1). 104 HCs were measured twice, ten HCs samples coming from the Swedish cohort were analyzed once. Positive sample values are included as mean of minimum two replicates.

The 104 sera from the Munich HC cohort were analyzed twice, 10 HCs from the Swedish cohort once. Positive samples above 3 SDs of the healthy control group, were analyzed at least twice. The index patient 2492 is represented as mean of 30 measurements. The coefficient of variation in the replicates is in average for the OMGP-TM 0.27 and therefore more precise than for OMGP-GPI with 0.39, which indicates, that OMGP-GPI has a greater level of dispersion around the mean.

Looking at the original data, it is evident that there are few clearly positive patients, while the vast majority is negative. Further, there is a gray zone and the classification of these patients depends on the threshold. In general, a low threshold results in false positive and a high threshold in false negative classifications. For both assays, OMGP-TM (Figure 3.7, A) and OMGP-GPI (Figure 3.7, B), the cutoff is calculated from 114 HCs. In Figure 3.7A and B, a low (mean of HCs + 3SDs) and additionally a high threshold (mean of HCs + 6 SDs) is indicated in Figure 3.7A. For 3 SDs, this results for OMGP-TM in a MFI ratio of 3.0 and for OMGP-GPI in 7.1 % of ΔQ2. For 6 SDs in OMGP-TM, this results in a MFI ratio of 4.4. This consideration indicates that a threshold of mean + 6SDs is meaningful for the OMGP-TM construct, but appears to be too stringent for OMGP-GPI, since the signal to noise ratio is better in the OMGP-TM, than in the OMGP-GPI assay.

Six different cohorts were included in the screening. When considering the less stringent cut-off, the highest frequency with 5.3 % (20/376) of OMGP-TM antibodies was seen in the MS/CIS cohort. These positive patients have all MS and some in addition NMOSD or ON. This number was reduced to 2.4 % in the same cohort, when analyzed on OMGP-GPI, which shows the differences in those two cell-based assays. The blue symbol in the graph show subjects double positive for OMGP-TM[+] and OMGP-GPI[+], purple for OMGP-TM[+]/OMGP-GPI[-] and orange for OMGP-TM[-]/OMGP-GPI[+]. The patients with the highest reactivity were positive in both assays (2492 index patient red triangle, 11-114, 1364, 3031, 3008, PPH035, 1825), whereas the intermediate patients were only positive in either OMGP-TM or OMGP-GPI assay. Combining both assays result in 5.9 % (22/376) of MS/CIS patients having autoantibodies against the human OMGP protein. Comparing this number to 1.8 % in healthy donors, the appearance of these autoantibodies in MS patients is three times higher.

Another patient cohort having autoantibodies against glutamic acid decarboxylase, had in addition with 4.5 % antibodies against OMGP-TM and with 9.1 % against OMGP-GPI. These two patients are diagnosed with limbic encephalitis or cerebellar syndrome. Pediatric patients with ADEM showed a frequency of 1.8 % autoreactivity towards OMGP. In OND/OIND group, 3.7 % off patients had antibodies to OMGP-TM and only 0.9 % to OMGP-GPI. These four patients are diagnosed with psychosis, paresthesia, neurosarcoidosis or SLE.

Concluding these findings, MS/CIS patients had with a frequency of 5.9 % a three times higher appearance of autoantibodies than healthy donors with a frequency of 1.8 %.

When considering the stringent cutoff of mean + 6SDs (Figure 3.7, A), then 2.1 % of MS, one patient with a psychosis and one child with ADEM would score positive. Thus, the conclusion would be the same: antibodies to OMGP are detected in serum of a few percent of MS patients.
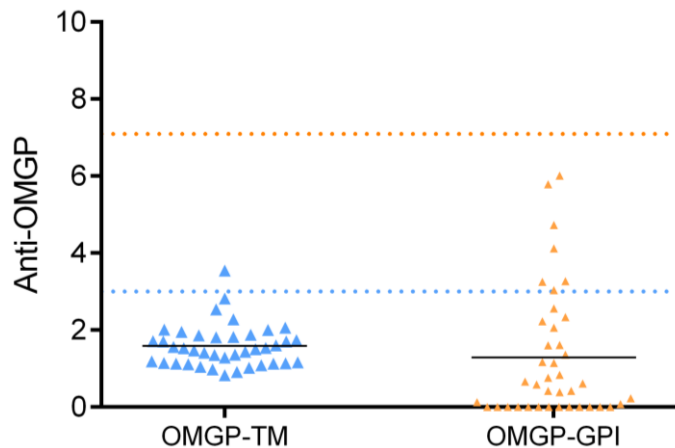
Figure 3.8 Autoantibody screening in CSF

CSFs from 42 MS patients were analyzed either on OMGP-TM (blue) or on OMGP-GPI (orange) transfected cells. The dotted horizontal line indicates the 3SDs-cutoff, calculated with sera for the different OMGP variants. OMGP-TM is represented as MFI ratio, whereas OMGP-GPI as ΔQ2.

Next, the presence of antibodies to OMGP was analyzed in the CSF. To this end, a total of 42 CSF samples from MS patients were screened with both OMGP-TM and OMGP-GPI (Figure 3.8). For the analysis of the CSF data, the HCs' sera cutoff was applied, which might be too harsh for this diluted body fluid. But still one patient had antibodies to OMGP and appeared in the OMGP-TM CBA above the cutoff. However, the signal is relatively low. Thus, while in a few patients autoantibodies to OMGP could be clearly detected in serum, anti-OMGP reactivity in CSF is low. From none of donors with antibodies to OMGP in serum, CSF was available.

3.3 IgG1 as main subclass of OMGP autoantibodies in patients

The screening for OMGP autoantibodies was conducted for all IgG isotypes by using an anti-human-IgG Fcγ fragment specific antibody. To analyze the subclasses by flow cytometry, seven different IgG1 and four IgG2/IgG3/IgG4 secondary antibodies (Table 2-11) were tested. None of those gave a signal for the OMGP seropositive patients. In Figure 3.9 (A) one series of isotyping

antibodies is illustrated, where the index patient 2492 was analyzed in OMGP-GPI CBA for the subclasses, by using anti-human-IgG-HRP or anti-IgM/IgG1-4 antibodies for detection. The staining of those subclass antibodies was carried out by an anti-HRP-alexa647. Although a clear signal with anti-IgG is visible, the IgG subtype secondary Abs are just indicative for an OMGP-specific IgG1 and IgG4 response.

Another antibody specific for IgG1 detection is shown in Figure 3.9 (B). This also gave a strong signal for one patient having MOG antibodies in the MOG CBA, where it serves as positive control. Although the function of this secondary antibody was proofed by the detection of IgG1 in MOG seropositive patient, there was no signal for the index patient with OMGP autoantibodies.

Since the identification of the isotype of the anti-OMGP response was not clear, another isotype-specific Ab from "The Binding Site", which was also used in another study (van Sonderen et al., 2016) was tested (Figure 3.9, C).
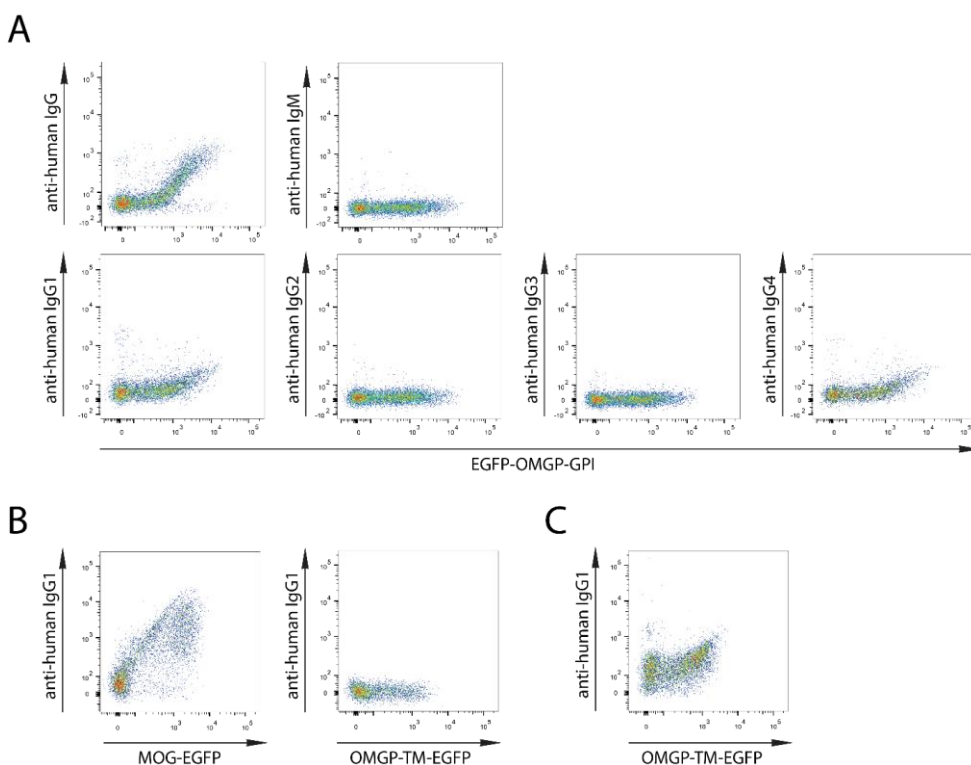
Figure 3.9 Comparison of isotype specific antibodies

(A) The serum of the index patient 2492 was analyzed in OMGP-GPI CBA with anti-IgG-HRP and subclass antibodies (anti-IgG1-4-HRP, anti-IgM-HRP), followed by an incubation with anti-HRP-alexa647 detection antibody. (B) To proof the function of another anti-human-IgG1 antibody (abcam), a MOG-IgG1 seropositive patient was tested. This antibody didn't give a signal for OMGP seropositive index patient tested by OMGP-TM CBA. (C) Only one primary anti-human-IgG1 antibody from "The Binding Site" was detecting IgG1 isotype in patients with OMGP autoantibodies, displayed here for the index patient.

This anti-human-IgG1 is the only antibody, which detected the IgG1 subclass in some OMGP seropositive patients. Regarding the positive result, this anti-human-IgG1 and anti-human-IgG4 of the same company were then used for the isotype screening. Using the lower cutoff, out of 29 positive patients, ten were identified having IgG1 isotype and none IgG4 autoantibodies. In the OMGP-TM positive cohort, out of 26 patients in 38 % of patients IgG1 was determinable, whereas in OMGP-GPI CBA out of 13 patients 23 % had detectable IgG1 autoantibodies. In 62 % for OMGP-TM CBA and 77 % for OMGP-GPI CBA no isotype could be analyzed. Considering the stringent cutoff, the nine positive patients are displayed in Figure 3.10, whereas the tenth patient (index 2492) is described in detail in section 3.9.
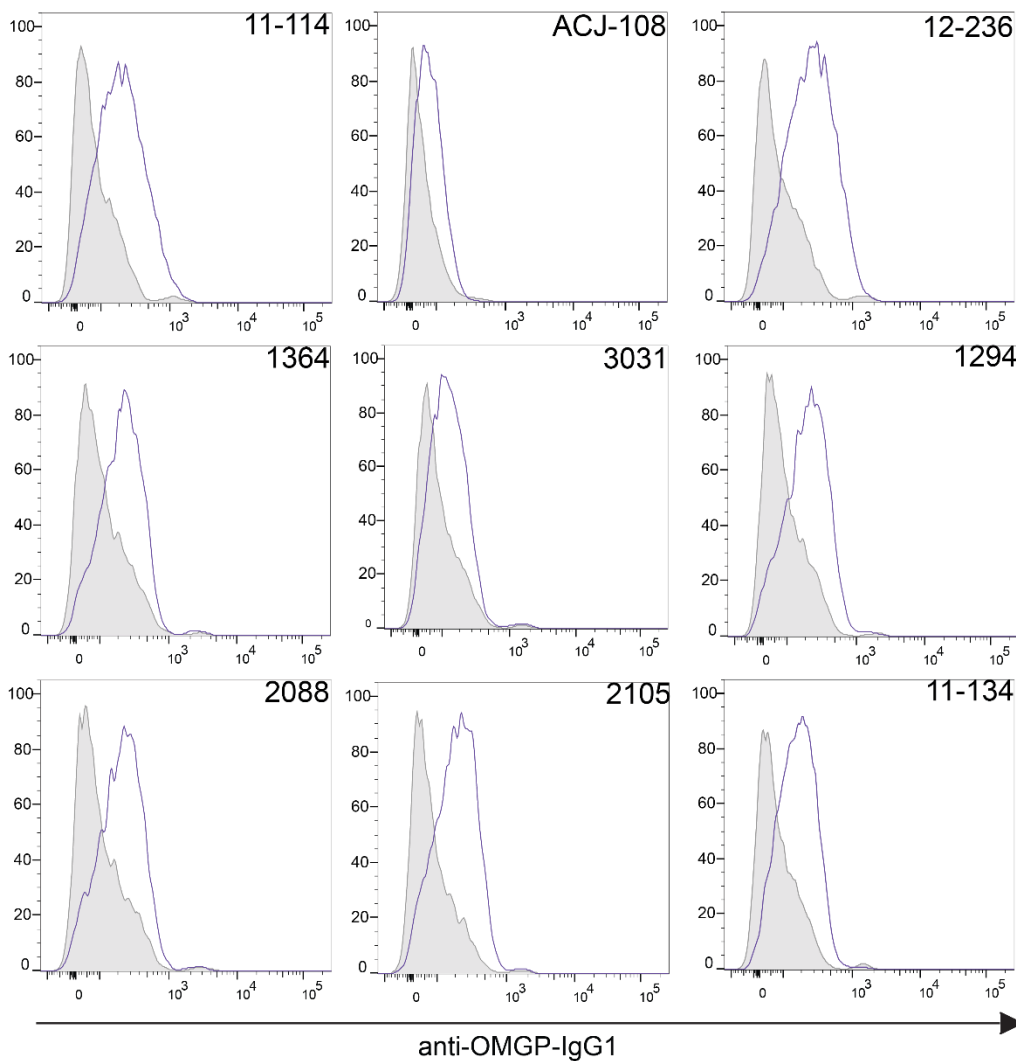

Figure 3.10 Overview of IgG1 isotype in OMGP seropositive patients

OMGP-TM CBA shows identification of IgG1 subclass in OMGP IgG seropositive patients. Grey Histograms represent background of EFGP transfected cells, whereas purple histogram represent antibody binding to OMGP-TM transfected cells.

3.4 Long-term persistence of OMGP autoantibodies in the serum of patients

Longitudinal samples were available from eleven patients, from which five had only one follow up sample and six could be analyzed in 3-7 time points. The highly reactive index patient 2492, who showed persistent Abs to OMGP, is discussed in detail in section 3.9. The other five longitudinal courses are illustrated in Figure 3.11.
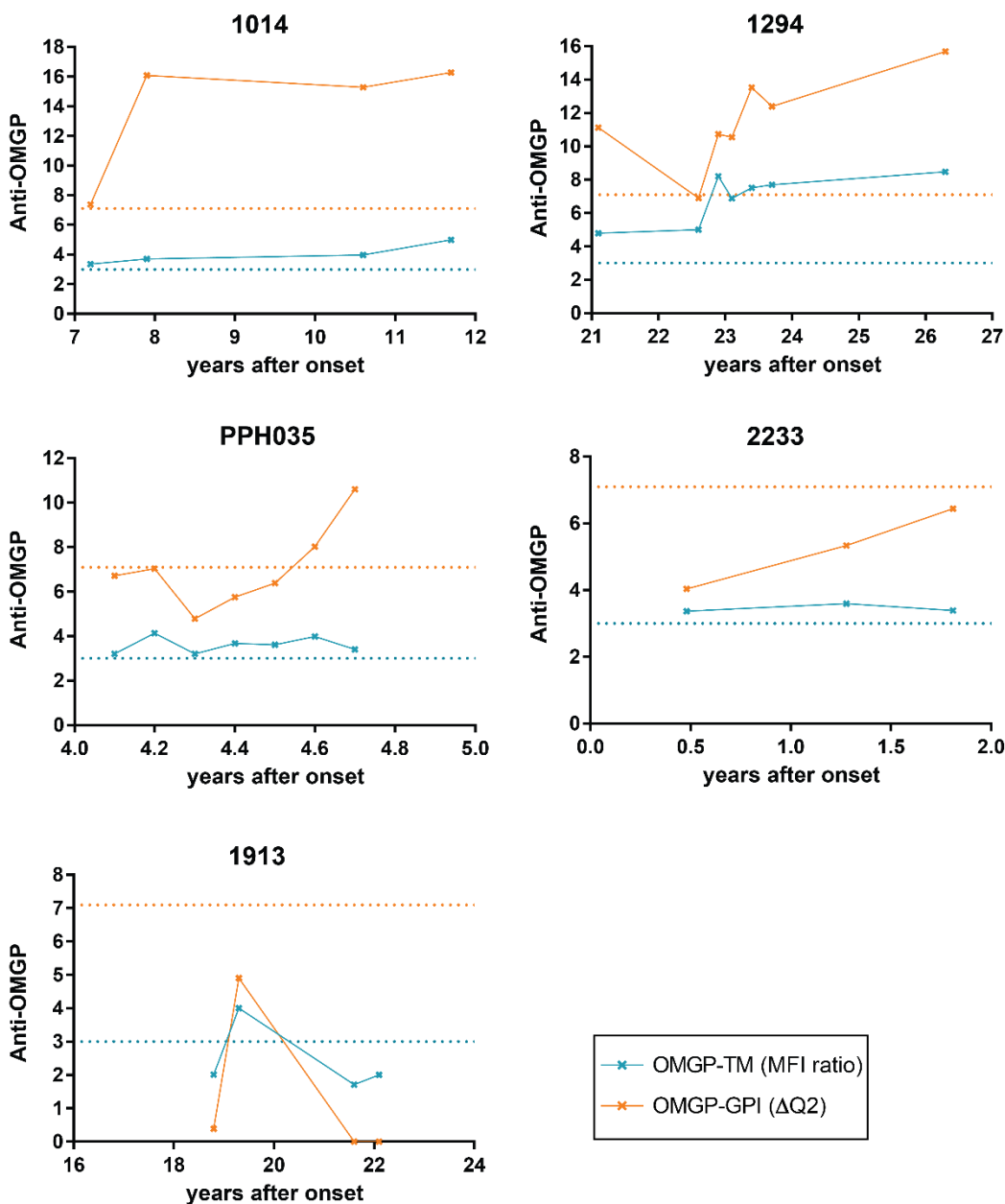
Figure 3.11 Longitudinal course of five patients

Patients were analyzed from 0.5 up to 26 years after disease onset. Blue color represents the measurement from OMGP-TM CBA, whereas orange from OMGP-GPI. The dotted horizontal line indicates the cutoff (mean of healthy controls + 3SDs) for each assay, 3.0 for OMGP-TM and 7.1 for OMGP-GPI.

For patient 1014 four samples could be evaluated and all time points were continuously positive for the OMGP-TM as well as OMGP-GPI CBA. The 71 year old (at first time point) female patient suffers from GAD antibody associated cerebellar syndrome and she was followed for 4.5 years from 7.2-11.7 years after disease onset.

The second patient 1294 was analyzed from 21.1-26.3 years after disease onset. At the first time point the female patient was 47 years old, where she was diagnosed with a severe form of RRMS, which is also expressed by the high clinical EDSS score of six. During the follow up period of 5.2 years, the autoantibodies were always present, as seen with both assays, OMGP-TM and OMGP-GPI CBA.

The patient indicated with PPH035 presented over a time period of about a year, almost every second month in the outpatient clinic. It was her fourth year after disease onset, where she experienced several relapses. The antibodies were always positive, when analyzed with the OMGP-TM, whereas only the two last time points scored positive in the OMGP-GPI CBA.

Patient 2233 could be measured relatively early after 0.5 years of disease onset and with an age of 41. The female RRMS patient with an EDSS score of two, was seropositive over a period of 1.3 years evaluated with OMGP-TM, whereas in OMGP-GPI the antibody values stayed under the cutoff.

For the female 32 year old (first time point) patient 1913 with an EDSS score of 4.5, only in one time point autoantibodies against OMGP-TM were detectable 19.3 years after disease onset. In the whole follow up period of 3.3 years no autoantibodies were detected with OMGP-GPI CBA.

Together, these longitudinal data indicate that OMGP autoantibodies tend to persist in most patients.

3.5 Purity of recombinantly expressed OMGP and subsequent biotinylation

Human OMGP was produced as a secreted protein in HEK293-EBNA cells as described in section 2.3.1 and purified through an IMAC (section 2.3.2). The antigen was used to establish an ELISA (section 3.6), for the affinity purification of patient derived Abs (section 3.9.2), to detect OMGP-specific T cells (section 3.13) and for generation of OMGP-specific T cells to be used in an animal model (section 3.12). To check the successful elution and quality of the purified protein, the crude supernatant, flow through, wash as well as elution fractions 50/75/150/1000 mM imidazole were loaded on a SDS gel (Figure 3.12). Before the purification, the supernatant contained also other proteins, which already passed the column while loading (flow through). An increasing purity of

the OMGP protein with raising imidazole concentrations is demonstrated in Figure 3.12, at a size of around 105 kDa. Due to the high glycosylation content, OMGP appears as a broad band in the gel.
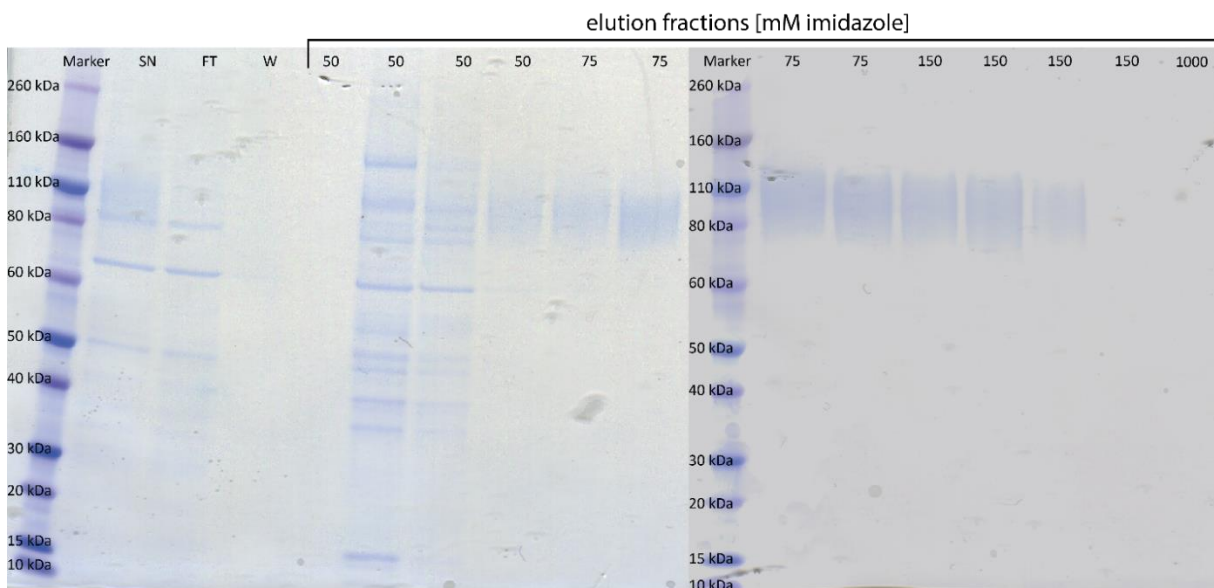
Figure 3.12 Coomassie stained SDS gel of recombinant produced human OMGP

The two gels show the unpurified supernatant (Renner et al.) of HEK293-EBNA cells, flow through (FT), wash (W) of the column and the elution steps using different concentrations of imidazole (50/75/150/1000 mM). The increasing purity of OMGP at 105 kDa is shown.

In average, all purifications yielded in 2.3 mg purified OMGP protein per 100 ml HEK293-EBNA culture (Table 3-2). This varied due to the quality of the cells regarding their passage number and the amount of death cells in the culture.
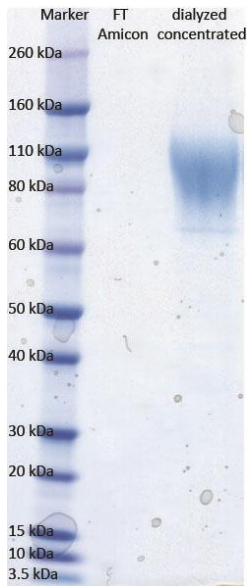
Table 3-2 Yield of hOMGP in HEK293-EBNA culture

| HEK293-EBNA culture volume [L]	purified hOMGP [mg]
0,2	3
0,6	10
0,8	28
0,7	26
0,65	26
1,5	7
1,1	11

The final purification step required the dialyzing against PBS and final concentration of OMGP by using an Amicon 50 kDa spin column. In Figure 3.13 the OMGP appears at 105 kDa and almost no contamination of other proteins is visible.

Figure 3.13 Purified hOMGP

The SDS gel proofed the absence of proteins in the flow through (FT Amicon) and a clean production of 105 kDa OMGP in the dialyzed and concentrated fraction.

For some assays (ELISA and antibody affinity purification), it was required to use biotinylated protein and therefore the Avi-tag of the protein was necessary. After enzymatic biotinylation (chapter 2.3.3) by BirA ligase, the efficiency was analyzed by Western Blot. Figure 3.14 demonstrates the positive biotinylation by staining with STV-HRP and a visible band of 105 kDa. The addition of biotin increased the protein by 0.24 kDa, which is not detectable by Western blot. The broad smear of the band is due to high amount of protein loaded and also the behavior of glycoproteins on a gel or Western blot.
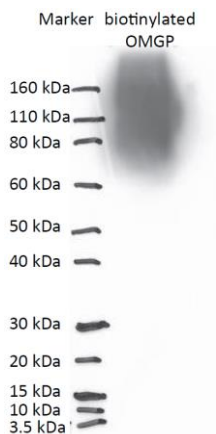
Figure 3.14 Proof of biotinylation by Western Blot

In the WB the biotinylation of OMGP could be analyzed by detection with STV-HRP. The protein shows a size of around 110 kDa, whereas the additional weight of 0.24 kDa from the biotin can't be seen.

## 3.6 Detection of OMGP autoantibodies by streptavidin ELISA

Purified and biotinylated OMGP was used for an ELISA screening, beside the CBA screening (section 3.2). The STV-ELISA was validated, using pAb AF1674 (Figure 3.15). Each screening plate contained as daily control the highly reactive index patient 2492 for OMGP autoantibodies. This allowed the normalization of each serum measurement to this daily value, since the OD varied regarding the substrate incubation time. Figure 3.15 represents 35 measurements of the index patient compared to its reactivity towards the STV background. For the analysis of the autoantibody in the different cohorts, the STV background was subtracted and then normalized to the daily control.
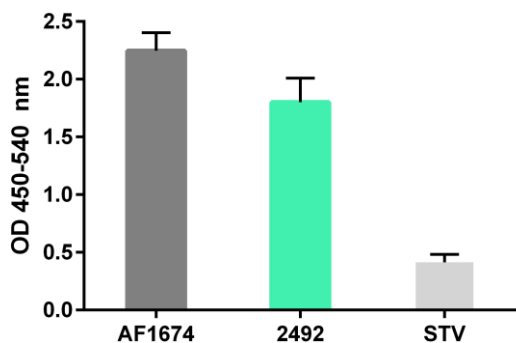
Figure 3.15 STV-ELISA validation and OMGP Ab reactivity of the index patient

The bar with pAb AF1674 validation shows the mean of five measurements, whereas the index patient 2492 is displayed as mean of 35 measurements, similar as for STV background. This serum 2492 served as daily control on each ELISA plate and was used for normalizing the OD values. Error bars represent SDs.

Different cohorts were analyzed for OMGP autoantibodies by ELISA (Figure 3.16). The cutoff for positivity was set to the mean value of the HC measurements plus three SDs and results in 0.4. All patients above the threshold were analyzed twice and the value represents the mean of these measurements. The coefficient of variation in the replicates was in average 0.13 and therefore lower than in CBAs.
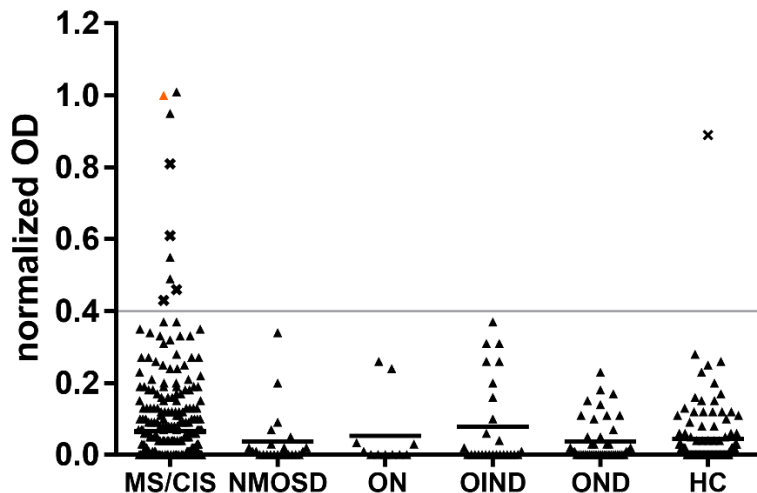
Figure 3.16 STV-ELISA screening for OMGP autoantibodies

The graph displays the normalized OD of the analyzed sera. From each value the STV background is subtracted and then normalized, by setting the OD of the index patient as daily control to 100 %. These groups were analyzed: multiple sclerosis/clinical isolated syndrome (MS/CIS, n=376), neuromyelitis optica spectrum disorder (NMOSD, n=24), opticus neuritis (ON, n=11), other inflammatory neurological disease (OIND, n=27), other neurological disease (OND, n=45) and healthy controls (HC, n=114). Horizontal line indicates cutoff at 0.4 (mean of HCs plus three SDs). All sera above the cutoff are mean values of at least two measurements. The cross symbols display patients newly identified by ELISA, which are not positive in CBAs. The orange triangle indicates the index patient and it's normalization to 100 %.

The biggest cohort is the MS/CIS group, where 2.4 % of the patients showed reactivity against OMGP, while in the HC cohort 1/114 (0.9 %) scored positive. Four patients were newly identified in this MS group and didn't score positive in any of the CBAs. In the other cohorts, NMOSD, ON and OND no patients were detected with OMGP autoantibodies.

3.7 Comparison of different assays established to detect autoantibodies to OMGP

Due to the SDs observed in the healthy donor group for the ELISA and the OMGP-GPI assay, a cutoff that is more stringent than mean + 3SDs does not appear meaningful. Therefore, the quantitative comparisons between ELISA and CBAs, outlined in this chapter, were performed

using the lower cutoff. Additionally, just for completeness the higher cutoff is displayed to indicate the grey zone between low and high threshold.

In the ELISA, 2.4 % of MS/CIS patients were detected with OMGP autoantibodies, whereas with the OMGP-TM CBA 5.4 % and OMGP-GPI CBA 2.4 %. For the comparative analysis between ELISA and CBA 596 sample pairs were tested in Spearman correlation and gives a weak but significant correlation of 0.19 between ELISA and OMGP-TM CBA (Figure 3.17). There are five samples which were seropositive for both assays. The ELISA detected overall less autoantibodies than the OMGP-TM CBA, but new patients were identified: two with high, one with intermediate and two with low reactivity.
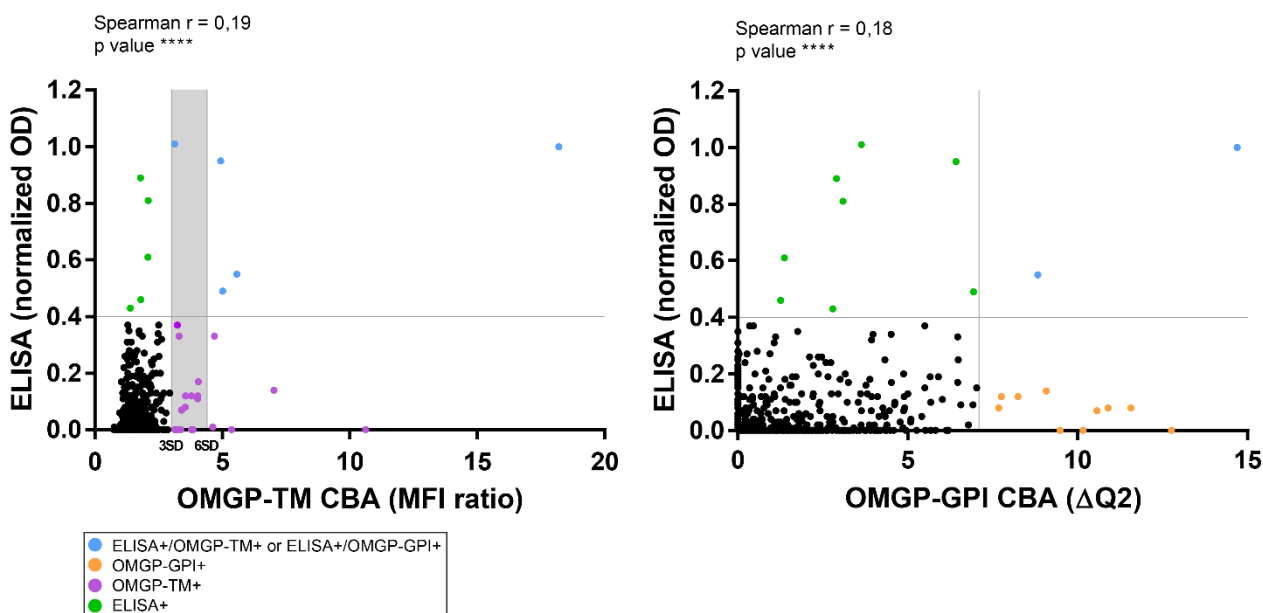

Figure 3.17 Spearman correlation analysis between ELISA and CBAs

The left graph shows for each ELISA measurement (cutoff at mean value of HCs + 3 SDs) the corresponding value in the OMGP-TM CBA with the lower (mean value of HCs + 3SDs) and higher cutoff (mean value of HCs + 6SDs) with its grey zone in-between. The right graph displays correlation between ELISA and OMGP-GPI CBA (cut off at mean value of HCs + 3SDs). 596 values were compared and double positives (ELISA+/OMGP-TM+ or ELISA+/OMGP-GPI+) are marked in blue, ELISA+ in green, OMGP-TM+ in violet and OMGP-GPI+ in orange.

If ELISA measurements are compared to the GPI anchored variant in CBA, only the values of two patients overlap for the OMGP autoantibody identification. The correlation between these two assays is significant, but also weak with r=0.18.

By comparing 675 pairs of data points from both TM and GPI anchored OMGP CBA variants, a higher significant correlation of r=0.69 can be obtained (Figure 3.18). In these assays, eleven

double positive patients with autoantibodies were detected, no matter if the OMGP was presented TM or GPI anchored. These patients have a higher titer and also the detection of Ig subclasses is more likely in double positives as well as more frequent long-term persistence of OMGP autoantibodies is observed.
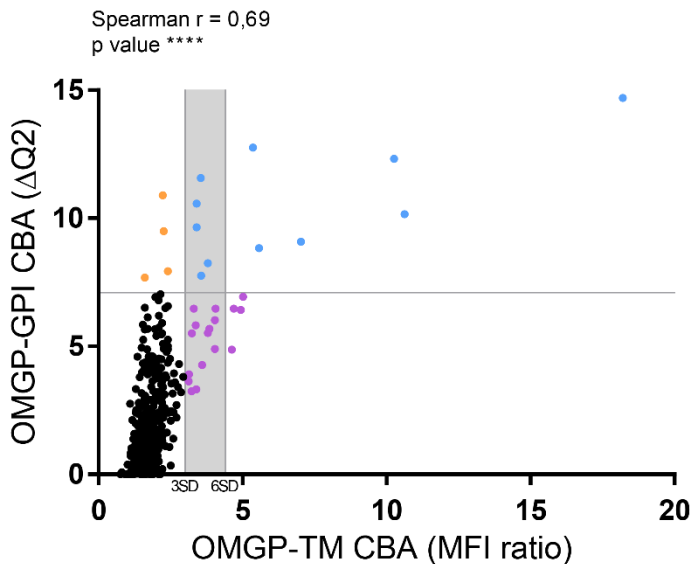
Figure 3.18 Spearman correlation between the two CBAs

The dots represent for each OMGP-GPI autoantibody measurement the corresponding value in the OMGP-TM CBA. 675 values were compared and double positives (ELISA+/OMGP-TM+ or ELISA+/OMGP-GPI+) are marked in blue, OMGP-TM+ in violet and OMGP-GPI+ in orange. Vertical grey lines indicate low (mean values of HCs + 3 SDs) and high (mean values of HCs + 6 SDs) cutoffs, with its grey zone in-between. Horizontal line displays cutoff (mean values of HCs + 3 SDs) for OMGP-GPI CBA.

Table 3-3 summarizes the autoantibody screening for OMGP-TM/-GPI CBA, using the lower cutoff. By combining both results, which means positivity in either OMGP-TM- or OMGP-GPI CBA, 5.9 % of MS/CIS patients had autoantibodies against the antigen. The highest ones scored positive with 1.9 % for both assays. For patients with GAD autoantibodies the OMGP-GPI CBA detected with 9.1 % one patient more than with the OMGP-TM assay. This is the only case where the GPI detection method had a higher frequency. Patients with ADEM were detected in both assays with a frequency of 1.8 % and the same was true for HCs. In the OND/OIND cohort 3.7 % had autoantibodies in the TM detection method and only 0.9 % with the GPI CBA. Overall with the OMGP-TM CBA more MS/CIS patients were identified than with OMGP-GPI CBA, whereas the frequency for HCs was in both assays identical.

Table 3-3 Summary of seropositive numbers in CBA measurements

Numbers in the table are calculated by using the less stringent cutoff (mean values of HCs + 3 SDs).

Patient cohort	total	OMGP-TM⁺ or OMGP-GPI⁺ CBA		OMGP-TM⁺ CBA		OMGP-GPI⁺ CBA		OMGP-TM⁺ & OMGP-GPI⁺ CBA	
		number	freq.	number	freq.	number	freq.	number	freq.
MS/CIS	376	22	5.90 %	20	5.3 %	9	2.4 %	7	1.9 %
GAD	22	2	9.10 %	1	4.5 %	2	9.1 %	1	4.5 %
ADEM	56	1	1.80 %	1	1.8 %	1	1.8 %	1	1.8 %
OND/OIND	107	4	3.70 %	4	3.7 %	1	0.9 %	1	0.9 %
HC	114	3	2.60 %	2	1.8 %	2	1.8 %	1	0.9 %
total	675	32	4.70 %	28	4.1 %	15	2.2 %	11	1.6 %

Together, here three assays were developed and all three assays were validated with commercial Abs to OMGP (Figure 3.3 for CBAs and Figure 3.15 for STV-ELISA). Although the results of the assays correlated with each other, the strongest association was observed between OMGP-TM and OMGP-GPI. When considering the dispersion, the difference between the strongly reactive ones and the mean background level, the OMGP-TM assay would be most reliable assay.

3.8 Clinical description of patients with autoantibodies against OMGP

The clinical details of donors with autoantibodies to OMGP are given in Table 3-4 and patients with a higher level of autoantibodies to OMGP, who scored positive with the stringent cutoff are indicated with a star symbol.

Most patients from the Munich cohort have lesions in the brain, several in the spinal cord and some in the brainstem. Interestingly, three highly positive patients (2492, 1294 and 2088) have a brain atrophy in the MRI scan. The sampling point varies from beginning of the disease, to more than 20 years after disease onset or manifestation. Five patients experience a more severe disease course having an EDSS score ≥ 4. All Munich cohort samples were tested negative for MOG autoantibodies and some were additionally tested for AQP4 reactivity and also showed negative results.

Table 3-4 Clinical features of patients with OMGP autoantibodies

Star symbol (*) indicates patients positive even with the stringent cutoff.

#	Positive sera/number of follow up	Sex	Age	Diagnosis	Clinical description	EDSS
Munich MS-NMOSD						
2492*	5/5	M	37	RRMS	Relapses: 4 (brainstem, myelitis, ON) Lesions: brainstem, spinal cord, cerebral MS typical, brain atrophy Disease duration: 17.7 years, OMGP seropositive in 60 month follow up	2.5
1294*	7/7	F	48	RRMS	Relapses >10 (brainstem, recurrent myelitis, ON, cognitive dysfunction) Lesions: brainstem, spinal cord, cerebral multiple MS lesions, brain atrophy Disease duration: 26.6 years, OMGP seropositive in 48 month follow up	6.0
2088*	1/2	M	51	RRMS	Relapse: 1 (myelitis, pathological VEP) Lesions: deep WM, LETM, brain atrophy Disease duration: 0.8 years	2.5
PPH035	7/7	F	32	RRMS	high relapse rate (3/year)	3.0
2233	3/3	F	58	RRMS	ocular and spinal manifestation	2.0
1913	1/4	F	33	RRMS	recurrent ON, spinal manifestation	4.5
3051	1/2	F	22	RRMS	high lesion load, brainstem manifestation	3.5
233	1/2	M	30	RRMS	disease activity reduced under natalizumab	2.0
3008	1/1	M	37	NMOSD	ON, myelitis along several vertebra	1.5
Munich typical MS						
2105*	1/1	M	58	RRMS	Relapse: 1 (myelitis) Lesions: spinal cord, several WM and subcortical Disease duration: 0.6 years	2.5
1825	2/2	F	30	RRMS	ON and increasing number of lesions due to therapy rejection of patient	2.0
1453	1/1	F	43	RRMS	visceral symptoms, Hashimoto's thyroiditis	3.0
1319	1/1	M	29	RRMS	multiple lesions, spinal manifestation	1.5
2252	1/1	M	30	RRMS	myelitis along several vertebra	2.0
2273	1/1	M	51	RRMS	brainstem and spinal lesions	5.5
Munich CIS						
1364*	1/2	F	37	CIS/MS	Relapse: 1 (large tumefactive cerebral lesion) Lesions: large parietal contrast enhancing deep WM Disease duration: 2.5 years	1.5
3031*	1/1	F	36	CIS/MS	Relapse: 1 (myelitis) Lesions: spinal cord, deep WM Disease duration: 0.5 years	0.0
Munich encephalitis						
1014	4/4	F	72	cerebellar syndrome	Non-paraneoplastic limbic encephalitis (NPLE), GAD antibody associated	/

3887	1/2	F	38	limbic encephalitis	GAD antibody associated, NPLE	/
Stockholm MS cohort						
11-114*	1/1	M	45	SPMS	more than nine lesions in MRI scan	4
11-134*	1/1	F	29	RRMS	remission, more than nine lesions in MRI scan	2
11-077	1/1	M	25	RRMS	remission phase, 3-5 lesions in MRI scan	0
12-176	1/1	F	45	PRMS	relapses without remission, 0-2 lesions in MRI scan	1.5
11-102	1/1	M	45	RRMS	remission phase, 0-2 lesions in MRI scan	6
Stockholm OND cohort						
12-236*	1/1	M	29	psychosis	no treatment, no OCBs, no lesions in MRI scan	
Canadian pediatric cohort						
ACJ-108*	1/1	F	10.5	ADEM	monophasic acquired demyelinating syndrome	/

In conclusion, most patients have an interesting clinical phenotype, since the majority with nine out of 19 Munich samples, have MS-NMOSD phenotype. This pattern was already described by our lab (Spadaro et al., 2016), where patients showing more often ON, lesions in brainstem and spinal cord involvement. Therefore, those were categorized as MS selected group with an NMOSD phenotype.

In addition to patients with MS, this study identified one patient with a psychosis and one child diagnosed with ADEM, having high level of OMGP autoantibodies.

The following section describes the highest positive patient 2492 with OMGP autoantibodies, which is subsequently named as index patient. This patient is also highlighted in Table 3-4 and has an interesting MS-NMOSD clinical phenotype.

3.9 Detailed analysis of the highest positive index patient 2492

3.9.1 Clinical case

The male patient was diagnosed with MS in 2002 when he was 18 years old. After a Hepatitis B vaccination and a measles infection he experienced paresthesia of his extremities. At this time point, no OCB were detectable in the CSF. The symptoms disappeared after steroid treatment. One year later, the patient got a relapse with signs of brain stem dysfunction and there OCBs, also with intrathecal IgM production, were present in the CSF. From 2002 until March 2014 the patient was treated with interferon beta but got two more relapses in 2006 and 2009 with ataxia of gait and ON. Since 2014 he has been visiting the LMU MS outpatient clinic yearly and started

at age of 30 years dimethyl fumarate (DMF) treatment. His MS course had several relapses, where he didn't completely recover and was therefore diagnosed with RRMS and incomplete remission. The patient had from beginning on a high titer of OMGP antibodies and scored positive in the OMGP-TM assay with a MFI ratio of 16.6 as well as in OMGP-GPI CBA with 31.16 % (Figure 3.19).
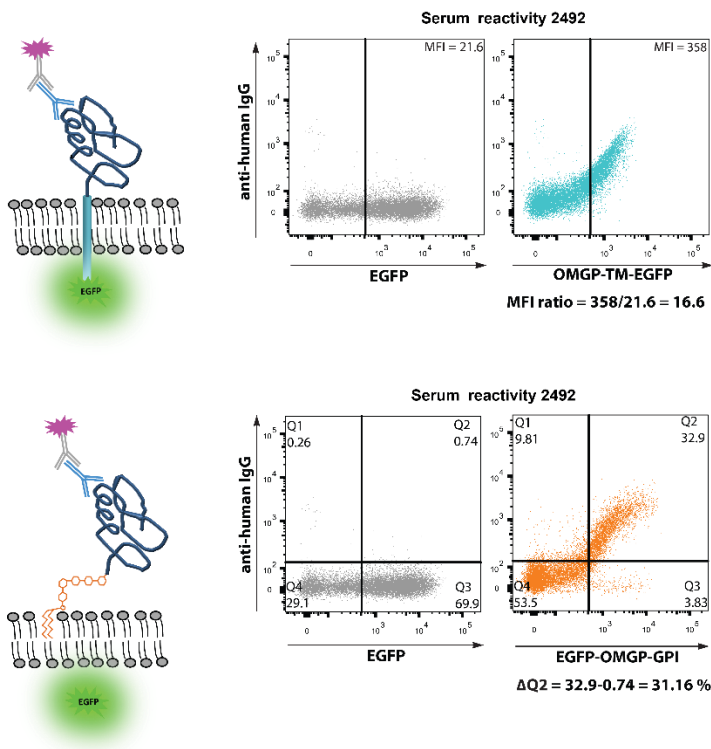

Figure 3.19 OMGP autoantibody reactivity of the index patient in CBAs

The serum of the patient was tested for OMGP autoantibodies in TM CBA (blue) where the MFI ratio is 16.6 and in GPI CBA (orange) with ΔQ2 of 31.16 %. The grey dot plot represents the antibody binding to EGFP transfected HeLa cells.

Five longitudinal samples could be collected over the time and were analyzed from 12.6 until 15.6 years after disease onset (Figure 3.20). In all time points the patient had autoantibodies against OMGP.

The clinical EDSS score of the patient varied from 2.5 in 2014, stayed at 2.0 from 2015-2017 and declined to 1.5 in February 2019. Under DMF treatment he is quite stable and didn't experience further relapses, as it was the case with interferon beta. In the MRI scan he already presented in 2014 with lesions in the cervical spinal cord, cerebellar on both sides and brainstem lesions in the pons region. Furthermore, periventricular, sub- and juxtacortical lesions in the cerebrum and the tissue destruction of the corpus callosum were visible. From 2014-2019 this findings were stable

and no contrast enhanced lesions, which represent active lesions, appeared. Only one lesion increased and therefore the patient's brain was analyzed with positron emission tomography (PET) using a translocator protein (TSPO) tracer, which detects microglial activation. There was no evidence for focal microglia activation in this specific periventricular lesion. During this observation period, the patient didn't develop new lesions, neither in the brainstem, cerebellum or cerebrum, nor in the spinal cord. However, brain atrophy over the years could be measured by MRI.
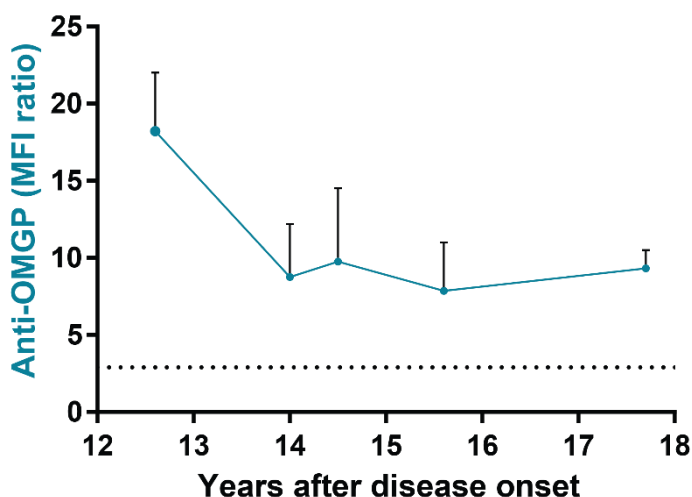
Figure 3.20 Longitudinal OMGP autoantibody analysis of the index patient

The graph shows the measurements of five follow up samples, analyzed with OMGP-TM CBA. Dotted horizontal line indicates the lower cutoff, which is the MFI ratio of 3.0. Values represent n≥2 replicates. Time point 2, 3 and 5 are plasma, whereas 1 and 4 display measurement of serum samples. Error bars represent SEM of 30 replicates for the first time point, six replicates of the last time point and of two measurements for the other time points 2/3/4.

The noticeable parameters in the blood were the high anti-nuclear antibody (ANA) titer, which decreased in 2015 from 1:3200 to 1:800 in 2016. No other autoimmune related autoantibodies like double-strand DNA (dsDNA), MOG, AQP4, rheumatoid factor (RF) or anti-phospholipid were detected. The blood was analyzed for cold agglutinins and cryoglobulins, since the serum clogged in the autoantibody preparations in the lab. The clinical chemistry in the LMU hospital detected positive titer for cold agglutinins with 1:10 dilution at 4 °C, which is still in the physiological range and might also vary in blood of patients regarding the season. These cryoglobulins can be seen in patients with HBV, HCV, HIV and rheumatoid disease or appear, if patients have high titers of antibodies, which is the case for OMGP and ANA autoantibodies in the index patient's blood.

The high titer of OMGP autoantibodies is illustrated in Figure 3.21 by diluting the serum of the patient from the second time point from 1:50, which is the screening dilution, to 1:1600. Also with higher dilutions, the reactivity was still detectable.
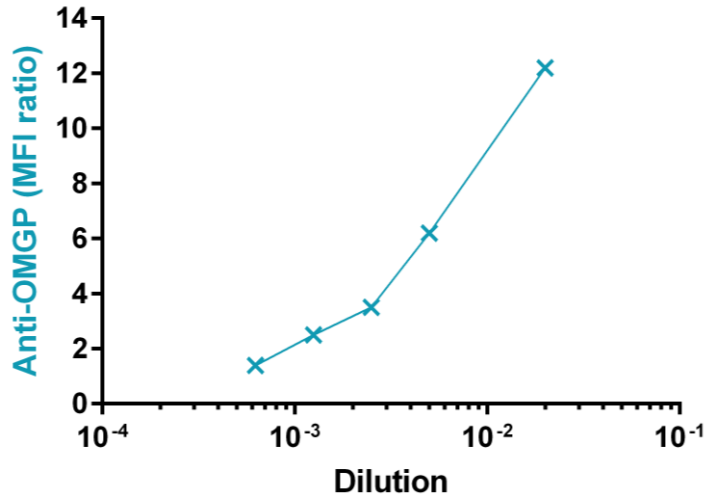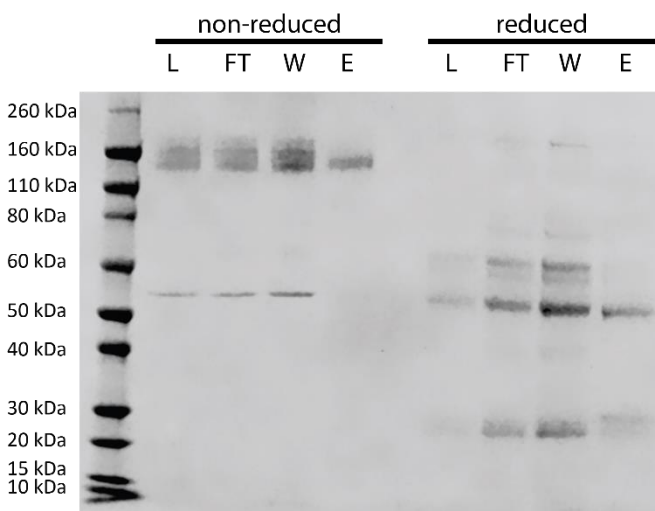

Figure 3.21 Serial dilution of the index patient's serum

The serum sample of the second time point was used for serial dilutions in OMGP-TM CBA. The following steps of dilution were used: 1:50/1:200/1:400/1:800/1:1600.

This patient showed the highest reactivity for OMGP autoantibody screening in OMGP-TM and OMGP-GPI CBA. Furthermore these antibodies could also be detected with a high OD in the OMGP STV-ELISA (Figure 3.15) and also in the longitudinal course, he stayed seropositive for the autoantibodies. Regarding the high titer of the OMGP antibodies, this patient was selected for an affinity purification of the autoantibodies out of plasma material.

### 3.9.2 Outcome of OMGP autoantibody affinity purification of patient's plasma

Starting with 450 ml of EDTA blood for affinity-purification with an OMGP-loaded column, 112 µg of OMGP autoantibodies could be obtained. The purity of these antibodies is demonstrated by SDS-PAGE in Figure 3.22 under reduced and non-reduced conditions. In the load, flow-through and wash fractions, the bands of all immunoglobulins as well as albumin between 50-60 kDa are visible. In the non-reduced samples the immunoglobulins have a size of 150 kDa, but by adding reducing agents they separate into heavy (50 kDa) and light chains (25 kDa). The elution fraction shows clean OMGP autoantibodies with 150 kDa under non-reduced conditions and at 50 kDa as well as 25 kDa under reduced conditions.

Figure 3.22 Non-/reduced SDS gel of OMGP autoantibody purification of the index patient

The gel shows the load (L), flow-through (FT), wash (W) and elution (E) fractions under non-reduced and reduced conditions. The immunoglobulins have a size of 150 kDa, heavy chain of 50 kDa and light chain of 25 kDa.

The bands from the elution fractions were cut out and analyzed by mass spectrometry in collaboration with the technician Reinhard Mentele from the lab of Dr. Klaus Dornmair. Regarding these results the existence of human immunoglobulins heavy and light chain was confirmed. The purified antibodies were still functional after the acidic elution and the enriched reactivity is shown in Figure 3.23. 50 ng of total immunoglobulins were tested on 5×10^4 OMGP-GPI transfected HeLa cells and only in the elution fraction autoantibodies bound to the antigen. These precious purified OMGP autoantibodies could be used for further functional analysis.
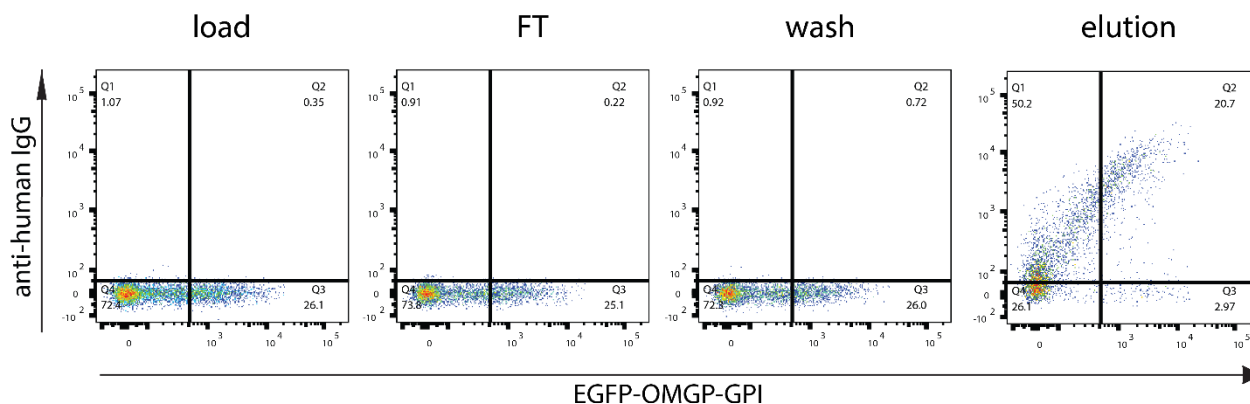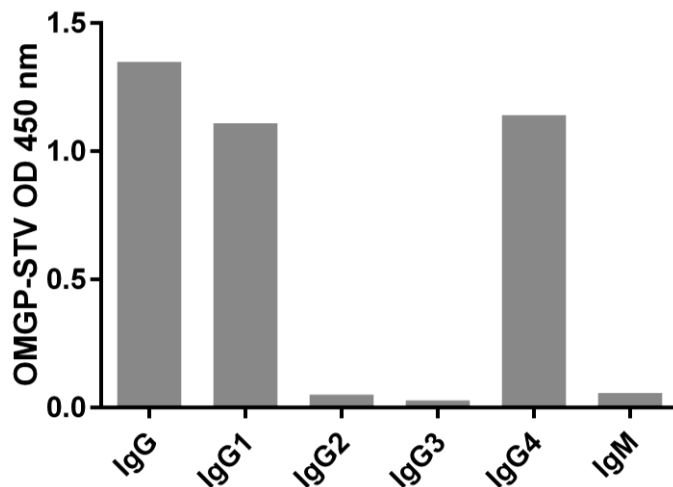

Figure 3.23 Purified OMGP autoantibodies in OMGP-GPI CBA

In all four columns 50 ng of immunoglobulins were tested on 5×10^4 OMGP-GPI transfected HeLa cells. Load, flow-through (FT) and wash didn't show antibody binding, but the elution fraction displays the enrichment of OMGP autoantibodies in Q2 gate.

3.9.3 IgG1 and IgG4 as subclasses of OMGP autoantibodies in the index patient

The isotype screening for the serum of the patient is depicted in section 3.3, which showed no strong signal in in the unpurified material with the OMGP-GPI CBA (Figure 3.9, A). If this unpurified serum sample was tested by STV-ELISA, IgG1 and IgG4 subclasses for OMGP autoantibodies were identified (Figure 3.24). There were no other signals for the detection of IgG2, IgG3 and IgM and therefore are not present as OMGP autoantibodies in this patient.

Figure 3.24 Determination of Ig subclasses by ELISA in unpurified serum of the index patient

The autoantibodies in serum were detected by OMGP STV-ELISA. After background correction (450 nm-540 nm), the STV background is subtracted from the OD signal of OMGP at 450 nm.

However, if autoantibodies were tested after the OMGP affinity purification, also IgG1 and IgG4 subclasses were detected by OMGP-GPI CBA (Figure 3.25). While the unpurified serum of this patient provided evidence for IgG1 and IgG4 Abs against OMGP (Figure 3.9), this was now firmly established, using the affinity-purified Abs. IgG2, IgG3 and IgM were still not found as isotypes of OMGP autoantibodies in this patient, even after purification.
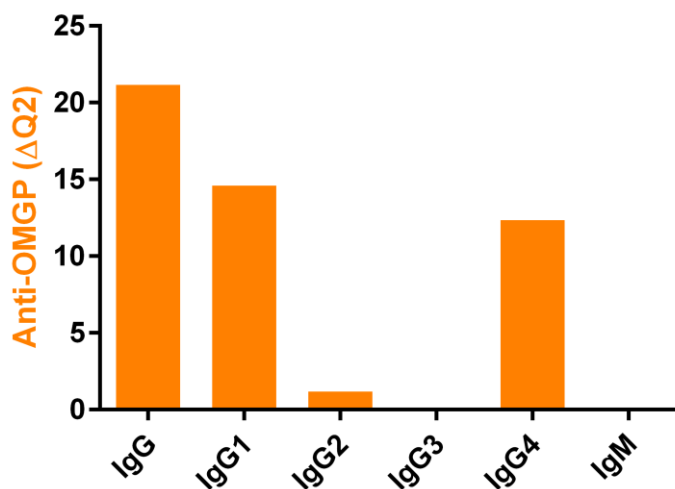
Figure 3.25 CBA isotyping of affinity purified OMGP autoantibodies of the index patient

600 ng of purified autoantibodies on $5x10^4$ transfected cells were tested for each subclass in OMGP-GPI CBA. Secondary antibodies were used from ELISA and detected with anti-HRP-alexa647 antibody by flow cytometry.

3.9.4 Potential induction of complement cascade by binding of C1q to autoantibodies

Having now the results of IgG1 and IgG4 isotypes of this OMGP-specific autoantibodies, it was of great interest to know, if they could also induce antibody mediated effector functions like the induction of the classical pathway of the complement cascade (Figure 3.26, A). In this whole process many proteins and steps in between are involved that result in the development of inflammatory mediators like C5a and also the final membrane attack complex (MAC) is formed *in vivo*. The detection of the MAC would be the most valuable effect, but it is very difficult to induce the entire process *in vitro*, since many factors are required and also a lot of inhibitory mechanisms need to be extinguished. For the detection of the potential initiation of the cascade, an ELISA was established, which detects the binding of the starter protein C1q to the autoantibodies of the patient (Figure 3.26, B). The C1q is only detected, if it is able to bind to the OMGP autoantibodies of the patient.

A
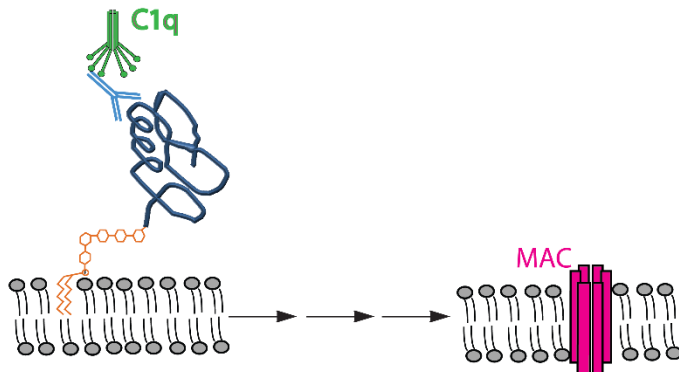
B
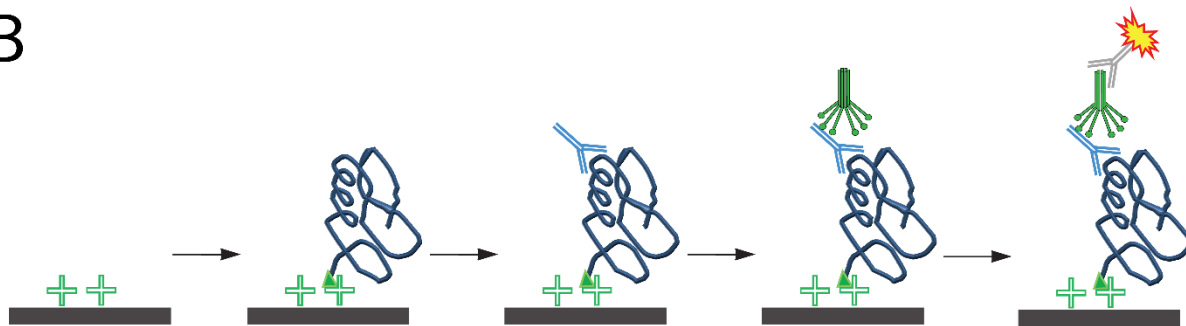
Figure 3.26 Classical pathway of complement system

(A) If complement cascade is activated by the binding of an antibody to its antigen *in vivo* and the starting protein C1q binds, a cascade of several proteins is induced with ends in the formation of a membrane attack complex (MAC). (B) The experimental set up is illustrated how the start of the complement cascade induction could be measured *in vitro*. STV (green cross) coated ELISA plate was incubated with biotinylated (green triangle) OMGP and detected by purified autoantibodies (blue). The bound C1q was detected by an anti-C1q-HRP. This is a simplified scheme to illustrate the detection of bound C1q. Recent work has provided evidence that C1q binding is enhanced by multimeric Ab platforms (Soltys et al., 2019).

The OMGP affinity purified autoantibodies of the index patient were titrated with 5/2.5/1.25/0.625 µg/ml in this ELISA (Figure 3.27). As CTR antibodies the intravenously administered immunoglobulins (IvIg) were used. The index patient's antibodies gave an OD of 0.5 with 5 µg/ml, whereas the signals of the control antibodies were in all concentrations around zero. With reducing concentrations of the OMGP autoantibodies, the signal declined to 0.18, but was still higher than with CTR antibodies.
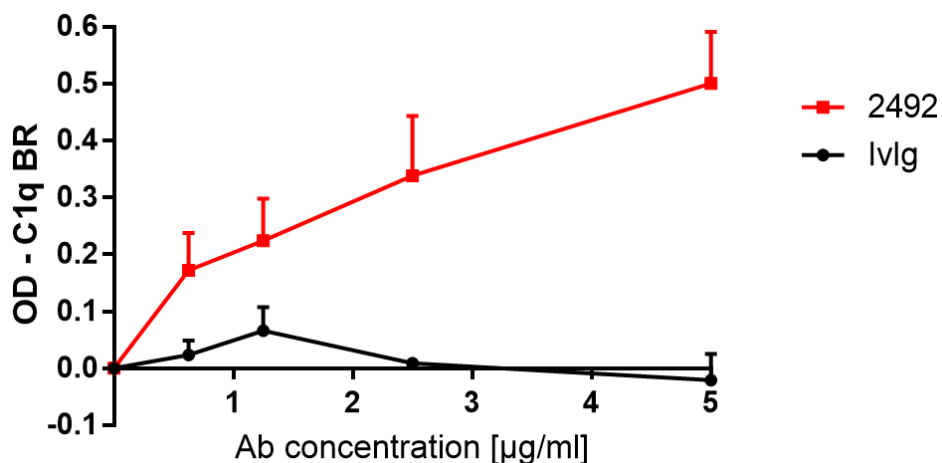
Figure 3.27 C1q protein binding to OMGP autoantibodies of the index patient 2492

The red line illustrates the results from the C1q binding to the autoantibodies of the patient, whereas the black line shows the values for the control immunoglobulins. These are Igs, which are given intravenously to patients and therefore called IvIg. OD signal was subtracted by C1q background signal (C1q BR). Error bars show SDs of two individual experiments.

3.9.5 Cross reactivity of hOMGP autoantibodies to rodent OMGP

The OMGP autoantibodies have a high specificity to the human protein, but due to the close evolutionary relationship of humans to rat and mice, these were also tested for the reactivity on mouse and rat m/rOMGP. This is of further interest, because the final and future aim of the OMGP autoimmunity study would be, to show the pathogenicity of these autoantibodies in an animal model.

The results of the protein alignments are demonstrated in Figure 3.28. The identity of human and of mouse protein is 88.6 % and between human and rat OMGP with 89.3 % quite similar. The green signal peptide from 1-24 aa shows only at one position an exchange of an amino acid between the rodent and human OMGP. Five variations in the sequence occur in the purple GPI signal peptide from 418-440 aa.

```
CLUSTAL O(1.2.4) multiple sequence alignment

SP|P23515|OMGP_HUMAN   MEYQILKMSLCLFILLFLTPGILCICPLQCICTERHRHVDCSGRNLSTLPSGLQENIIHL 60
SP|Q63912|OMGP_MOUSE   MEYQILKMSSCLFILLFLTPGILCICPLQCTCTERHRHVDCSGRNLTTLPPGLQENIIHL 60
TR|Q7TQ25|Q7TQ25_RAT   MEYQILKMSSCLFILLFLTPGILCICPLQCICTERHRHVDCSGRNLTTLPPGLQENIIHL 60
                       ******** ***.***********.******** ********:*** *********

SP|P23515|OMGP_HUMAN   NLSYNHFTDLHNQLTQYTNLRTLDISNNRLESLPAHLPRSLWNMSAANNNIKLLDKSDTA 120
SP|Q63912|OMGP_MOUSE   NLSYNHFTDLHNQLTPYTNLRTLDISNNRLESLPAQLPRSLWNMSAANNNIKLLDKSDTA 120
TR|Q7TQ25|Q7TQ25_RAT   NLSYNHFTDLHNQLTPYTNLRTLDISNNRLESLPAQLPRSLWNMSAANNNIKLLDKSDTA 120
                       ************** *******************:**********************

SP|P23515|OMGP_HUMAN   YQWNLKYLDVSKNMLEKVVLIKNTLRSLEVLNLSSNKLWTVPTNMPSKLHIVDLSNNSLT 180
SP|Q63912|OMGP_MOUSE   YQWNLKYLDVSKNMLEKVVLIKNTLRSLEVLNLSSNKLWTVPTNMPSKLHIVDLSNNSLT 180
TR|Q7TQ25|Q7TQ25_RAT   YQWNLKYLDVSKNMLEKVVLIKNTLRSLEVLNLSSNKLWTVPTNMPSKLHIVDLSNNSLT 180
                       ************************************************************

SP|P23515|OMGP_HUMAN   QILPGTLINLTNLTHLYLHNNKFTFIPDQSFDQLFQLQEITLYNNRWSCDHKQNITYLLK 240
SP|Q63912|OMGP_MOUSE   QILPGTLINLTNLTHLYLHNNKFTFIPEQSFDQLLQLQEITLHNNRWSCDHKQNITYLLK 240
TR|Q7TQ25|Q7TQ25_RAT   QILPGTLINLTNLTHLYLHNNKFTFIPDQSFDQLLQLQEITLHNNRWSCDHTQNITYLLK 240
                       **************************:******:*******:********.********

SP|P23515|OMGP_HUMAN   WMMETKAHVIGTPCSTQISSLKEHNMYPTPSGFTSSLFTVSGMQTVDTINSLSVVTQPKV 300
SP|Q63912|OMGP_MOUSE   WVMETKAHVIGTPCSKQVSSLKEQSMYPTPPGFTSSLFTMSEMQTVDTINSLSMVTQPKV 300
TR|Q7TQ25|Q7TQ25_RAT   WMMETKAHVIGIPCSKQVSSLKEQSMYPTPPGFTSSLFTMSEMQTVDTINSLSMVTQPKV 300
                       *:********* ***.*:*****:.***** ********:* ***********:******

SP|P23515|OMGP_HUMAN   TKIPKQYRTKETTFGATLSKDTTFTSTDKAFVPYPEDTSTETINSHEAAAATLTIHLQDG 360
SP|Q63912|OMGP_MOUSE   TKTPKQYRGKETTFGVTLSKDTTFSSTDRAVVAYPEDTPTEMTNSHEAAAATLTIHLQDG 360
TR|Q7TQ25|Q7TQ25_RAT   TNIPKQYRGKDTTFGVTLSKDTTFSSTDRALEPYPEDTPTEMTSSREAAAATLTIHLQDG 360
                       *: ***** *:****.********:***:*.   ***** **  .*:*************

SP|P23515|OMGP_HUMAN   MVTNTSLTSSTKSSPTPMTLSITSGMPNNFSEMPQQSTTLNLWREETTTNVKTPLPSVAN 420
SP|Q63912|OMGP_MOUSE   MSSNASLTSATKSPPSPVTLSIARGMPNNFSEMPRQSTTLNLRREETTANGNTRPPSAAS 420
TR|Q7TQ25|Q7TQ25_RAT   MSSNASLTSAAKSSPAPVTLSITSGMPNNFSEMPQQSTTLNLRREETTANVKTQPPSSAS 420
                       * :*:****::** *:*:****: **********:****** *****:* :*  ** .*.

SP|P23515|OMGP_HUMAN   AWKVNASFLLLLNVVVMLAV 440
SP|Q63912|OMGP_MOUSE   AWKVNASLLLMLNAVVMLAG 440
TR|Q7TQ25|Q7TQ25_RAT   AWKVNASLLLMLNAVVMLAG 440
                       *******:**:**.*****
```

Figure 3.28 OMGP protein alignment

The amino acid sequences of human (P23515), mouse (Q63912) and rat (Q7TQ25) OMGP from Uniprot were aligned by using the online program Clustal Omega. Stars indicate similarity and dots are present if there are differences. In green the signal peptide 1-24 aa is marked and in purple from 418 to 440 aa the GPI-anchor signal peptide.

Human and rodent OMGP share 89 % identical amino acid sequence and therefore the autoantibodies of the index patient 2492 were able to bind beside the human variant also the rodent form (Figure 3.29). If serum was used, which represents unpurified material, the binding to the human protein was strong with 19.6 % of hOMGP-GPI expressing cells bound with autoantibodies and a mean fluorescence signal of 637. Rat OMGP was detected less with 15.3 % and MFI of 137. The mouse variant was stained with unpurified serum with 23.1 % in OMGP-GPI and MFI of 241 in OMGP-TM assay.

After the successful affinity purification of patients' plasma, the elution fraction contains enriched OMGP autoantibodies. This was evaluated in the OMGP-GPI CBA by a similar or enhanced percentage number in Q2 gate and more obvious by an increase of the MFI signal. The detection of human OMGP increased from MFI of 637 to 6055 in Q2 gate, for rat OMGP from 137 to 197 and for mouse OMGP from 241 to 3691.
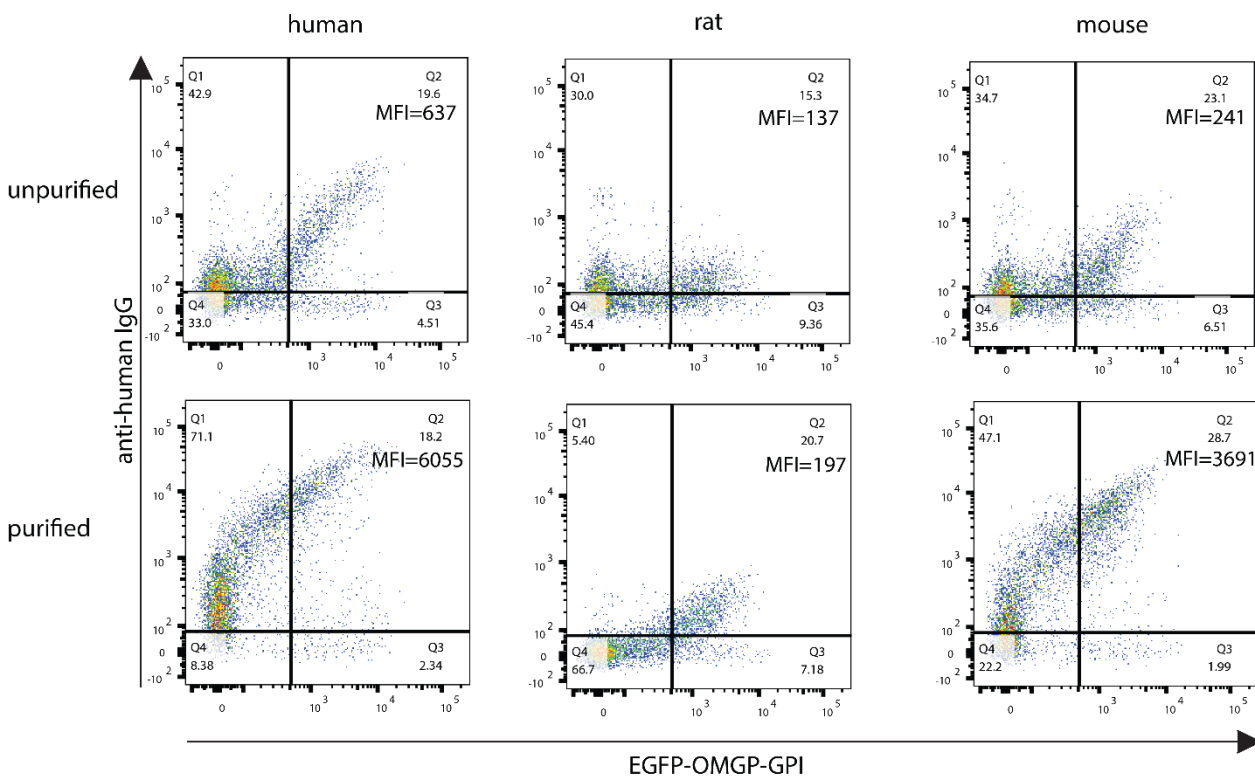
**Figure 3.29 Detection of rodent cross reactivity of OMGP purified Abs from the index patient**

Serum of patient was tested in regular CBA with 1:50 dilution as unpurified sample (upper row) on human, rat and mouse OMGP-GPI. The lower row displays the OMGP affinity purified sample tested with 50 ng of IgG on 5×10^4 transfected HeLa cells. Mean fluorescence intensity is shown in each Q2 gate below the number of percentage.

This patient showed a high cross reactivity to mouse OMGP and a bit to rat OMGP, which had a higher signal after the autoantibody affinity purification. Therefore, this purified material could be used for further studies in an animal transfer experiment.

3.9.6 Identification of circulating OMGP-specific B cells in the blood of the index patient

In the serum of different time points of the patient, OMGP autoantibodies were constantly detected (Figure 3.20). To study if circulating OMGP-specific B cell can be differentiated into antibody secreting cells, PBMCs were stimulated with TLR ligand R848 and IL2. This protocol was already established in our lab for analyzing GAD and MOG circulating B cells (Thaler et al., 2019; Winklmeier et al., 2019).

Figure 3.30 shows the analysis of 13 stimulated wells of the index patient 2492. One out of 13 scored clearly positive in both CBAs, whereas the second highest was also producing OMGP Abs into the supernatant, but with a lower concentration or affinity.
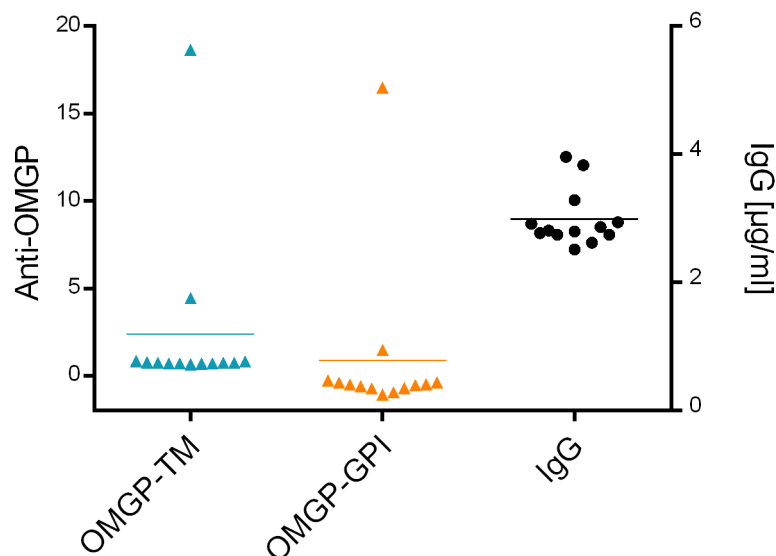
Figure 3.30 Production of OMGP Abs after *in vitro* differentiation of B cells to Ab-secreting cells

13 wells with 6 x 10^5 PBMCs/well of the index patient 2492 were stimulated and tested for OMGP autoantibody production in the supernatant by OMGP-TM- (blue symbols) and OMGP-GPI- (orange symbols) CBAs (left y-axis). The two highest values are coming from the same well. Additionally, all 13 wells were analyzed further for their IgG concentration by human IgG ELISA, indicated on the right y-axis. Horizontal lines represent the mean in each group.

In all wells the IgG production was quantified by human IgG ELISA (Figure 3.30, B). The concentration varied from 2.5 µg/ml to 4 µg/ml. This is in the lower range of IgG production, when comparing to the patients and healthy controls analyzed in the MOG study (Winklmeier et al. 2019).

3.10 Development and characterization of monoclonal antibodies against OMGP

In collaboration with the group of Dr. Regina Feederle from Helmholtz Centrum München we developed our own monoclonal antibodies by immunizing mice and rats with the recombinant produced hOMGP as well as the rat specific OMGP peptide (Table 2-9). The evaluation of these 133 hybridoma supernatants was the MD project of Lena Kristina Pfeffer and described in detail in her thesis. Three antibodies (22H6-rIgG2A, 31A4-mIgG2B and 14A9-rIgG2B) from all clones were used for further investigations and also appear in this study (Table 2-10).

Additionally in this project, one clone (22H6) was transformed from rat IgG2A Fc part to human IgG1 and successfully produced as a recombinant antibody in HEK293-EBNA cells (section 2.2.12.). The functionality of this monoclonal antibody is displayed in Figure 3.31.
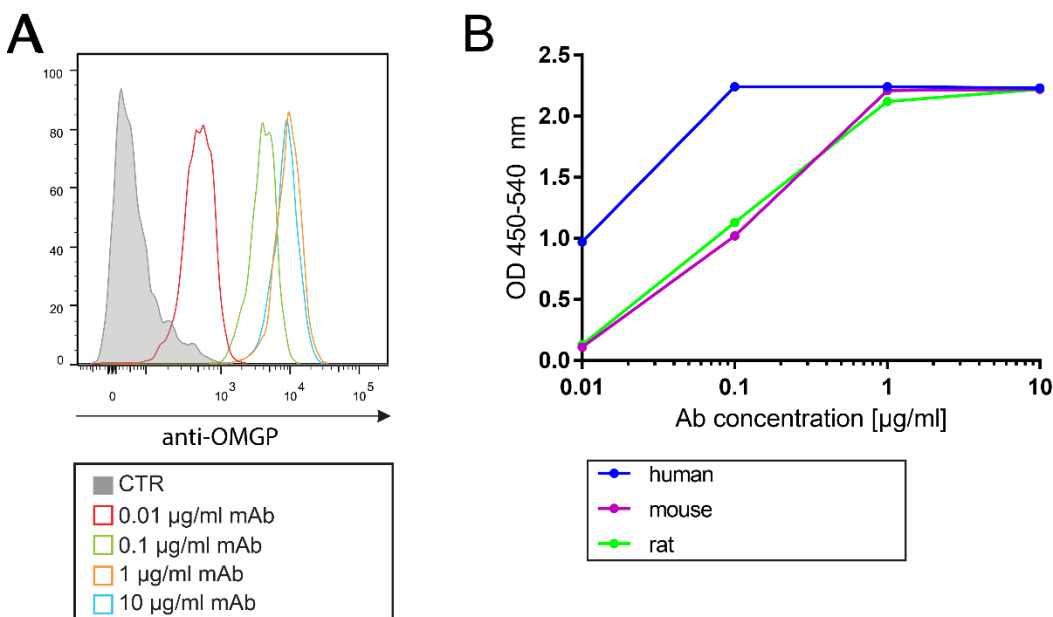
Figure 3.31 Characterization of monoclonal antibody 22H6-hIgG1 in CBA and ELISA

(A) The functionality of 22H6-hIgG1 was proofed in OMGP-TM CBA with four concentrations 10/1/0.1/0.01 µg/ml of the antibody. (B) After Fc part exchange from rIgG2A to hIgG1, the antibody 22H6 still recognized the OMGP antigen from three different species: human (blue), mouse (purple) and rat (green) in MaxiSorp ELISA, coated with 1 µg/ml of human/mouse/rat OMGP. The signals of the antibody of the BSA background wells were subtracted from OMGP coated wells. For plate background correction signal at 540 nm was subtracted from values at 450 nm.

The specificity of this recombinant Ab was elaborated with the human OMGP-TM CBA, showing that this Ab reacted even with a low concentration of 10 ng/ml (Figure 3.31, A). This recombinant mAb was also able to detect mouse and rat OMGP in an ELISA, but the reactivity to rat and mouse OMGP was weaker than to human OMGP (Figure 3.31, B).

The final aim was to test antibodies against OMGP in an animal model and therefore all three selected mAbs (22H6-rIgG2A, 31A4-mIgG2B and 14A9-rIgG2B) as well as 22H6-hIgG1 were evaluated for their C1q binding ability *in vitro* (Figure 3.32).
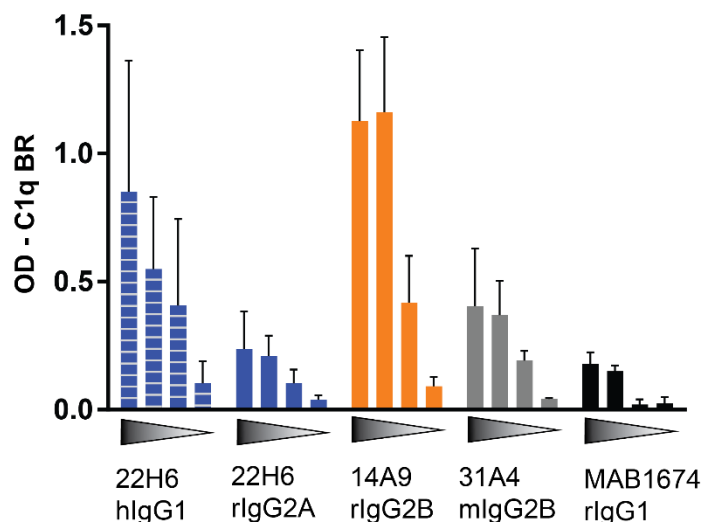
Figure 3.32 C1q protein binding to newly developed OMGP mAbs

C1q complement protein binding ELISA with all selected OMGP mAbs and commercial MAB1674. Grey triangles represent decreasing Ab concentrations 10/1/0.1/0.01 µg/ml. Bars display mean of two replicates with SEM.

Some new antibodies, e.g. 22H6-rIgG2A, 31A4 and commercial MAB1674 hardly bound C1q, whereas 14A9 showed the highest binding affinity. As soon as rIgG2A Fc part from 22H6 was exchanged to hIgG1, a stronger binding to C1q could be achieved.

3.11 Staining of oligodendrocytes and neurons as OMGP expressing cells

Primary mouse oligodendrocyte cultures from O4 positive oligodendrocyte precursor cells (OPCs) and MBP positive oligodendrocytes were stained by Lena Kristina Pfeffer in the lab of Prof. Tanja Kuhlmann together with Laura Starost and Dr. Stefanie Albrecht. It was shown, that O4$^+$ OPCs express OMGP. After maturation to oligodendrocytes, MBP and OMGP double staining was observed, indicating that also mature oligodendrocytes display OMGP. Further results are discussed in her MD project.

3.11.1 Expression of OMGP in human oligodendrocytes

Laura Starost in the lab of Prof. Tanja Kuhlmann in Münster generated human oligodendrocytes from induced pluripotent stem cells (Ehrlich et al., 2017). These cells were fixed and stained with the new established and humanized antibody 22H6-hIgG1 (section 3.10).
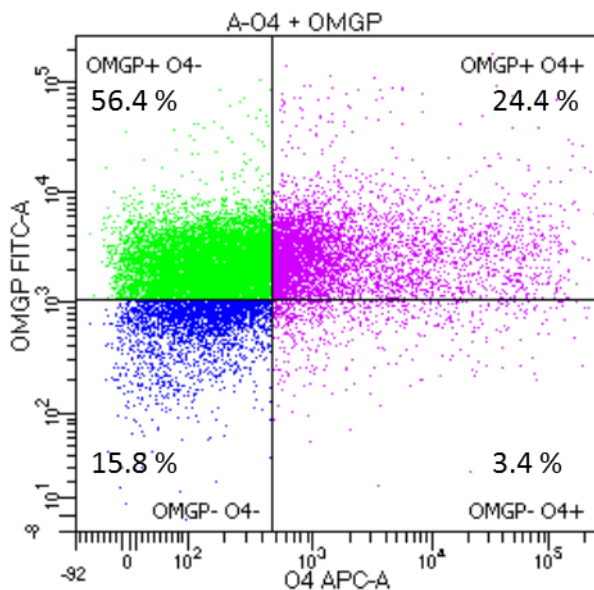
Figure 3.33 Flow cytometer analysis of human induced oligodendrocytes

Dot plot of the flow cytometer shows O4-APC staining on the x-axis, whereas OMGP-FITC signal is displayed on the y-axis. Percentage of cells in each gated group are labeled (analysis done by Laura Starost).

Double positive staining of the early oligodendrocyte marker O4 and OMGP with subsequent analysis by flow cytometer, allowed the identification of 24.4 % of OMGP$^+$/O4$^+$ human induced oligodendrocytes (Figure 3.33). 56.4 % of the cells displayed OMGP on their surface but not O4 and 3.4 % had only the O4 marker whereas 15.8 % had none of those.

### 3.11.2 Expression of OMGP in hippocampal and cortical mouse neurons

It is already described that neurons express OMGP (Habib et al., 1998), but for validation of the newly developed mAbs against OMGP (22H6-rIgG2A, 31A4-mIgG2B and 14A9-rIgG2B), they were tested on primary mouse neurons and double stained with β-III-tubulin. As representative staining of cortical and hippocampal neurons, 22H6 is displayed in Figure 3.34.

OMGP showed a double staining with β-III-tubulin on cortical and hippocampal neurons (Figure 3.34, A), where tubulin was localized in the soma together with OMGP, while in the axons it was less co-expressed. For tissue sections of the spinal cord (Figure 3.34, B), OMGP co-localized with β-III-tubulin in the soma of neurons in the grey matter.

A
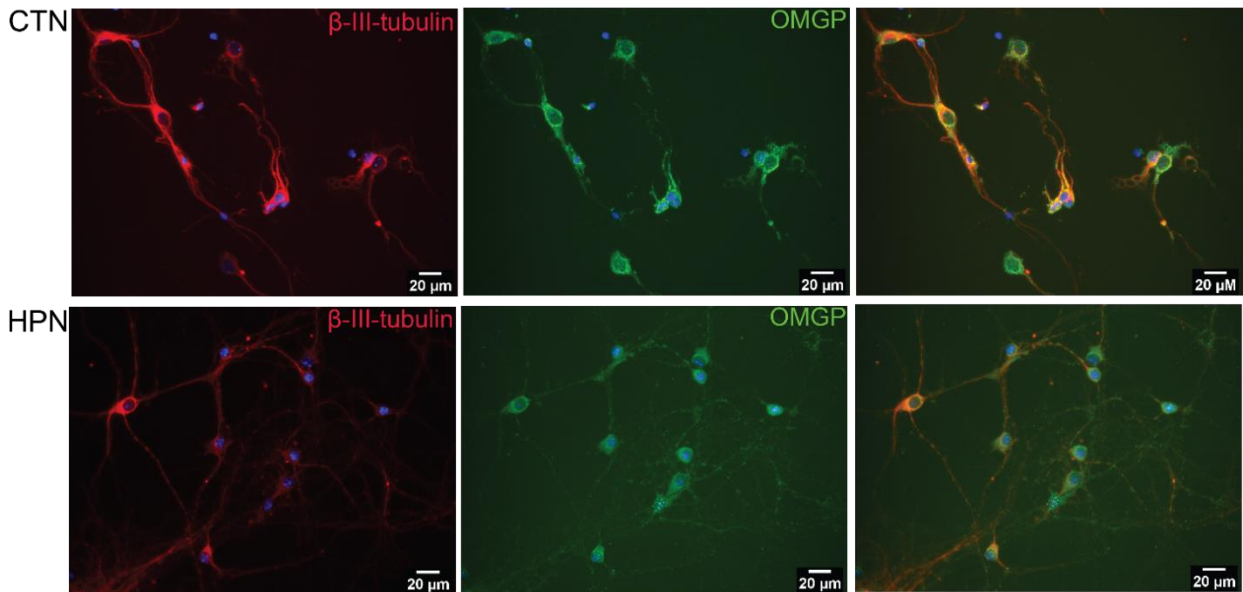
B Spinal cord - grey matter
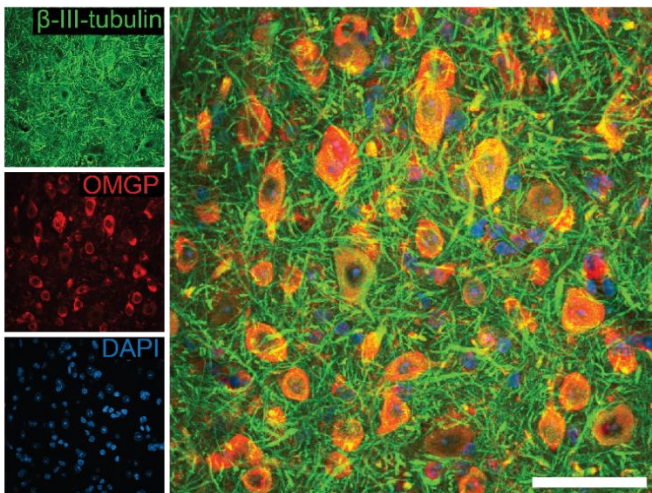
Figure 3.34 Immunofluorescence staining of mouse primary neurons and spinal cord tissue

Staining of anti-OMGP (mAb 22H6, green) on cortical (CTN) and hippocampal (HPN) neurons in combination with β-III-tubulin marker, displayed in red (A). Scale bar represents 20 µm. Furthermore, spinal cord tissue sections of 55 µm were stained with anti-OMGP (red) and β-III-tubulin (green) for visualization in grey matter. Images are stacks from confocal microscopy with 60x magnification and white scale bar indicates 50 µm.

In the previous section, the successful staining of human oligodendrocytes could be shown. Mouse oligodendrocytes were positively stained by Lena Kristina Pfeffer in Münster and discussed in detail in her MD thesis. Furthermore, on mouse neurons the existence of OMGP could be additionally proofed. Therefore, the next step address the evaluation of OMGP autoimmunity in an animal model.

3.12 Pathogenicity of OMGP autoimmunity in an animal model

In this project, Dr. Naoto Kawakami carried out all animal experiments in Lewis rats. Ovalbumin specific cell line T_{OVA} were used as a negative control (CTR), whereas T_{MBP} directed against MBP as positive CTR, since these cells have a strong effect on opening the blood-brain barrier (BBB) (Kawakami et al., 2004). Table 3-5 summarizes the experimental setup and combinations of T cells with antibodies. As positive antibody CTR, the anti-MOG 818C5 was used with the humanized IgG1 Fc part. The ability of its demyelination potential was already proofed in a previous study (Spadaro et al., 2018).

Table 3-5 Overview of i.v. injected T cells and i.t. injected antibodies in EAE rat model

Digits in the table indicate the number of animals injected with the respective T cells and Abs.

	T_{OVA} (15 x 10^6)	T_{MBP} (1.1 x 10^6)	T_{OMGP} (10 x 10^6)
no antibody	3	-	3
818C5-hIgG1	3	3	3
14A9-rIgG2B	-	2	-
31A4-mIgG2B	-	2	-
22H6-rIgG2A	-	2	2
22H6-hIgG1	-	-	3
MAB1674-rIgG1	-	-	3
IvIg	3	-	3
HK3-hIgG1	-	3	3
CTR-rIgG2B	-	2	-
CTR-mIgG2B	-	2	-
CTR-rIgG2A	-	2	2
CTR-IgG1	-	-	3

3.12.1 Inflammation of cortical meninges and SC gray matter caused by T_{OMGP} cells

The first experiment compares i.v. injected T_{OVA} to the newly developed T_{OMGP} cells. These rats neither lost weight nor showed any clinical symptoms. The histology by Prof. Hans Lassmann showed a massive meningitis (Figure 3.35, A), which was mainly located in the cerebral cortex and perivascular, but not in the cerebellum or brain stem (Figure 3.35, B). Nonetheless, some aggregation close to the Virchow Robin space between medulla and cerebellum was observed.
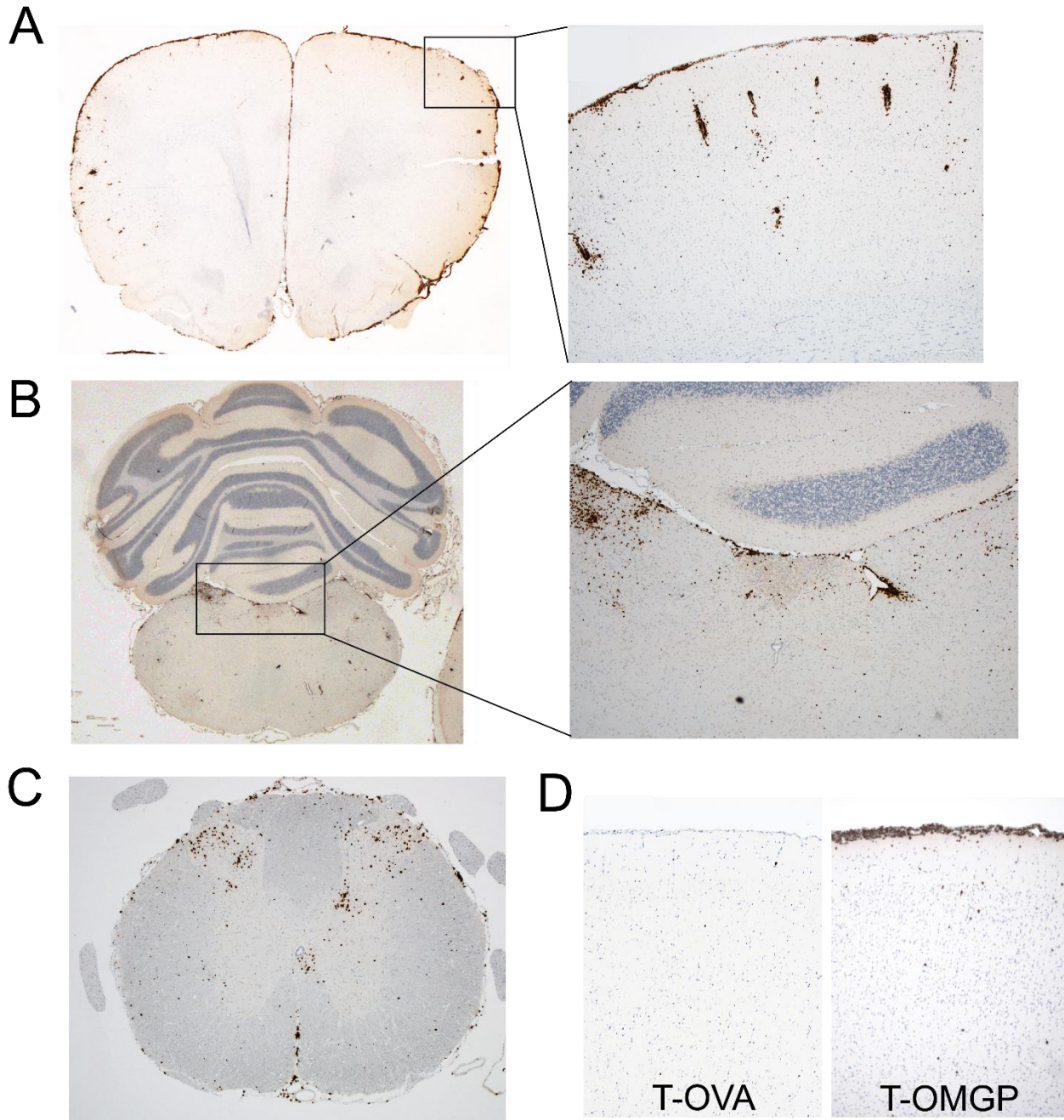
Figure 3.35 Histology of T$_{OMGP}$ cell transfer

The tissue sections were stained for CD3 T cells. Immunostaining was developed with peroxidase and diaminobenzidine as substrate resulting in a brown color, whereas nuclei were counterstained with haemalum solution, giving a blue color. (A) Overview of rat brain displaying cortical meningitis and perivascular inflammation of T cells. (B) No meningitis in brain stem and cerebellum, but spread of T cells close to Virchow Robin space between medulla and cerebellum. (C). Inflammation of T cells in dorsal horn of spinal cord. (D) Negative control cells T$_{OVA}$ were compared T$_{OMGP}$ cell transfer with CD3 staining in the cortex.

Furthermore infiltrations of T_{OMGP} cells into the grey matter of the dorsal horn of the spinal cord were detected (Figure 3.35, C). As negative control for this experimental setup, T_{OVA} cells were injected and compared to the CD3 staining of T_{OMGP} cells in the cortex (Figure 3.35, D).

Overall these newly generated OMGP autoreactive T cells induced an unusual massive meningitis, which was not demonstrated in any other EAE model. With this animal experiment a cortical and grey matter pathology was induced with a strong BBB disruption.

3.12.2 T_{OMGP} synergize with MOG but not OMGP antibodies to mediate demyelination

For the evaluation of the pathogenicity of the OMGP antibodies, five different antibodies (Table 3-5, blue) and one positive CTR MOG antibody (818C5-hIgG1) as well as respective negative CTR antibodies (Table 3-5, grey) were injected two days after the T cell transfer. Largely none of the OMGP antibodies induced any clinical symptoms or showed a histological effect. Even when the strong encephalitogenic MBP specific T cell line was used, there was only the pathology due to the T cells but no enhancement by antibodies. Even, the injection of the humanized antibody 22H6-hIgG1 with the same Fc part as 818C5-hIgG1 didn't lead to demyelination or neurodegeneration. Thus, none of the applied mAbs to OMGP clearly enhanced the pathology mediated by the OMGP-specific T cells.

Interestingly when using T_{OMGP} cells together with the potent MOG antibody, these animals developed a clinical score of 0.5, which indicates a loss of tail tonus and partial paralysis of legs. The histology demonstrated that T_{OMGP} cells open the BBB and pave the way for anti-MOG mediated demyelination. Figure 3.36 illustrates the demyelination of ventral areas in the spinal cord by the MOG antibody. The HE and the LFB staining indicate the loss of white matter. With the CTR antibody no destruction of the spinal cord tissue was seen.
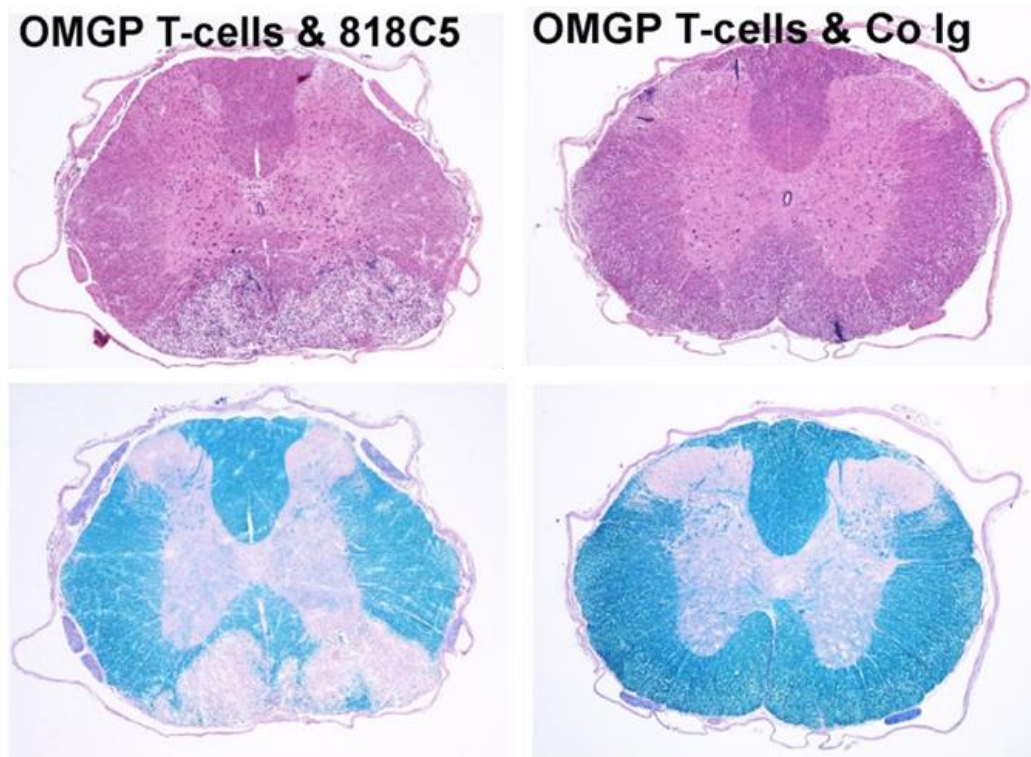
Figure 3.36 T~OMGP~ cells pave the way for anti-MOG mediated demyelination

The left panel displays T~OMGP~ cells injected with 818C5-hIgG1 MOG antibody and the right panel T~OMGP~ cells injected together with CTR antibody (Co Ig). The first row shows hematoxylin and eosin (HE) staining and the second line luxol fast blue (LFB) staining.

In this experimental setup with the MOG antibody also focal demyelinating lesions in the cortex of the rat brain were detected (Figure 3.37). In these lesions an aggregation of CD3 positive T cells, a slight activation of ED1 CD68 macrophages and a massive activation of Iba1 microglia compared to the CTR animal can be seen (Figure 3.37, A). Furthermore, there is an intense staining for rat Ig, human Ig (Fc part of 818C5 MOG antibody) and C9neo complement precipitation due to the BBB disruption (Figure 3.37, B). The loss of MOG indicates the myelin loss and the reduction of the AQP4 marker of astrocytes as manifestation of reactive gliosis (Figure 3.37, C), which is a response to CNS damage, also seen in lesions of NMOSD patients (Misu et al., 2013). Additionally, there is also an increase of the signal for amyloid precursor protein observed in this panel, due to the axonal injury.
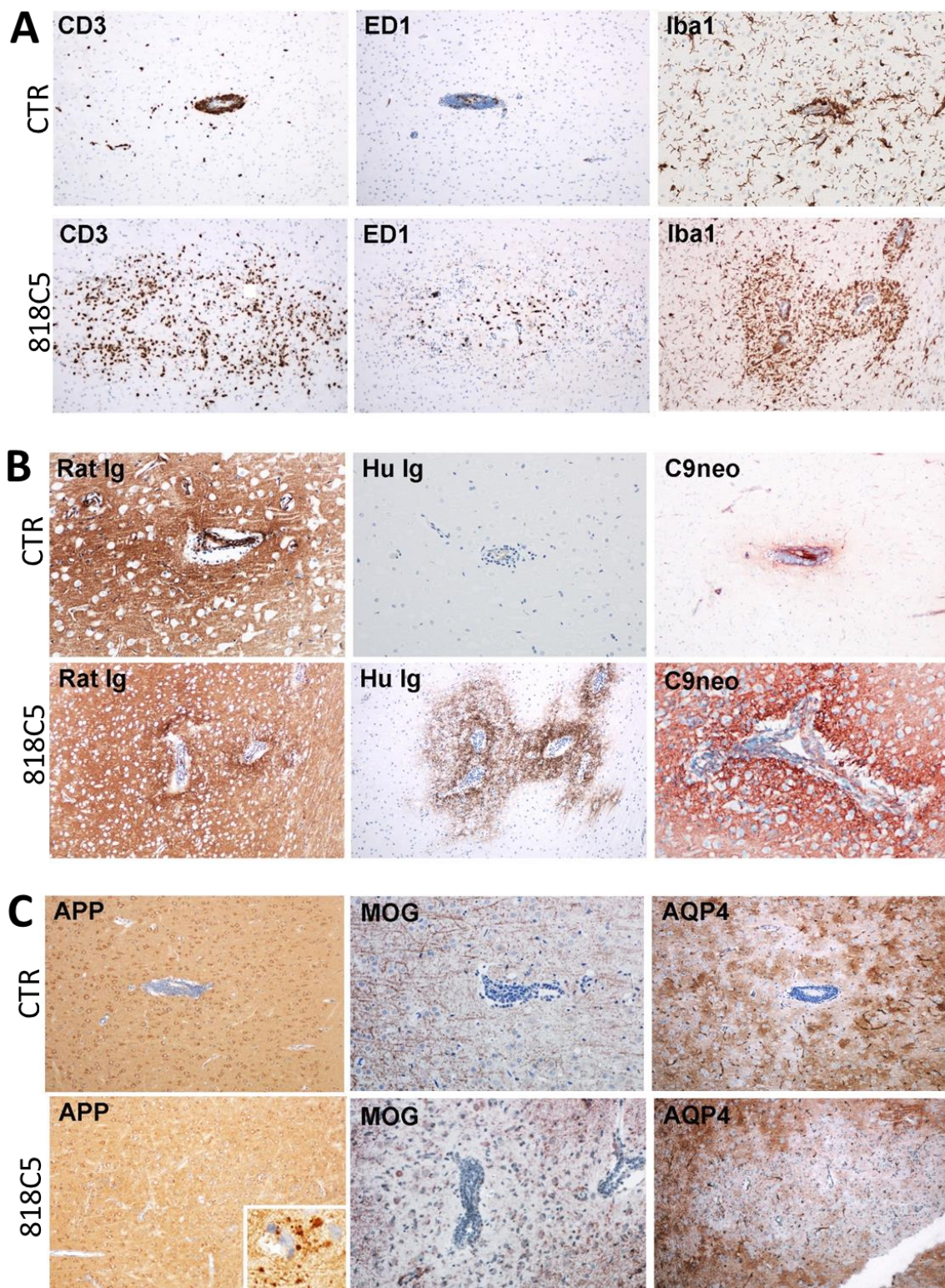
Figure 3.37 Cortical area with a lesion after T$_{OMGP}$ cell transfer together with a MOG Ab

In all panels 818C5-hIgG1 MOG antibody is compared to CTR antibody. (A) T cell staining with CD3, CD68 macrophages (ED1) and microglia (Iba1). (B) The histology is displayed for rat Ig, human Ig and complement deposition of C9neo. (C) Amyloid precursor protein, MOG and AQP4 were stained.

In this animal model OMGP-specific T cells lead to a massive BBB disruption and therefore the i.t. injected antibodies evaded through the inflamed vessels into the peripheral blood and could recirculated into the perivascular space. This view is supported by detection of MOG Abs by ELISA in the blood of animals that had received anti-MOG intrathecally (Figure 3.38).
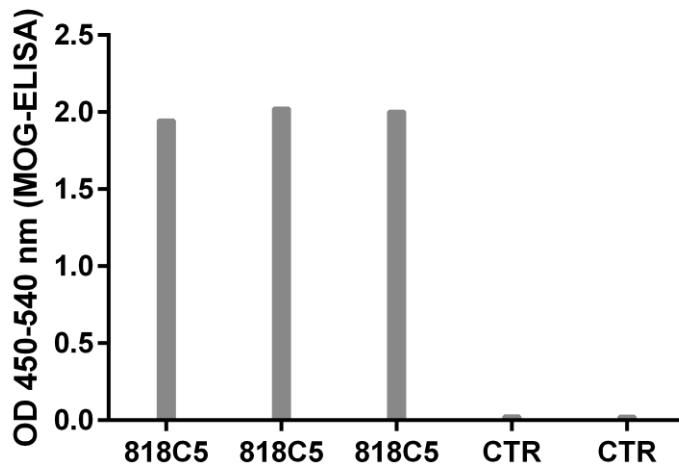
Figure 3.38 Detection of intrathecally injected MOG antibody in the peripheral blood

The MOG antibody 818C5-hIgG1 was detected by MOG STV-ELISA. Before rats were sacrificed, peripheral blood was withdrawn and tested for presence of circulating MOG Abs. The results display the OD measurements of each serum from the five different animals, three for anti-MOG and two for CTR Ig injection. Values are calculated by subtraction of 540 nm value from 450 nm. Further STV background value is subtracted from MOG measurement.

3.13 Human autoreactive T cells against OMGP

Subsequent to the findings in the Lewis rat model, where OMGP T cells induced an inflammatory phenotype with meningitis and BBB disruption, the question arose if patients with MS also have autoreactive T cells which are directed towards OMGP. To address this question, T cell proliferation assays and cytokine analysis of stimulated T cells were conducted.

3.13.1 T cell proliferation analysis upon OMGP stimulation – CFSE and EdU assay

The PBMCs of HCs and patients were cultured with measles, tetanus, OMGP and with the lectin ConA as positive control. This is a potent T cell activator by triggering crosslinking of the T cell receptor complex (Dwyer and Johnson, 1981).

After four and seven days the results of proliferating CD3 positive T cells were compared with CFSE signal reduction or EdU dye uptake. Both methods work in a different way since with EdU

staining the uracil was added 24 h prior analysis and got incorporated into the DNA, which resulted in a gain of the signal as proliferation response of the 24 h time window. Whereas CFSE was added as cell permeable dye on day zero, it coupled covalently to intracellular molecules (Lyons and Parish, 1994). According to this, the dye got diluted out due to proliferation and the signal decreased, but represents a summation of the response of the whole time frame.

In Figure 3.39 one HC donor is demonstrated and the proliferation was analyzed on day four (Figure 3.39, A) and day seven (Figure 3.39, B). Respectively, the gate of proliferation is defined by the unstimulated control. On day four, T cells had a high proliferation response of 66 % analyzed with CFSE and 71.8 % with EdU towards ConA, whereas on day seven it was already reduced to 15.6 % with EdU since the cells were exhausted. The CFSE staining increased a bit to 85.6 % and represent the summation of the proliferation events over the last seven days. The tetanus antigen induced also a T cell response, which was hardly detectable on day four with 2.9 % for EdU and 0.25 % for CFSE, but much more on day seven with 4.97 % for EdU and 2.57 % for CFSE. The same goes for the measles antigen where 5.55 % of the EdU stained T cells and 0.33 % of the CFSE proliferated on day four. On day seven this increased for CFSE stained T cells to 9.19 %, whereas for Edu it stayed with 4.69 % in the same range as detected on day four. The low proliferation response of T cells against OMGP with 1.73 % for EdU and 0.16 % for CFSE on day four increased slightly on day seven to 2.01 % for CFSE, whereas it stayed for EdU with 1.79 %.

These experiments with healthy controls showed that the analysis on day seven is better since the signal can still increase over the time and a proliferation of rare T cells might be better seen by the summation of the response when using CFSE.

In the following experiments the response of patients having autoantibodies against OMGP were analyzed for their T cell autoreactivity after seven days using the CFSE assay. Also frozen PBMCs, as in previous experiments with HC, were stimulated using ConA, measles, tetanus, OVA as negative control and OMGP. In Figure 3.40 the responses of the index patient 2492 and the limbic encephalitis patient 1014 are displayed. Patient 2492 had a higher spontaneous proliferation in the unstimulated condition of 0.53 % compared to 0.034 % in the other patient. Both reacted with 81 % similarly to the positive control ConA and also to tetanus with 2.13 % in 2492 and 1.76 % in 1014. For measles antigen the proliferation response was 4.32 % for patient 2492 and 2.12 % for patient 1014. The OMGP response for the sample 2492 was comparable to the negative control OVA and below 1 %. In one OMGP stimulation well, patient 1014 responded with 2.28 % of proliferation, which was higher than the OVA background of 0.11 % proliferation.
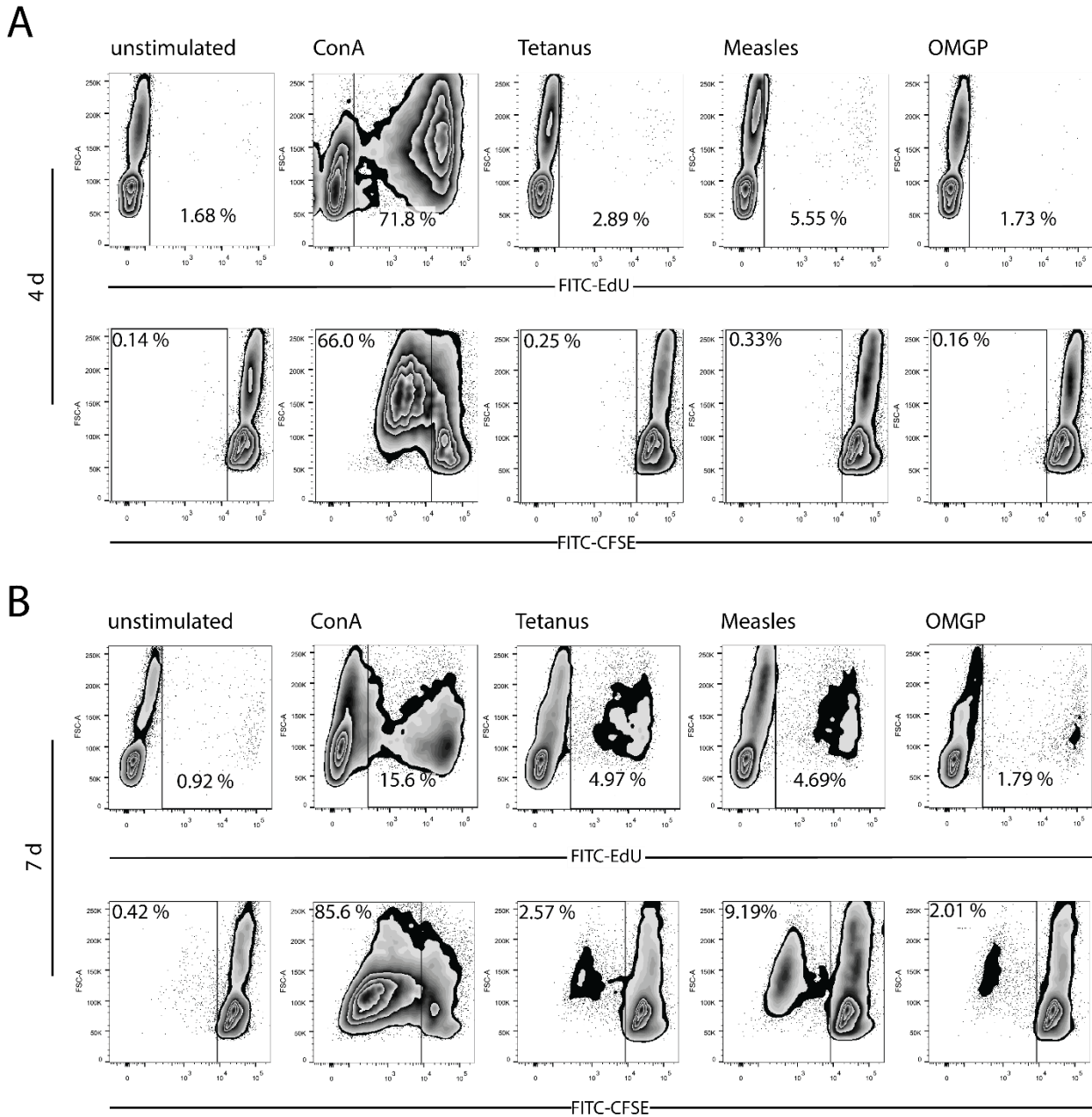
**Figure 3.39 Proliferation analysis of HC PBMCs using EdU and CFSE staining**

The zebra plots show the proliferation of T cells from a healthy control after stimulation with Concavalin A (ConA), tetanus, measles and OMGP antigens on day four (A) and day seven (B). The x-axis indicates the used staining solution EdU or CFSE, whereas CFSE indicates proliferation by signal reduction and EdU displays proliferation through dye uptake and therefore an increase in signal. The gate of proliferation is set by the unstimulated control, respectively.
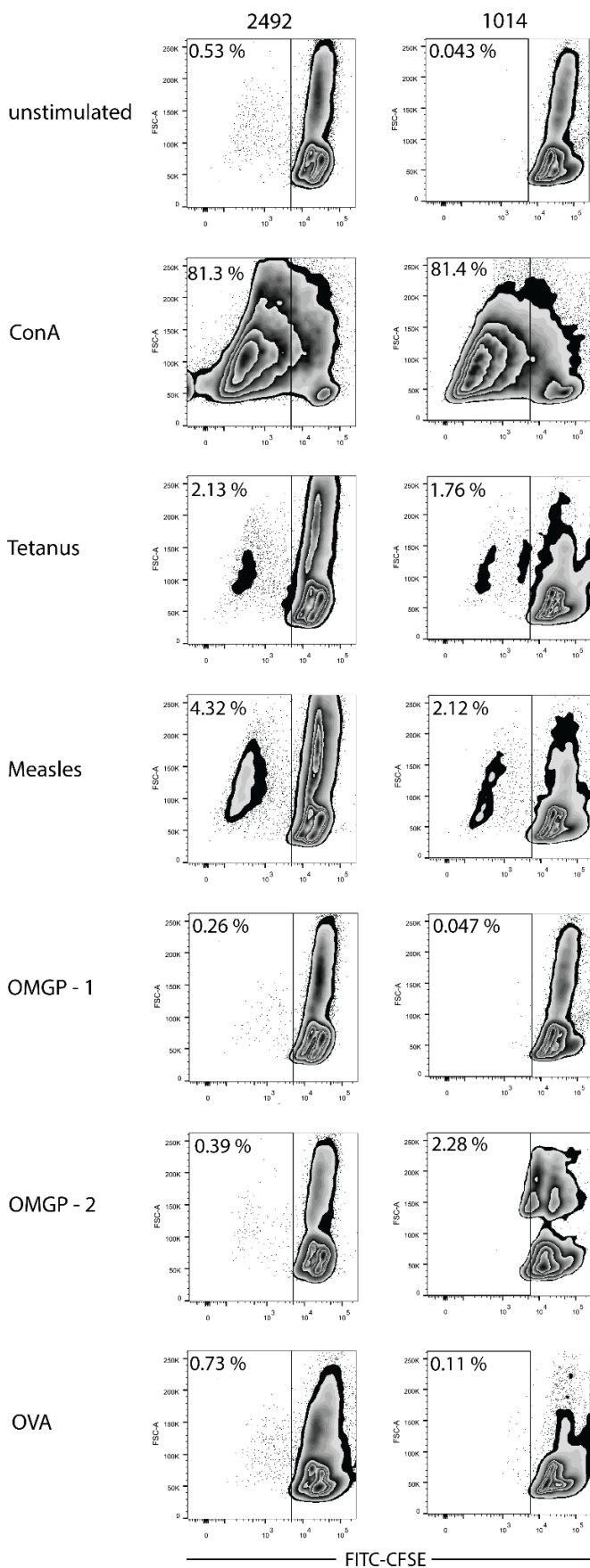
Figure 3.40 CFSE T cell proliferation analysis of two patients with frozen PBMCs

The index patient 2492 and the limbic encephalitis patient (1014) were stimulated with Concanavalin A (ConA), tetanus, measles, duplicates of OMGP (OMGP-1, OMGP-2) and ovalbumin. The x-axis of the graphs represent the loss of CFSE signal due to proliferation, whereas the y-axis displays signals of the forward scatter (FSC). Proliferation gate is set regarding the unstimulated control.

Another possibility for increasing the proliferation rate of autoreactive T cells was the usage of fresh preparations of PBMCs instead of frozen PBMCs. The index patient 2492, could be analyzed with freshly isolated and stimulated PBMCs (Figure 3.41).
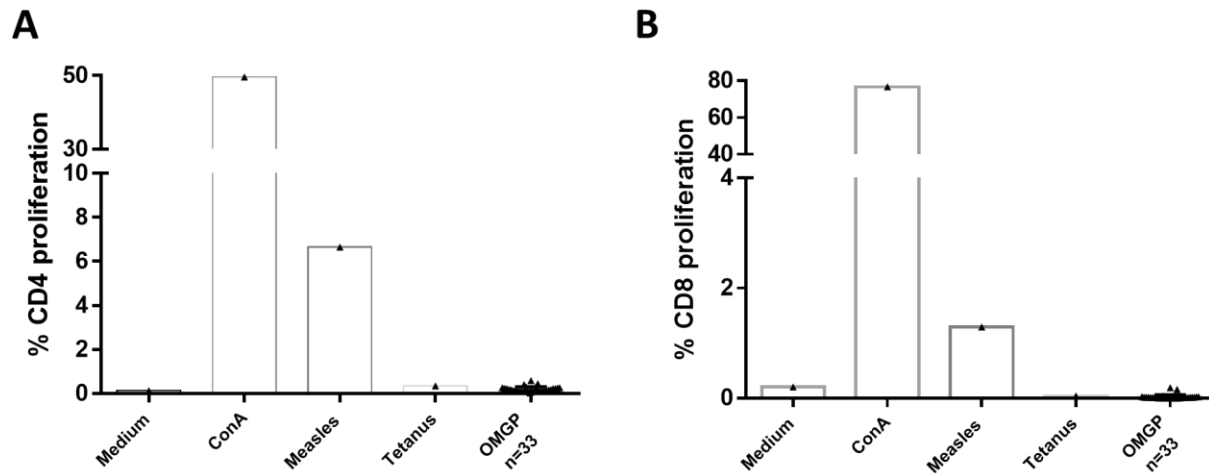
Figure 3.41 CD4/CD8 positive T cell proliferation of freshly isolated PBMCs of patient 2492

The graphs represent the proliferation of $CD3^+/CD4^+$ (A) or $CD3^+/CD8^+$ (B) in the CFSE assay after seven days. As stimulus Concavalin A (ConA), measles, tetanus and OMGP were used.

By using fresh PBMCs the ConA proliferation rate of $CD3^+/CD4^+$ T cells (Figure 3.41, A) was 49.6 %, with measles 6.64 %, tetanus 0.34 % and the mean proliferation rate of all 33 OMGP stimulated wells with 0.19 % similar to the background level of medium with 0.13 %. The results looked similar for $CD3^+/CD8^+$ T cells (Figure 3.41, B): 76.6 % proliferation with ConA, 1.29 % with measles, tetanus induced 0.04 % and the mean proliferation rate of all 33 OMGP stimulated wells was 0.02 %. The medium background was with 0.2 % proliferation rate similar to the value observed with $CD3^+/CD4^+$ T cells.

In summary, no OMGP-specific T cell response in 33 stimulation wells was induced by using fresh PBMCs and analyzing the CD4 and CD8 percentage of CFSE proliferation by flow cytometer. This patient responded to measles more than to tetanus, which was already seen in the previous experiment with frozen PBMCs (Figure 3.40). In conclusion with these experiments, no OMGP-specific T cells could be reliably identified in the blood of the analyzed patients.

3.13.2 Cytokine analysis of T cells as readout upon OMGP stimulation

Higher sensitivity in detection of rare autoreactive T cells might be given by the analysis of cytokine production in the supernatant of stimulated T cells. For these experiments eight new and untreated CIS/MS patients were collected and the stimulation was carried out on freshly isolated PBMCs. In addition, seven healthy controls with fresh PBMCs were included.

The first try was the measurement of the T cell specific cytokine IL-17 in the supernatant on day seven after stimulation with OMGP and positive control antigens like tetanus and measles. The IL-17 signals was extremely low and hardly reached the lowest value of the standard curve from the ELISA. Thus, another cytokine IFNγ, which results in much higher levels, was analyzed. In summary each patient was stimulated with 6-56 wells of OMGP and control wells respectively. In total 287 OMGP stimulated wells were analyzed regarding the IFNγ production in the supernatant. Thereby an OMGP-specific IFNγ production in both patient and control group could be detected.

As it turned out later, these results do not give any conclusions about OMGP autoreactive T cells, since different OMGP preparations were used and throughout the evolution of the project various endotoxin contaminations in the protein preparations were detected.

3.13.3 Strong lipopolysaccharide (LPS) effect on T cell stimulation assays

For analyzing the effect of the endotoxin contaminations from the in house produced OMGP, the CFSE assay and IFNγ analysis were re-evaluated using LPS as control stimulations. Fresh PBMCs of the index patient 2492 were stimulated with 100/10/1/0 pg/ml of LPS and CD4 as well as CD8 proliferation were analyzed (Figure 3.42). $CD3^+/CD4^+$ T cells (Figure 3.42, A) responded still with low concentration of 10 pg/ml of LPS with 2.46 % proliferation. The results were a bit lower, but the effect was comparable with $CD3^+/CD8^+$ T cells (Figure 3.42, B), that small concentrations of LPS induced a proliferative response.

A **B**
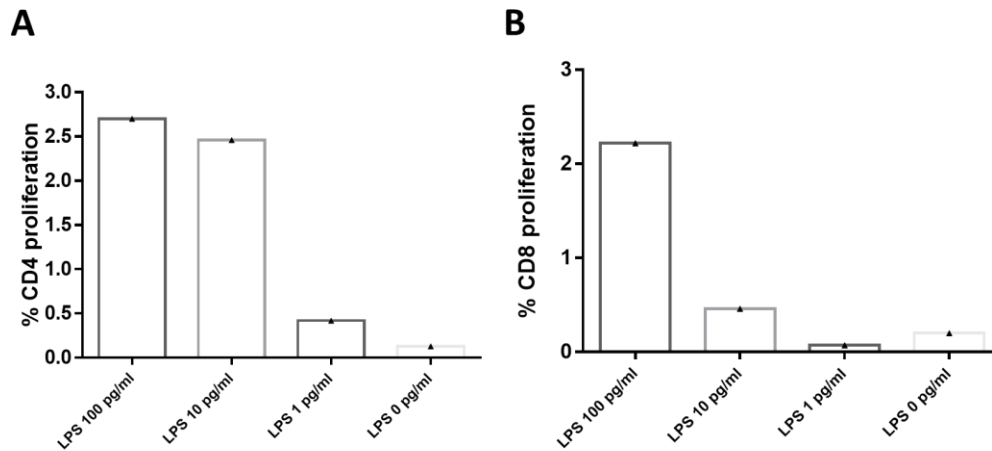
Figure 3.42 LPS effect on T cell proliferation in CFSE assay

Graphs show the result of CD3^{+} gated cells of the flow cytometer analysis. PBMCs of patient 2492 were stimulated with the indicated concentrations of LPS and CD3^{+}/CD4^{+} proliferation rate (A) or CD3^{+}/CD8^{+} proliferation rate (B) is calculated on day seven after stimulation.

There was a strong effect of LPS on the proliferation of T cells. Already small amounts of 10 pg/ml of this endotoxin induced an immune response compared to 0 pg/ml of LPS. It is necessary to use this as control parameters in all experiments to exclude false positive results due to LPS induction of an immune response. Having endotoxin contaminations above 1 pg/ml, it is hardly possible to detect a correct autoreactive T cell response, which might additionally result in only a few percentage.

The same effect could be seen by analyzing the IFNγ response after stimulating PBMCs with LPS (Figure 3.43). 30 wells in each condition of one freshly stimulated healthy donor are displayed. There was a big variation throughout the wells in one condition. Furthermore, it was indicated that already small amounts of 1 pg/ml induce a mild IFNγ secretion of 5 pg/ml in average, whereas 100 pg/ml of LPS resulted in 415 pg/ml of IFNγ in the supernatant.
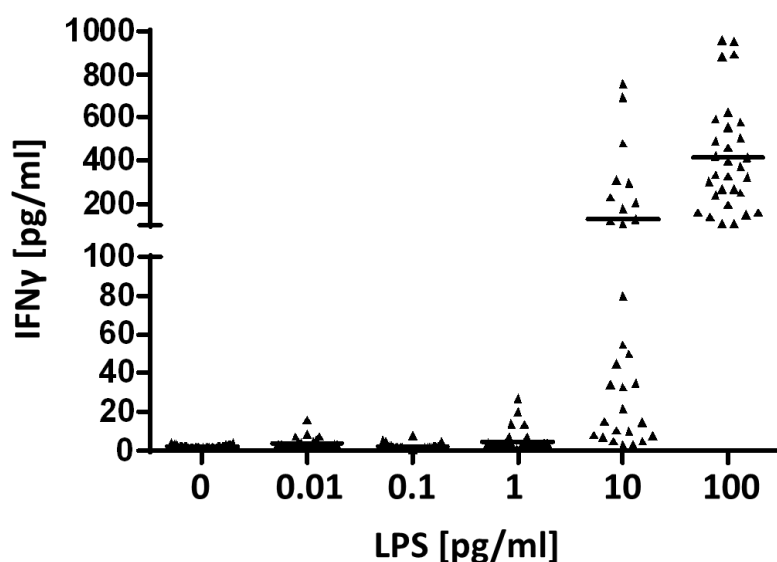
Figure 3.43 LPS stimulates IFNγ production of PBMCs

PBMCs of one healthy donor were stimulated with indicated concentrations of LPS and IFNγ values were measured by ELISA. Individual concentrations of LPS were tested in 30 wells of a 96 well plate and each triangle represents one well.

Since a strong effect was seen, all in house produced OMGP preparations were analyzed in limulus amebocyte lysate assay and various LPS contaminations from 0.22 to 132 ng/ml are detected (Table 3-6).

Table 3-6 LPS contaminations in OMGP protein preparations

OMGP preparations	Stock protein concentration [mg/ml]	LPS stock concentrations [ng/ml]	Other center LPS measurements [EU/ml]	Final LPS concentrations [pg/ml] in 50 µg/ml of OMGP in assays
March 2016	4.5	0.22 (=2.2 EU/ml)		2.5
Feb 2017	7.9	2.7 (=27 EU/ml)		17
Nov 2017	7.9	11.7 (= 117 EU/ml)	2.5 and 6	75
Dec 2017	10	132 (=1320 EU/ml)	1533 and 2243	660

These used proteins have a high variability in the endotoxin/LPS contaminations. The range in the final concentration in CFSE T cell proliferation assay or in IFNγ ELISA is from 2.5 pg/ml to 660 pg/ml. It is shown in Figure 3.42 and Figure 3.43 that already 1 pg/ml induced proliferation or cytokine production in a few wells, which might lead to false positives in the readout for rare OMGP autoreactive T cells. Neither the CFSE proliferation assay, nor the IFNγ evaluation in the supernatant could therefore give reliable results by the use of the endotoxin contaminated OMGP protein.

Purification processes via LPS removal columns failed and therefore a collaboration with Mattias Bronge in the lab of Prof. Hans Grönlund at the Karolinska Institute in Stockholm was initiated.

3.13.4 Identification of a few MS patients with OMGP-specific T cells by FluoroSpot assay

Mattias Bronge and Prof. Hans Grönlund published in 2019 a bead-based T cell stimulation method, where antigen coupled beads can be washed for LPS removal (Bronge et al., 2019b). The LPS was removed by washing steps with 0.01/0.1/0.5/1 M NaOH. The quality control of successful coupled antigen to magnetic beads was carried out by positive staining of anti-OMGP or anti-His-tag antibody in flow cytometry. As control beads, uncoupled (neg-CTR) and Avi-His-tag coupled beads were used. This allowed to control, if patients react to those tags, which also appear in the OMGP construct.

As antigen OMGP-Dec17 preparation with 132 ng/ml LPS (Table 3-6) was used for the coupling to the magnetic beads. The results of successful coupling of OMGP antigen or Avi-His peptide are displayed in Figure 3.44. The analysis was carried out on single, aggregated and total number of beads. As example of gating, negative CTR beads (Figure 3.44, A) are displayed in the forward (FSC) and side scatter (SSC) with 51 % of aggregate formation and 48.9 % of single beads. Similar results were observed for the OMGP beads aggregation and Avi-His beads. Furthermore, the anti-OMGP antibody didn't bind unspecific to the neg-CTR beads. The coupling of OMGP to the beads resulted in 98.7 % positive staining of these beads (Figure 3.44, B), whereas the control of the secondary antibody was negative. Also the coupling of Avi-His peptide with 95.5 % was highly efficient and no or extreme low unspecific staining of the secondary antibody was seen.

The beads with OMGP, having a high LPS contamination due to preparation, were washed with harsh conditions of 1 M NaOH. Nevertheless the detection by the OMGP antibody in the flow cytometer was with 98.7 % highly positive. The Avi-His peptide was produced LPS free by chemical synthesis and therefore these control beads were only washed with PBS.
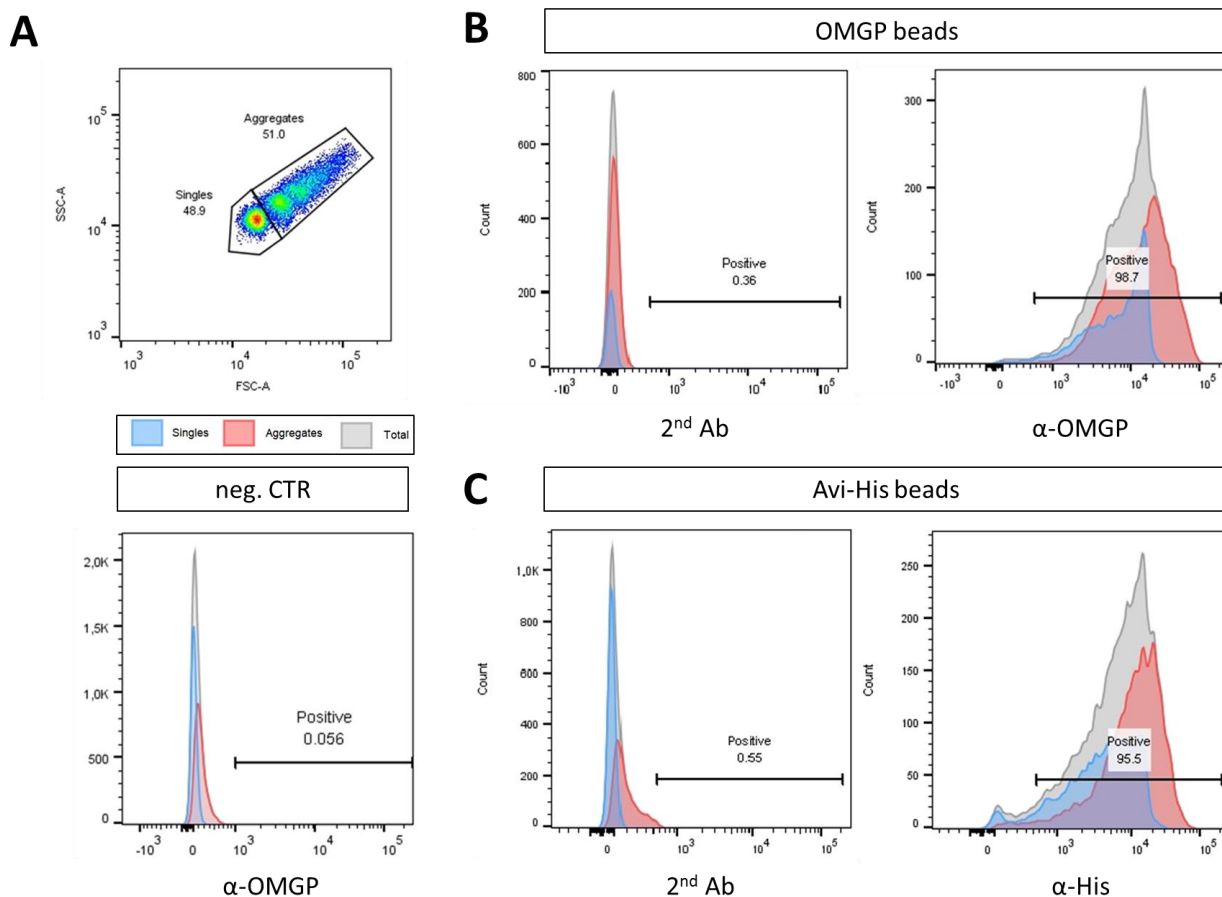
Figure 3.44 Flow cytometry quality control of OMGP and Avi-His-tag coupling to the beads

The gating of the analysis is displayed in A as example on negative control beads (neg-CTR, uncoupled), where single (blue), aggregates (red) and total beads (grey) can be separated in the forward scatter (FSC-A) and side scatter (SSC-A). No unspecific binding of OMGP antibody to the neg-CTR beads is displayed. Coupling of OMGP to the beads is illustrated in B, where the secondary antibody CTR (2nd Ab) stains nothing and on the right side of B the positive antibody staining of anti-OMGP is displayed. These OMGP beads were washed with 1 M NaOH. (C) Avi-His beads were washed with PBS. There the 2nd Ab staining as control is shown on the left side and the positive anti-His staining on the right side.

To analyze the washing efficiency and also the required amount of NaOH, a wash titration from 0.01 M to 1 M NaOH treated OMGP beads was tested with six healthy controls and evaluated by IFNγ, IL-22 and IL-17A FluoroSpot assay (Figure 3.45). A decline in the signal of all three cytokines was observed by washing with high NaOH concentrations of 0.5 or 1 M. The number of IFNγ spot forming units (SFUs) per 2.5 x 10^5 stimulated PBMCs was always higher than for the other cytokines IL-22 and IL-17A.
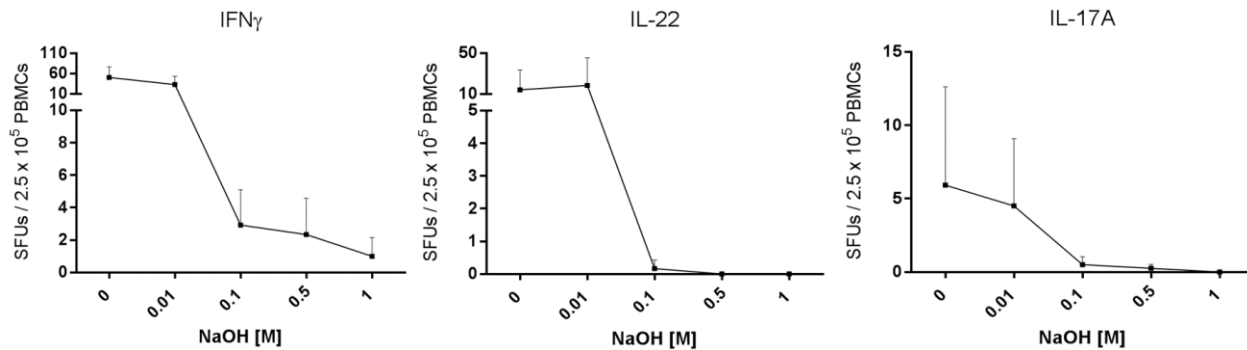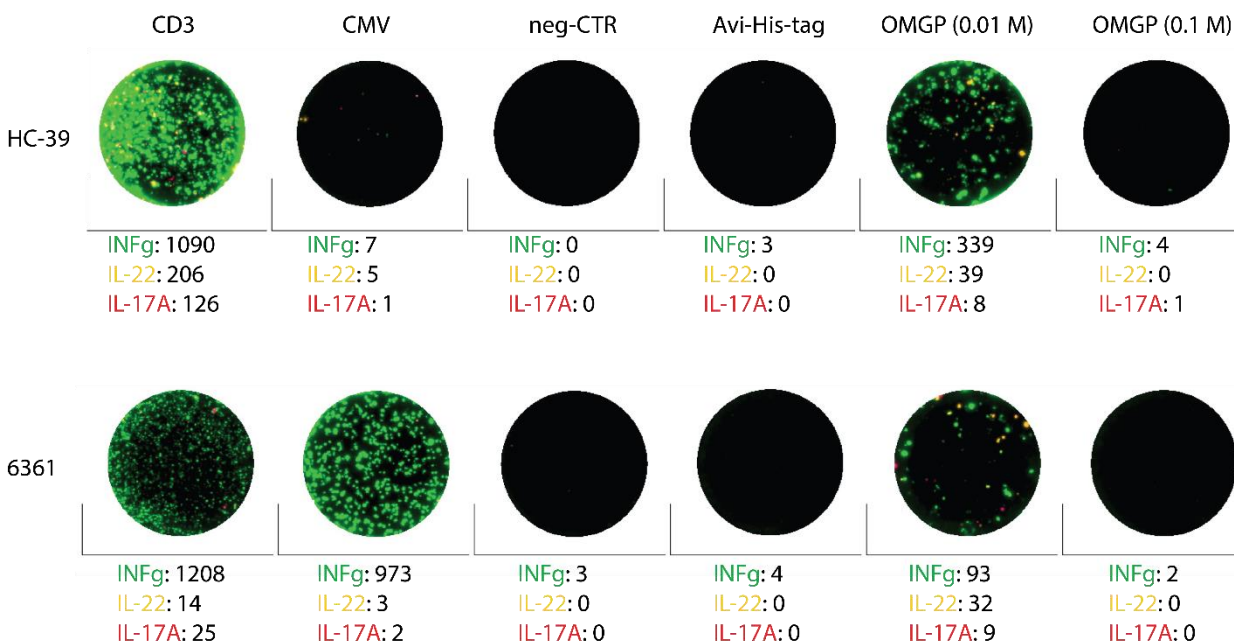
Figure 3.45 Wash titration analysis of OMGP beads in FluoroSpot assay

The graphs illustrate the LPS removal effect by 0.01/0.1/0.5/1 M NaOH (x-axis) washing procedure. Values display the mean and standard deviation of six healthy individuals. IFNγ, IL-22 and IL-17A secretion were measured by spot forming units (SFUs) per 2.5×10^5 PBMCs of technical duplicates from each donor.

These results indicated the best signal to noise ratio by using 0.1 M NaOH washing condition on OMGP beads. To exclude the loss of some low positive autoreactive patients, also less harsh washing condition with 0.01 NaOH OMGP beads was included in the analysis.

The screening for autoreactive T cells was conducted with 53 donors: 17 HCs, 19 untreated and 17 natalizumab (anti-α4-integrin) treated patients. Due to exclusion criteria, which is first anti-CD3 positive stimulation response with SFUs below 100, ten donors were removed from analysis (two healthy, three untreated and five natalizumab treated donors). Regarding second and third criteria, one HC donor had no comparable technical duplicates and another HC sample reacted unspecific to the negative uncoupled control beads were excluded. The remaining cohorts with 13 HCs, 12 natalizumab and 16 untreated patients were then included in the final analysis.

Figure 3.46 shows the immunofluorescence pictures of one HC-39 and one untreated patient 6361 with all six stimulation conditions. CD3 induced in both samples a strong response of cytokine IFNγ, 1090 in HC and 1208 spots in untreated patient sample detected with a secondary antibody coupled to FITC (LED490). The yellow signal, detected by Cy3 (LED550) secondary antibody, represents IL-22 production, 206 spots in the HC-39 and 14 spots produced by patient 6361. CD3 stimulation induced 126 red IL-17A spots in the HC-39 and 25 spots in the untreated patient. This was detected in LED640 channel by an antibody coupled to Cy5. The stimulation with CMV beads (coated with antigenic peptides from cytomegalovirus) lead only in the untreated patient to a response of 973 IFNγ spots, three IL-22 spots and two IL-17A spots but no cytokine production by the PBMCs of the healthy donor was induced.

	CD3	CMV	neg-CTR	Avi-His-tag	OMGP (0.01 M)	OMGP (0.1 M)
HC-39	INFg: 1090 IL-22: 206 IL-17A: 126	INFg: 7 IL-22: 5 IL-17A: 1	INFg: 0 IL-22: 0 IL-17A: 0	INFg: 3 IL-22: 0 IL-17A: 0	INFg: 339 IL-22: 39 IL-17A: 8	INFg: 4 IL-22: 0 IL-17A: 1
6361	INFg: 1208 IL-22: 14 IL-17A: 25	INFg: 973 IL-22: 3 IL-17A: 2	INFg: 3 IL-22: 0 IL-17A: 0	INFg: 4 IL-22: 0 IL-17A: 0	INFg: 93 IL-22: 32 IL-17A: 9	INFg: 2 IL-22: 0 IL-17A: 0

Figure 3.46 IF pictures from FluoroSpot analysis showing all screening conditions

The upper row displays as an example one HC-39 and the lower row one untreated patient (6361) with all six screening conditions: positive CTR anti-CD3, CMV (antigenic peptides from cytomegalovirus) beads, neg-CTR (uncoupled beads), Avi-His-tag coupled beads (PBS washed) and OMGP beads washed before with either 0.01 M or 0.1 M NaOH. IFNγ was detected by an antibody coupled to FITC (LED490), IL-22 by Cy3 (LED550) and IL-17A by Cy5 (LED640). In all wells 2.5×10^5 PBMCs were stimulated, except in the CD3 condition, where only 1.25×10^5 PBMCs were seeded.

The neg-CTR beads and the Avi-His-tag beads did neither produce IL-22 spots, nor IL-17A spots. Only a low number of 3-4 IFNγ spots in the HC and patient 6361 were detected. OMGP beads, washed with 0.01 M NaOH, induced in the HC a moderate number of 339 IFNγ spots, 39 IL-22 spots and eight IL-17A spots. In the patient 6361, IL-22 and IL-17A were similar with 32 and nine spots, but IFNγ response was with 93 spots 3.6 times lower than in the HC. Most likely, these numbers are unspecific results and coming from the higher LPS contamination, since the numbers decline if PBMCs, which were stimulated with cleaner OMGP (washed with 0.1 M NaOH). This bead preparation induced four IFNγ spots in the HC and two in the patient. For this reason the final evaluation of OMGP-specific autoreactive T cells was carried out on samples stimulated with the 0.1 M NaOH washed antigen.

In all samples of the entire screening, anti-CD3 and CMV beads as positive controls were included. These responses from 13 HCs, 12 natalizumab and 16 untreated patients towards this stimuli are shown in Figure 3.47.
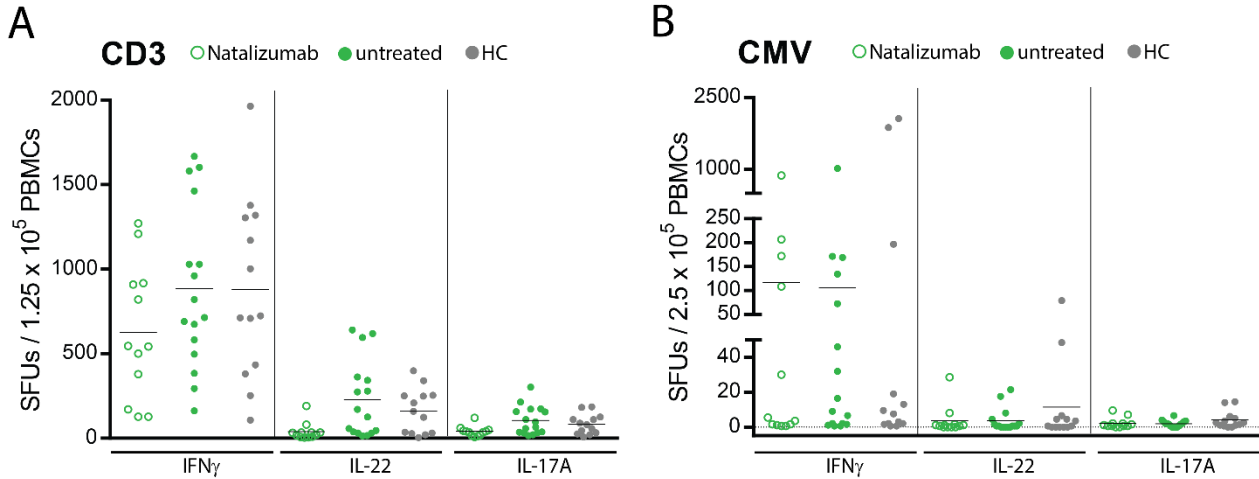
Figure 3.47 IFNγ, IL-22 and IL-17A response after anti-CD3 or CMV beads stimulation

FluoroSpot analysis of 12 natalizumab (green open circles), 16 untreated (green closed circles) patients and 13 HCs (grey circles) donors are displayed. The spot forming units (SFUs) of CD3 are based on 1.25×10^5 PBMCs in the stimulation well (A), whereas CMV response (B) is coming from 2.5×10^5 PBMCs per well. Each cytokines were evaluated separately and are indicated on the x-axis. Every symbol represents the mean of two technical replicates.

CD3 stimulation response of IFNγ from 1.25×10^5 PBMCs was on average in all three cohorts similar: 627 SFUs in natalizumab cohort, 885 SFUs in untreated and 882 spots in HC group (Figure 3.47, A). IL-22 cytokine response varied from 39 spots in natalizumab group to 228 spots in untreated cohort and 162 spots in HCs. The numbers of SFUs by IL-17A producing cells were in average 40 in natalizumab, 105 in untreated and 83 in HC group.

The reactivity to CMV (Figure 3.47, B) was mainly coming from T cells producing IFNγ. Numbers of SFUs were based on 2.5×10^5 stimulated PBMCs. 105 SFUs in untreated, 117 SFUs in natalizumab and 322 SFUs in HC cohort were detected on average. The values of IL-22 and IL-17A were very low and can be disregarded since CMV response is known to induce mainly IFNγ cytokine (Tay and Welsh, 1997).

In PBMC cultures responding to the positive control anti-CD3, the autoreactivity of these samples towards OMGP was evaluated. Therefore, single cytokine SFUs from IFNγ, IL-22, IL-17A, as well as double and triple positives were analyzed in Figure 3.48. Values are displayed as ΔSFUs / 2.5×10^5 stimulated PBMCs, since numbers of Avi-His beads as background signal are subtracted. For each cytokine, a cutoff was calculated which represents the mean value of the HC measurements plus three SDs.

The response against the autoantigen OMGP, was in all cohorts with values from 0 to 9.5 compared to CMV responses (Figure 3.47, B) with SFUs till 2060 quite low. This is not surprising, since it is an autoreactive target and not as often attacked as a viral peptides coming from CMV.
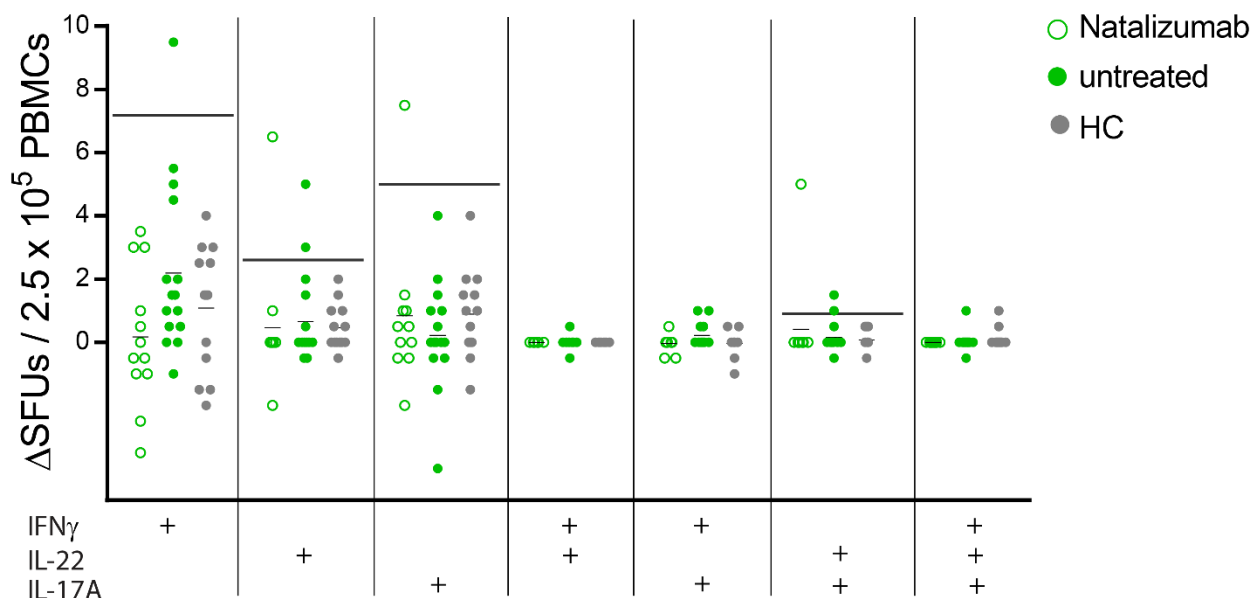
Figure 3.48 OMGP beads stimulated IFNγ, IL-22 and IL-17A production

OMGP beads, washed with 0.1 M NaOH, stimulated IFNγ, IL-22 and IL-17A production of PBMCs from 12 natalizumab (green open circles), 16 untreated (green closed circles) and 13 HCs (grey circles). Values represent ΔSFUs per 2.5 x 10^5 PBMCs in each well, since Avi-His-tag SFUs numbers were subtracted from OMGP numbers respectively. Each circle represents the mean of two technical replicates. Plus symbols below x-axis indicated the analysis of the labeled cytokine. The last column displays the analysis of triple positive SFUs. Horizontal lines in the cytokine columns are cutoff lines, which are calculated by mean of HC values plus three SDs. Columns with no cutoff line have either a value of zero or no sample reaches numbers above it. The cutoff SFUs are: 7 in IFNγ, 2.6 in IL-22, 5 in IL-17A and 0.9 in IL-22$^+$/IL-17A$^+$ assay. The green natalizumab patient above the cutoff is the same donor, whereas five values in the untreated cohort are coming from four different donors.

The IFNγ signal after OMGP stimulation resulted in one untreated patient with 9.5 ΔSFUs, which is above the cutoff of 7. The analysis of IL-22 lead to two untreated patients and one natalizumab patients above the cutoff of 2.6. Additionally, the same natalizumab patient scored positive for the IL-17A cytokine. By evaluating the most prominent autoreactive cytokines, IL-22 and IL-17A double positives, the same natalizumab patient 6334 was detected with 5 ΔSFUs above the cutoff of 0.9. Additionally, two other untreated patients 5397 and 5681 reached values of 1.5 and 1.0 ΔSFUs, which are slightly above the cutoff.

Finally, this bead-based stimulation method is a reliable detection method for rare autoreactive T cells towards OMGP, since the effect of LPS can be controlled by NaOH washing, which allows the removal of endotoxins. Furthermore, it is sensitive enough to pull out four untreated and one natalizumab treated patient by higher IFNγ, IL-22 and IL-17A cytokine production.

4. DISCUSSION

This study identified autoantibodies to OMGP in a few percent of patients with MS using stringent criteria and different assays. For the detection of autoantibodies, CBAs were developed, with two different anchoring methods of the antigen and an ELISA. Further, in cooperation with Dr. Naoto Kawakami and Prof. Hans Lassmann it was found by a newly developed EAE animal model, that autoimmunity to OMGP is pathogenic. Thus, detection of autoantibodies might be useful in the future to stratify patients with inflammatory CNS disorders.

4.1 Development of assays for the identification of OMGP autoantibodies in patients

The first aim of this thesis was to identify patients with Abs to OMGP. To this end, several tests were developed. Autoantibodies can be assessed by various methods using ELISA or WB among others (Xiao et al., 1991). Live CBAs are the gold standard for the detection of several autoantibodies against many membrane-bound surface antigens, such as MOG-IgG (Yeh and Nakashima, 2019). Therefore, reactivity against OMGP was evaluated using two variants of the antigen, transiently expressed by HeLa cells, which display the antigen more efficiently than HEK293T cells (Figure 3.1). The method for detecting OMGP autoantibodies was performed following a protocol developed in our lab for the identification of MOG-IgG. OMGP antibodies are screened on unfixed cells, which express OMGP protein and bound antibodies are detected using a biotinylated secondary antibody and a streptavidin labelled fluorescent dye for subsequent analysis by flow cytometry (Mayer et al., 2013; Spadaro et al., 2016). Other groups use distinct antibodies for detection, such as anti-human-IgG1, instead of anti-human-IgG biotin (Waters et al., 2015). In addition autoantibody binding can be assessed by IF microscopy as an alternative for flow cytometry (Mader et al., 2011). During establishment of the OMGP CBAs, it was worked out that in the case of this antigen, trypsin digestion of transfected cell reduces the assay sensitivity and are therefore removed by ice cold PBS.

The OMGP constructs used in these CBAs were either transmembraneously anchored to the membrane or GPI-linked as found *in vivo* (Mikol and Stefansson, 1988). On the one hand, by using the OMGP-TM, the transient expression varies less than with OMGP-GPI, because a ribosome skipping element is introduced between EGFP and OMGP-GPI. On the other hand the GPI-anchor might lead to a more flexible and accessible antigen targeting by autoantibodies. Comparing these assays, patients with high reactivity score positive in both CBAs, whether OMGP is TM- or GPI-linked to the membrane.

Furthermore, these two assays display a great correlation of r=0.69 (Figure 3.18). The presence of autoantibodies in healthy donors is also seen for autoantibodies against MOG (O'Connor et al., 2007; Spadaro, 2017) and NF (Ng et al., 2012), which holds true for OMGP autoantibodies as well. The group of HCs was used for determination of a threshold for the identification of OMGP Abs in patients. Therefore, a reasonable cutoff is calculated by using the mean of HC measurements plus three SDs, as it is also used for MOG Ab detection in our lab (Spadaro and Meinl, 2016). However, some groups also use a higher cutoff such as HCs' mean plus six SDs (Waters et al., 2015). As such, in our assay, no HCs would score positive above the threshold of 4.4 in OMGP-TM CBA. By using this stringent cutoff, eight out of 376 from the MS/CIS cohort would display autoreactivity against OMGP. Here, in this study the evaluation of OMGP autoantibodies was carried out based on the cutoff at 3.0, which is calculated by mean value of HCs plus three SDs. Combining both CBAs, OMGP-TM or OMGP-GPI positivity, then 22 patients with OMGP autoantibodies in the MS/CIS cohort, two in the GAD Abs positive cohort, one ADEM and four in OND/OIND diagnosed with psychosis, paresthesia, neurosarcoidosis and SLE are considered positive. Looking at double positive candidates for OMGP-TM[+]/OMGP-GPI[+], a total number of ten patients is detected with autoantibodies: seven MS/CIS, one GAD[+], one ADEM and one psychosis patient.

Beside sera, plasma and PPH also CSF samples were analyzed for the presence of OMGP Abs, since for some autoantibodies like AQP4-IgG they can also present in this body fluid (Bennett et al., 2009; Jarius et al., 2010). The result for OMGP autoantibodies in CSF is low, because only one patient from 42 screened MS samples, scored positive above the cutoff which is calculated by sera. This threshold is not optimal, but it is hard to evaluate HCs' CSF for cutoff calculation.

The determination of isotypes from patient specific OMGP autoantibodies was challenging, as only some samples were detected to harbor IgG1 OMGP Abs and in the majority no isotype for OMGP Abs was detectable by flow cytometry. Nonetheless, after affinity purification of OMGP autoantibodies from the MS index patient 2492, besides IgG1 also IgG4 was detectable (chapter 3.9.3). This indicates, that the total number of determinable isotypes in OMGP autoantibodies might be underestimated, since it is only detectable in purified material. Furthermore, these enriched purified antibodies displayed *in vitro* the binding ability of complement cascade initiator protein C1q (Figure 3.27) and additionally an enhanced cross reactivity to rodent OMGP (Figure 3.29).

Persistence of OMGP antibodies could be observed for the whole observation period of 60 months in the index patient (Figure 3.20) and for 48 months in a severely affected MS patient 1294 (Figure 3.11). The titration of OMGP antibodies in the index patient revealed positivity until a 1:400 dilution,

whereas with a 1:800 dilution the value would sank below the cutoff at MFI ratio of 3.0. But this threshold was determined from HCs with 1:50 dilution and is not meaningful in this experiment.

All findings mentioned, are based on the detection by CBAs, but for the use in ELISA, full length protein was successfully produced by HEK293-EBNA cells (Figure 3.13). It is important, that the antigen is produced by this human cell line, as it was shown for NF that proteins produced from murine NS0 cells harbor abnormal immunogenic glycosylation patterns and are not suitable for autoantibody detection in patients (Ng et al., 2012). Therefore in this study, HEK293-EBNA derived OMGP was enzymatically biotinylated and used for detection of autoantibodies in STV-ELISA (Figure 3.16). A total number of 596, from all 675 samples analyzed by CBAs, were screened in STV-ELISA, resulting in nine patients with OMGP Abs in the MS/CIS cohort. Four of these patients were newly identified and didn't score positive in any CBAs. The correlation between STV-ELISA and OMGP-TM with r = 0.19 as well as r = 0.18 for OMGP-GPI CBA is low and only a few patients overlap in detection of OMGP Abs. Until now it is not understood, why by ELISA different patients are identified than in CBAs, but this is also reported for the detection of MOG Abs (Spadaro, 2017). However, it is possible to display also other autoreactive targets like NF by both assays, ELISA and CBA, for identification of seropositive patients (Ng et al., 2012; Vural et al., 2018).

The evaluation of OMGP autoantibodies was carried out using three different assays, which have some internal variability. Nevertheless, highly reactive patients as the index patient 2492 among others, show OMGP antibody autoreactivity in all assays. Although the determination of a fixed cutoff at mean plus three or six SDs values from HCs is discussable, patients with a high titer will always be identified as seropositive, similarly by using the criteria OMGP-TM/OMGP-GPI double positives. This avoids the identification of false positives, also by using three different assays for detection of OMGP Abs and setting a stringent cutoff for the evaluation of OMGP-IgG seropositivity.

Furthermore, using PBMCs of the index patient, the identification of circulating OMGP-specific B cells in the peripheral blood was possible. By using this assay, as it was established for the identification of MOG- and GAD- specific B cells (Thaler et al., 2019; Winklmeier et al., 2019), two out of 13 stimulated wells produced OMGP autoantibodies, which were secreted into the cell supernatant (Figure 3.30) and analyzed by CBAs. With this method, it was easy and robust to detect OMGP-specific B cells and this suggests also a similar frequency for circulating autoreactive T cells. Nonetheless, the detection of these autoantigen specific T cells is more difficult, because measuring the Abs is more robust and sensitive than current T cell methods.

4.2 Strategies to identify autoreactive OMGP T cells in patients

This part of the thesis aims at identifying autoreactive T cells against OMGP. The previously described OMGP Abs were of the IgG isotype, indicating cognate T cell help. The detection of rare autoreactive T cells is challenging, due to the low frequency of many myelin reactive T cells, e.g. 0.61 T_{MBP} cells per 10^5 PBMCs in MS patients (Chou et al., 1992). Therefore, different methods were established from limiting dilution to proliferation assays measuring ^{3}H-thymidine, EdU incorporation, the dilution of CFSE dye or the analysis of IFNγ secretion by ELISA (Elong Ngono et al., 2012). High sensitivity can be achieved by using ELISpot or FluoroSpot assays, whereas the latter allows simultaneous detection of a higher number of cytokines (Bronge et al., 2019a).

In this study, the first try for the identification of OMGP-specific T cells was carried out using EdU and CFSE proliferation assays. Thereby, the assay was established with a healthy donor (Figure 3.39), showing low unspecific background proliferation with EdU staining and less in CFSE condition after 7d of stimulation. The protocol was established successfully, seen by high CD3$^+$ T cell proliferation response with ConA treatment or stimulation with measles or tetanus antigen. T cells of this HC reacted after 7d with EdU and CFSE proliferation upon OMGP stimulation, showing less response than with the recall antigens, but more than observed for the background level.

For two patients, 1014 and 2492, the OMGP T cell response in the CFSE assay after 7d is displayed in Figure 3.40. The unspecific background proliferation in these patients is low and two OMGP stimulation wells display 0.26 % and 0.39 % of proliferating CD3$^+$ T cells in patient 2492, whereas for patient 1014 there is a variation from 0.047 % in the first to 2.28 % in the second well. This may reflect the rare frequency of OMGP-specific T cells by having 10^6 stimulated PBMCs in a well, that only in some a response can be detected. Analyzing the CD4$^+$ and CD8$^+$ T cell response, the mean frequency of OMGP-specific T cells is in both subsets with 0.04-0.19 % is comparable to the background level with 0.13-0.2 % of unstimulated proliferating T cells. Furthermore, the use of fresh PBMCs instead of frozen in this assay, didn't increase the number of proliferating T cells upon OMGP stimulation (Figure 3.41).

The second try to identify OMGP-specific T cells with a higher sensitivity, was conducted by IL-17/IFNγ cytokine measurement in the supernatants of stimulated PBMCs from MS patients and HCs. Whereas IL-17 signals were hardly detected at all, IFNγ could be measured in the supernatants of patients and HCs, stimulated with our in house produced OMGP. As it turned out later, these results can't be used, because it was observed throughout the evolution of the project, LPS contaminations contribute to the IFNγ concentrations (Figure 3.43). Additionally, it was

demonstrated, that proliferation of $CD4^+$ and $CD8^+$ T cell is influenced already by low concentrations of 1 pg/ml of LPS (Figure 3.42). In these assays, various OMGP preparations with final LPS concentrations of 2.5-660 pg/ml were used (Table 3-6).

To overcome the effect of LPS contaminations and using a highly sensitive as well as specific FluoroSpot assay, a new method from 2019 was applied (Bronge et al., 2019b). Therefore, OMGP was coupled to paramagnetic beads, which could be washed with NaOH for LPS removal. Afterwards, the binding success of the antigen to beads with 98.7 % positive anti-OMGP staining and 95.5 % anti-His staining for Avi-His control peptide was evaluated by flow cytometry (Figure 3.44). For an optimal signal to noise ratio, the wash titration analysis of OMGP beads (Figure 3.45) pointed out 0.1 M NaOH as optimal condition. Upon stimulation with these beads, a few MS patients with OMGP-reactive T cells could be identified by FluoroSpot assay, measuring IFNγ, IL-17A and IL-22 secretion (Figure 3.48). In total after OMGP beads treatment, one natalizumab patient and five untreated patients responded with cytokine secretion.

Interestingly, patients with $IL-22^+/IL-17A^+$ T cells are identified. This cytokine pattern is found by Th17 cells, which might play a role in the pathogenesis of MS (Dos Passos et al., 2016; Knochelmann et al., 2018). In the MOG T cell study, natalizumab treated patients were included in the screening, since this anti-α4 integrin monoclonal antibody is directed against a cell adhesion molecule and therefore blocks the leukocyte extravasation, resulting in a higher number of circulating lymphocytes and PBMCs (Bronge et al., 2019b; Krumbholz et al., 2008). Therefore, this effect is beneficial for increasing the chance to detect rare autoreactive T cells and might be useful for other autoimmunity studies as well (Jelcic et al., 2018). Although, this assay identified a few patients with OMGP T cells, the number of SFUs is low and it might be valuable to perform replicates as well as longitudinal analysis in patients to investigate the persistence of these autoreactive T cell subsets. Nevertheless, using those purified beads for stimulation and evaluation by FluoroSpot, the LPS as well as the sensitivity issue could be overcome.

Together, three different methods have been applied in this thesis to identify OMGP-specific T cells. First, measuring T cell proliferation using CFSE or EdU. Thereby, no OMGP-specific T cells could be detected, although an immune response against recall antigens was detected. Second, cytokine production. However, this assay is too sensitive towards low amounts of LPS contaminations, which could be detected even in the eukaryotic produced antigen. The identification of OMGP-specific T cells was possible with a novel assay and research period at the Karolinska Institute, Stockholm. This assay has three advantages: a) enhanced sensitivity through efficient antigen-uptake via beads, b) washing away any possible LPS contamination of the beads, and c) high sensitivity through detection by FluoroSpot assay.

116

To identify an immune reaction against certain infectious agents, like CMV and tuberculosis, antigen specific T cell activation is used (Bacher et al., 2015; Schmidt et al., 2014). For the diagnosis of autoimmune diseases, the identification of autoantibodies (e.g. against MOG or AQP4) is much more sensitive and robust, than the identification of autoreactive T cells. However, the identification of autoreactive T cells might give insight into possible pathogenic mechanisms of the disease (Cao et al., 2015; Cruz-Herranz et al., 2017; Hohlfeld et al., 2016a; Hohlfeld et al., 2016b; Lodygin et al., 2019; Planas et al., 2018).

For the development of a personalized treatment, the identification of target antigens is of fundamental importance. An ultimate aim of future therapies is either the targeted therapy, where pathogenic autoreactive T cells should be specifically removed or by restoring the self-tolerance (Hohlfeld et al., 2016a). This could be applied in numerous ways by vaccines or oral administration of myelin peptides among others (Steinman et al., 2019). One recently developed method uses MOG/MBP/PLP peptides coupled to blood cells for induction of tolerance in MS patients in a clinical trial (Lutterotti et al., 2013). For that reason, it is important to find novel antigens, like OMGP, which might be included in the toleration cocktails of future studies.

4.3 Pathogenic relevance of OMGP autoimmunity

This study demonstrated for the first time the pathogenic potential of autoimmunity to OMGP in a rat model, where T_{OMGP} cells induced a novel type of EAE with gray matter lesions in the spinal cord and cortical meningitis. For several autoantigens, it is reported, that the clinical outcome depends on the expression of the target. Injection of MOG or S100β specific T cells led to mild disease, but with intense CNS inflammation (Kawakami et al., 2004). In contrast, T_{MBP} cells mediate a potential lethal EAE in Lewis rats and drive inflammation mainly in the white matter, whereas T cells for neuronal specific antigens affect the grey matter. For example contactin-2 specific T cells induce grey matter pathology of the cortex and the spinal cord (Derfuss et al., 2009) or β-synuclein directed T cells lead to neuronal destruction, gliosis as well as to brain atrophy (Lodygin et al., 2019).

To understand the clinical picture observed in animals treated with T_{OMGP} cells, the expression pattern of OMGP needs to be analyzed. In this study, OMGP is detected on oligodendrocytes, hippocampal as well as cortical neurons and in SC tissue sections (Figure 3.34). Early O4$^+$ OPCs and also mature MBP$^+$ oligodendrocytes display OMGP on their surface and could be detected with our new mAbs (MD thesis of Lena Kristina Pfeffer). Similarly, human oligodendrocytes express OMGP on O4$^+$ and O4$^-$ cells. This is consistent with previous studies, where OMGP could

be detected together with MBP on the outermost surface of myelin of a dissected optic nerve (Chang et al., 2010). Furthermore, it was shown that cortical and hippocampal neurons express OMGP (Gil et al., 2010; Habib et al., 1998). There the staining of OMGP in the spinal cord was located at the dorsal horn, which reflects our findings seen in histology after OMGP T cell transfer.

As OMGP is a GPI anchored protein and can be shed by lipases (Mikol and Stefansson, 1988; Wang et al., 2002b), it might be existing as soluble form in the CSF. In a study of 2012, OMGP peptides were identified by mass spectrometry in CSF of MS patients (Dhaunchak et al., 2012). Seeing cortical meningitis in Lewis rats injected with T_{OMGP} cells, may reflect T cells activated by potential high soluble OMGP levels in the CSF. Comparing this EAE model to MS, meningeal inflammation in patients is linked to cortical injury (Bevan et al., 2018). Furthermore, cortical meningitis might be followed by subpial cortical demyelination, which is described as characteristic feature in MS (Kutzelnigg et al., 2005). Whether soluble OMGP helps to mediate meningitis and the underlying mechanism of OMGP processing, if despite lipases other enzymes, like ADAM 10 for the GPI anchored PrP protein (Liang and Kong, 2012) can be involved, remains to be elucidated in future studies.

Knowing that T_{OMGP} cells do not induce clinical symptoms, but have the potential to mediate cortical meningitis and grey matter pathology in the spinal cord, the question arose if they can open the BBB for pathogenic antibodies. Co-injection of 818C5-hIgG1 MOG antibody resulted in an intense demyelination. The demyelinating characteristic of 818C5-hIgG1 was already seen, when injected with T_{MBP} or T_{MOG} cells (Spadaro et al., 2018). T_{OMGP} cells breach the BBB, induce a massive inflammation, but only little ED1 macrophage activation and allow MOG antibodies to enter the CNS, where they induce demyelination. It is mainly observed perivascular, in which the lesions are composed of Ig-precipitation, complement C9neo deposition and a low number of Iba1 macrophages. This indicates, that the demyelination is most likely mediated through complement rather than by antibody dependent cellular cytotoxicity. Additionally, intrathecally injected MOG antibodies were also found in high levels in the periphery, which presumably explains the perivascular demyelination.

Looking at the subpial cortex, to analyze the characteristic subpial demyelination, typically found in MS (Kutzelnigg et al., 2005), only mild complement activation with no demyelination was observed. Regarding the short observation period of 3d after MOG antibody injection, the mAb might induce subpial demyelination by prolonging the exposure time and allowing therefore a persistent binding.

Beside the demyelination potential of MOG antibodies, this study also evaluated the pathogenicity of OMGP autoantibodies, injected together with T_{OMGP} or T_{MBP} cells. A summary of all used antibodies and combinations with T cells is listed in Table 3-5. A total of four different OMGP mAbs with distinct isotypes were used for induction of demyelination in the EAE rat model. Beforehand, they were tested regarding there in vitro C1q binding ability, resulting in 14A9 as strong binder (Figure 3.32). But neither 14A9 anti-OMGP, nor one of the others induced demyelination with T_{OMGP} or T_{MBP} cells. To exclude the lack of the appropriate Fc part of these OMGP mAbs, rat 22H6 antibody Fc part was exchanged and produced recombinantly as 22H6-hIgG1 with the same part used for 818C5-hIgG1 (Spadaro et al., 2018). However, this didn't induce demyelination, when injected together with T_{OMGP} cells.

For now, comparing to MOG antibodies, mAbs against OMGP didn't reveal a demyelination potential. One possible reason might be an absorption of antibodies by soluble OMGP in the CSF and parenchyma. Furthermore, the mechanism of shedding is completely unknown and OMGP might be quickly released upon antibody binding and therefore no tissue destruction can occur. Although two mAbs generated against OMGP bind C1q *in vitro*, it might be that these have too low affinity, not as high as 818C5-hIgG1 to MOG and lack appropriate features for complement activation *in vivo*, as it was shown for AQP4 mAbs, a certain antigen structure is required (Soltys et al., 2019).

This study didn't address the function of OMGP among Nogo/MAG as member of ligands for neurite outgrowth and remyelination inhibitors. Throughout antibody binding to OMGP, these functions might be limited. It can be speculated, that antibodies targeting OMGP could promote remyelination and axonal repair. This is reported for Nogo, which is together with OMGP a ligand for NgR. In a lysolecitin demyelinating mouse model the anti-Nogo treatment induced remyelination and enhanced axonal repair (Ineichen et al., 2017a). There are several clinical trials phase I studies testing anti Nogo-A mAbs for MS, spinal cord injury and amyotrophic lateral sclerosis. Indicating the importance, that drugs protecting the nervous system from chronic progressive diseases are an urgent need and might be beneficial in progressive MS (Ineichen et al., 2017b).

Another target of antibody treatment in phase II clinical studies is LINGO-1. The protein acts as co-receptor to NgR/p75NTR receptor complex and therefore is involved in the same signaling as OMGP (Lee and Petratos, 2013). Both are negative regulators of axonal sprouting and are overexpressed in EAE animal models (Lee et al., 2011; Loov et al., 2012). Therefore, neutralization of LINGO-1 results in an expansion of immature neurons and might be a promising target for promoting neurogenesis in neurodegenerative disorders or after spinal cord injuries

(Loov et al., 2012). Whether binding LINGO-1 by Opicinumab, used in phase II studies for MS and optic neuritis induces regeneration, remains to be elaborated in ongoing studies. Until now, the effect seen in animal models is not as strong in treated patients (Cadavid et al., 2019). Therefore, it might be interesting, to evaluate the role of another similar target like OMGP and study the relevance of therapeutic antibodies against it.

4.4 OMGP-associated disease as a new subgroup of MS and related disorders?

This study elaborates OMGP as an autoreactive target, by identification of antibodies and T cells against this antigen. Furthermore, the pathological potential of T_{OMGP} opening the BBB, could be displayed in an animal model.

This study identifies for the first time patients with inflammatory CNS diseases, who have autoantibodies to OMGP. As illustrated in Figure 4.1 (A), autoantibodies to AQP4 and MOG constitute own entities, NMOSD- and MOG-Ab associated diseases (Fujihara et al., 2018; Wynford-Thomas et al., 2019). Will autoantibodies to OMGP constitute also a separate disease? This will be answered by further studies identifying more patients. These future studies can use the methods of Ab detection described here.

A critical issue will be the development of standardized assays and thresholds. This thesis shows, that by using a low threshold a spectrum of diseases from MS, NMOSD, ADEM, LE and psychosis is identified (Figure 4.1, B). By using a very stringent threshold the MS, ADEM and psychosis is still seropositive for OMGP autoantibodies. In these cohorts, none of the patients with MOG or AQP4 Abs do have autoantibodies against OMGP, but one patient with LE and GAD Abs has additional OMGP Abs. For the unspecific diagnosis of psychosis, not much more clinical information about this patient is available. In some disorders like NMDAR encephalitis, which was describe for the first time in 2007 (Dalmau et al., 2007), patients present early with psychiatric symptoms, whereas autoantibodies are not yet evaluated and only in retrospective analysis the presence of NMDAR Abs was confirmed (Pruss et al., 2010).
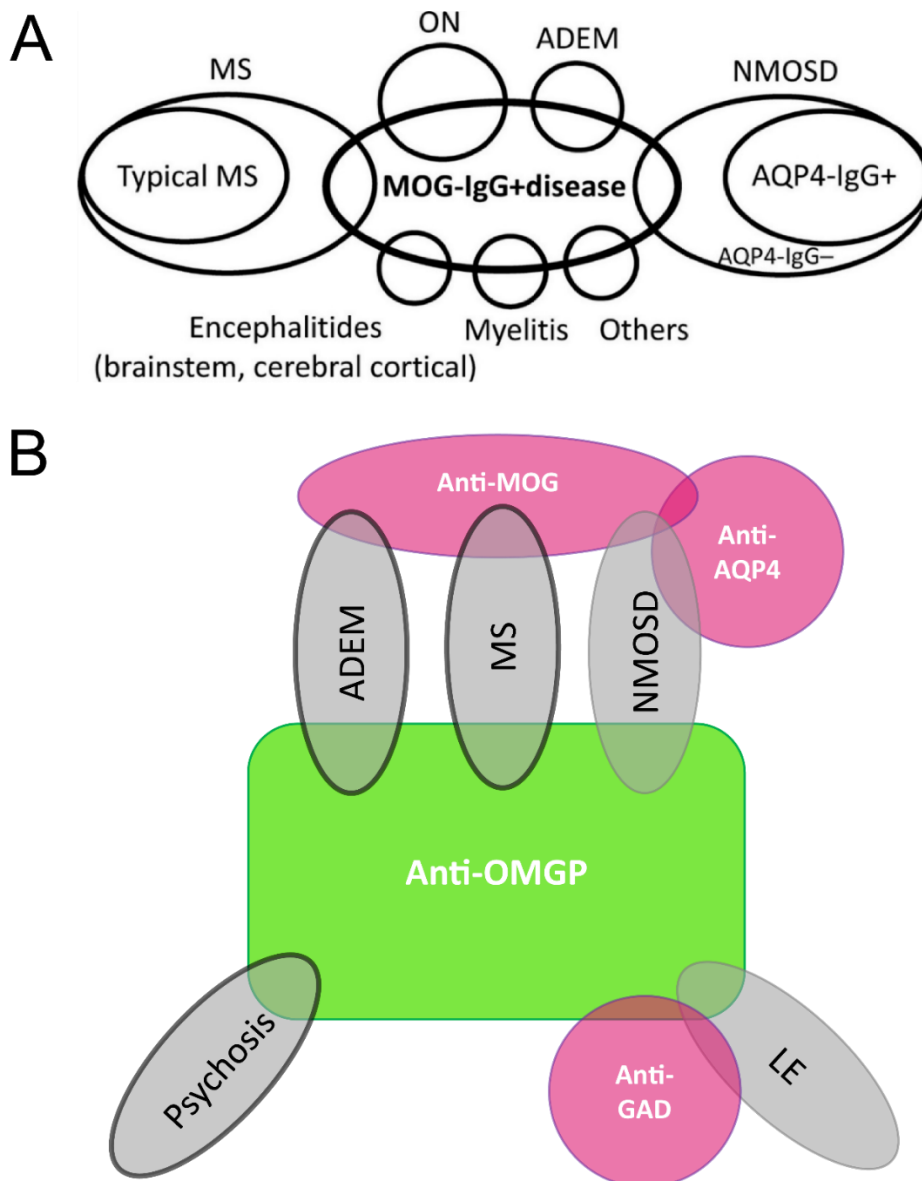
Figure 4.1 Spectrum of antibody associated diseases

(A) Studies about MOG and AQP4 autoantibodies helped for the stratification of patients with different diseases and constitute now separate entities (Fujihara et al., 2018). (B) OMGP Abs are identified in patients with different diseases. The purple circles illustrate other autoantibodies against, MOG, AQP4 or GAD, whereas the latter shows overlap with OMGP Abs. Black circles around ADEM, MS and psychosis indicate patient groups, which score seropositive, even with the stringent cutoff.

The second part of this study evaluated the pathogenicity of OMGP autoimmunity and the presence of OMGP-specific T cells in humans. In the animal model, T_{OMGP} cells induced meningitis, breached the BBB and allowed MOG Abs to induce demyelination, whereas OMGP Abs didn't show a pathogenic effect.
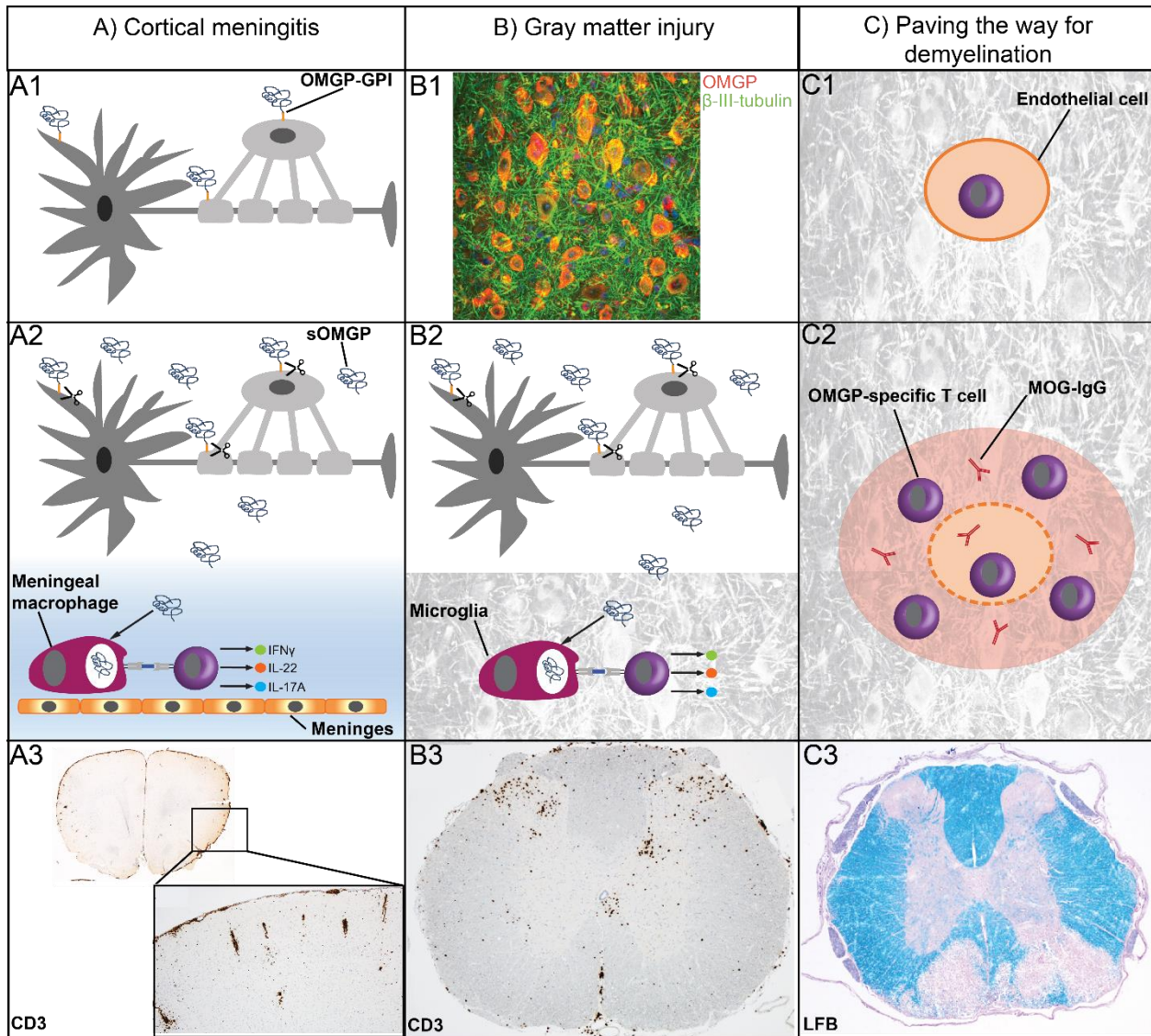
Figure 4.2 Aspects of CNS pathology mediated by OMGP-directed autoimmunity

OMGP autoimmunity mediates three pathologies: (A) cortical meningitis, (B) grey matter injury of the spinal cord and (C) breaching the BBB to pave the way for MG-Ab induced demyelination. Level 1: presence of OMGP on neurons as well as oligodendrocytes and OMGP-specific immune cells. Level 2: concept of antigen-specific activation in tissue and its consequences in the CNS milieu. Level 3: pathology observed in animal transfer experiments with CD3 and luxol fast blue (LFB) staining, coloring myelin in blue.

All findings of this study and additional hypotheses are summarized in Figure 4.2. It is shown, that OMGP is displayed on the surface by neurons and oligodendrocytes (Figure 4.2, A1), where it might be directly targeted by autoantibodies. Since neither neuronal destruction, nor demyelination are observed following injection of OMGP Abs, a potential mechanism behind it may be the release of OMGP from its GPI-anchor (Figure 4.2, A2/B2). PLC could cut the protein from its anchor, as it was reported by exogenously added enzyme (Wang et al., 2002b). Additionally, ADAM10 proteases have the ability to shed proteins close to the c-terminal end as it

was demonstrated for the GPI anchored prion protein (McDonald and Millhauser, 2014). Soluble OMGP is released into the CSF, also found by mass spectrometry (Dhaunchak et al., 2012), where it might absorb antibodies or is taken up by meningeal macrophages and presented to OMGP-specific T cells (Figure 4.2, A2), which produce effector cytokines like IFNγ, IL-22 or IL-17A. Similarly, in spinal cord tissue the OMGP might be taken up by microglia and presented to OMGP-specific T cells and induce inflammation in the dorsal horn of the SC (Figure 4.2, B2-3). Furthermore, injection of T_{OMGP} cells leads to BBB disruption and therefore allows demyelinating MOG Abs to enter the CNS (Figure 4.2, C).

All this may lead to the pathological pattern, seen in an animal model after injection with T_{OMGP} cells (Figure 4.2): a) cortical meningitis with perivascular aggregation of T cells, b) grey matter injury of spinal cord, mainly of the dorsal horn which is consistent with literature (Habib et al., 1998) and c) by breaching the BBB T_{OMGP} cells mediate MOG Ab induced demyelination.

4.5 Conclusion

This work evaluates for the first time autoimmunity against the OMGP protein in an animal model and patients. The target was selected by its exclusive presence on neurons and oligodendrocytes in the CNS, as MS is a disease of grey and white matter. With the development of two CBAs and an ELISA, autoantibodies against OMGP could be identified in patients with MS and related diseases. By purification of OMGP-specific antibodies from a highly reactive MS patient, additional features like isotypes and complement binding could be elucidated. The further aim would be to inject these patient derived antibodies in an animal model to study the relevance of OMGP Abs from patients. The pathogenic relevance of T_{OMGP} cells in Lewis rats was pointed out, as they open the BBB and pave the way for demyelination by MOG Abs. Furthermore, these autoreactive T_{OMGP} cells were also detected in natalizumab and untreated MS patients.

In conclusion, the findings of the novel autoreactive target OMGP for antibodies and T cells helps to get more insights into the pathological mechanisms behind MS and related autoimmune diseases. For the MOG antigen it took more than ten years to define it as a separate MOG-antibody associated disease entity. Therefore, this study just gives an idea of how OMGP autoimmunity could work, but for understanding the role and relevance, future studies are needed. Furthermore, these data help to support the idea of personalized treatment strategies, as OMGP Abs might be used in future as biomarker or OMGP T cells could be targeted by drugs, composed of a mixture of myelin peptides to bring back the physiological self-tolerance.

5. LIST OF ABBREVIATIONS

aa	amino acid
Ab	antibody
ADEM	acute disseminated encephalomyelitis
ANA	antinuclear antibodies
ANO2	anoctamin 2
AQP4	aquaporin-4
BAFF	B cell activating factor
BBB	blood-brain barrier
BCA	bicinchoninic acid assay
BR	background
BSA	bovine serum albumin
Caspr	Contactin associated protein
CBA	cell-based assay
cDNA	complementary DNA
CFSE	carboxyfluoresceinsuccinimidylester
CIDP	chronic inflammatory demyelinating polyneuropathy
CIS	clinical isolated syndrome
CMV	cytomegalovirus
CNP	cyclic-nucleotide-phosphodiesterase
CNS	central nervous system
ConA	Concavalin A
CRION	chronic inflammatory optic neuropathy
CRMP-2	collapsin response mediator protein 2
CSF	cerebrospinal fluid
C-terminus	carboxy-terminus of the protein
CTR	control
CV	column volume
DNA	desoxyribonucleic acid
dsDNA	double-stranded desoxyribonucleic acid
DMF	dimethyl fumarate
DTT	dithiothreitol
EAE	experimental autoimmune encephalitis
EBNA	Epstein-Barr virus nuclear antigen
EBV	Epstein-Barr virus
ED1	mAb against CD68
EDSS	expanded disability status scale
EDTA	ethylenediaminetetraacetate
EdU	5-Ethynyl-2´-deoxyuridine
EGFP	enhanced green fluorescent protein
ELISA	enzyme-linked immunosorbent assay
ELISPOT	enzyme-linked immune absorbent spot
FACS	fluorescence-activated cell scanning
FCS	fetal calf serum
FSC	forward scatter
FT	flow through
FWD	forward
GAD	glutamic acid decarboxylase
GFAP	glial fibrillary acidic protein

124

GM	grey matter
GnT1	N-acetylglucosaminyltransferase I
GPI	glycosylphosphatidylinositol
HBV	hepatitis B virus
HC	healthy control
HCV	hepatitis C virus
HE	hematoxylin and eosin
HEK	human embryonic kidney cell line
HeLa	Henrietta Lacks cell line
His	histidine tag
HIV	human immunodeficiency virus
HLA	human leukocyte antigen
HNK-1	human natural killer-1
HRP	horseradish peroxidase
IBA1	ionized calcium-binding adapter molecule 1
IF	immunofluorescence
IFNγ	interferon gamma
Ig	immunoglobulins
IL	interleukin
IMAC	immobilized metal ion affinity chromatography
i.t.	intrathecal
i.v.	intravenous
IvIg	Intravenous immunoglobulin
LAL	limulus amebocyte lysate
LB	lysogeny broth medium
LE	limbic encephalitis
LETM	longitudinal extensive transverse myelitis
LFB	luxol fast blue
LINGO-1	leucine rich repeat and immunoglobin-like domain-containing protein 1
LPS	Lipopolysaccharide
mAb	monoclonal antibody
MAC	membrane attack complex
MADSAM	multifocal acquired demyelinating sensory and motor polyneuropathy
MAG	myelin-associated glycoprotein
MBP	myelin basic protein
MFI	mean fluorescence intensity
MOG	myelin oligodendrocyte glycoprotein
MRI	magnetic resonance imaging
MS	multiple sclerosis
MSC	multiple cloning site
N-terminus	amino-terminus of the protein
NF	neurofascin
NgR	neurite outgrowth inhibitor receptor
NMDAR	N-methyl-D-aspartate receptor
NMOSD	neuromyelitis optica spectrum disorders
Nogo	neurite outgrowth inhibitor
NPLE	non-paraneoplastic limbic encephalitis
NRSPMS	non-relapsing secondary progressive multiple sclerosis
OCB	oligoclonal bands
OD	optical density

OMGP	oligodendrocyte myelin glycoprotein
OMGP-GPI	oligodendrocyte myelin glycoprotein glycosylphosphatidylinositol
OMGP-TM	oligodendrocyte myelin glycoprotein transmembran
OIND	other inflammatory neurological diseases
ON	optic neuritis
OND	other neurological diseases
OPC	oligodendrocyte precursor sells
OVA	ovalbumin
P0	myelin protein zero
pAb	polyclonal antibody
PBMCs	peripheral blood mononuclear cells
PCR	polymerase chain reaction
PEI	polyethylenimine
PET	positron emission tomography
PFA	paraformaldehyde
PI	propidium iodide
PI-PLC	phosphatidylinositol specific phospholipase C
PirB	paired immunoglobulin-like receptor B
PLC	phospholipase C
PLP	proteolipid protein
PPH	plasmapheresis
PPMS	primary progressive multiple sclerosis
PVDF	polyvinylidene difluoride
R848	resiquimod
Rev	reverse
RF	rheumatoid factor
RION	relapsing inflammatory optic neuropathy
RIS	radiological isolated syndrome
RNA	ribonucleic acid
RRMS	relapsing remitting multiple sclerosis
RSPMS	relapsing secondary progressive multiple sclerosis
RT	reverse transcriptase
SC	spinal cord
SCNI	subclinical neuroinflammation
SD	standard deviation
SDS-PAGE	sodium dodecyl sulfate polyacrylamide gel electrophoresis
SEM	standard error of the mean
SFU	spot forming unit
SLE	systemic lupus erythematosus
SMART	switching Mechanism At the 5' end of RNA Template
SPMS	secondary progressive multiple sclerosis
SSC	side scatter
STV	streptavidin
T2A	thosea asigna virus 2A peptide
TCR	T cell receptor
TLR	toll-like receptor
TM	transmembrane
TNF	tumor necrosis factor
TSO	template switching oligonucleotide
TSPO	translocator protein

WB	Western blot
WM	white matter
WT	wild type

6. LIST OF FIGURES

7. LIST OF TABLES

8. REFERENCES

Akaishi, T., et al., 2017. Neuromyelitis Optica Spectrum Disorders. Neuroimaging Clin N Am. 27, 251-265.

Anderson, A.C., et al., 2000. High frequency of autoreactive myelin proteolipid protein-specific T cells in the periphery of naive mice: mechanisms of selection of the self-reactive repertoire. J Exp Med. 191, 761-70.

Atwal, J.K., et al., 2008. PirB is a functional receptor for myelin inhibitors of axonal regeneration. Science. 322, 967-70.

Ayoglu, B., et al., 2016. Anoctamin 2 identified as an autoimmune target in multiple sclerosis. Proc Natl Acad Sci U S A. 113, 2188-93.

Bacher, P., et al., 2015. Fungus-specific CD4(+) T cells for rapid identification of invasive pulmonary mold infection. Am J Respir Crit Care Med. 191, 348-52.

Beck, R.W., et al., 2003. High- and low-risk profiles for the development of multiple sclerosis within 10 years after optic neuritis: experience of the optic neuritis treatment trial. Arch Ophthalmol. 121, 944-9.

Beltran, E., et al., 2019. Early adaptive immune activation detected in monozygotic twins with prodromal multiple sclerosis. J Clin Invest. 129, 4758-4768.

Bennett, J.L., et al., 2009. Intrathecal pathogenic anti-aquaporin-4 antibodies in early neuromyelitis optica. Ann Neurol. 66, 617-29.

Bettelli, E., et al., 2003. Myelin oligodendrocyte glycoprotein-specific T cell receptor transgenic mice develop spontaneous autoimmune optic neuritis. J Exp Med. 197, 1073-81.

Bevan, R.J., et al., 2018. Meningeal inflammation and cortical demyelination in acute multiple sclerosis. Ann Neurol. 84, 829-842.

Bourahoui, A., et al., 2004. CSF isoelectrofocusing in a large cohort of MS and other neurological diseases. Eur J Neurol. 11, 525-9.

Boyanapalli, M., et al., 2005. Oligodendrocyte-myelin glycoprotein is present in lipid rafts and caveolin-1-enriched membranes. Glia. 52, 219-27.

Brandle, S.M., et al., 2016. Distinct oligoclonal band antibodies in multiple sclerosis recognize ubiquitous self-proteins. Proc Natl Acad Sci U S A. 113, 7864-9.

Brilot, F., et al., 2009. Antibodies to native myelin oligodendrocyte glycoprotein in children with inflammatory demyelinating central nervous system disease. Ann Neurol. 66, 833-42.

Brimberg, L., et al., 2015. Antibodies as Mediators of Brain Pathology. Trends Immunol. 36, 709-724.

Bronge, M., et al., 2019a. Sensitive detection of antigen-specific T-cells using bead-bound antigen for in vitro re-stimulation. MethodsX. 6, 1635-1641.

Bronge, M., et al., 2019b. Myelin oligodendrocyte glycoprotein revisited-sensitive detection of MOG-specific T-cells in multiple sclerosis. J Autoimmun. 102, 38-49.

Brunner, C., et al., 1989. Differential ultrastructural localization of myelin basic protein, myelin/oligodendroglial glycoprotein, and 2',3'-cyclic nucleotide 3'-phosphodiesterase in the CNS of adult rats. J Neurochem. 52, 296-304.

Bukhari, W., et al., 2017. Incidence and prevalence of NMOSD in Australia and New Zealand. J Neurol Neurosurg Psychiatry. 88, 632-638.

Cadavid, D., et al., 2019. Safety and efficacy of opicinumab in patients with relapsing multiple sclerosis (SYNERGY): a randomised, placebo-controlled, phase 2 trial. Lancet Neurol. 18**,** 845-856.

Cafferty, W.B., et al., 2010. MAG and OMgp synergize with Nogo-A to restrict axonal growth and neurological recovery after spinal cord trauma. J Neurosci. 30**,** 6825-37.

Cao, Y., et al., 2015. Functional inflammatory profiles distinguish myelin-reactive T cells from patients with multiple sclerosis. Sci Transl Med. 7**,** 287ra74.

Chang, K.J., et al., 2010. Oligodendrocyte myelin glycoprotein does not influence node of ranvier structure or assembly. J Neurosci. 30**,** 14476-81.

Chitnis, T., 2007. The role of CD4 T cells in the pathogenesis of multiple sclerosis. Int Rev Neurobiol. 79**,** 43-72.

Chivatakarn, O., et al., 2007. The Nogo-66 receptor NgR1 is required only for the acute growth cone-collapsing but not the chronic growth-inhibitory actions of myelin inhibitors. J Neurosci. 27**,** 7117-24.

Chou, Y.K., et al., 1992. Frequency of T cells specific for myelin basic protein and myelin proteolipid protein in blood and cerebrospinal fluid in multiple sclerosis. J Neuroimmunol. 38**,** 105-13.

Compston, A., Coles, A., 2002. Multiple sclerosis. Lancet. 359**,** 1221-31.

Compston, A., Coles, A., 2008. Multiple sclerosis. Lancet. 372**,** 1502-17.

Confavreux, C., Aimard, G., Devic, M., 1980. Course and prognosis of multiple sclerosis assessed by the computerized data processing of 349 patients. Brain. 103**,** 281-300.

Cooper, G.S., Bynum, M.L., Somers, E.C., 2009. Recent insights in the epidemiology of autoimmune diseases: improved prevalence estimates and understanding of clustering of diseases. J Autoimmun. 33**,** 197-207.

Cortese, A., et al., 2020. Targeted next-generation sequencing panels in the diagnosis of Charcot-Marie-Tooth disease. Neurology. 94**,** e51-e61.

Cree, B.A., Goodin, D.S., Hauser, S.L., 2002. Neuromyelitis optica. Semin Neurol. 22**,** 105-22.

Cruz-Herranz, A., et al., 2017. T cells targeting neuromyelitis optica autoantigen aquaporin-4 cause paralysis and visual system injury. J Nat Sci. 3.

Dalmau, J., et al., 2007. Paraneoplastic anti-N-methyl-D-aspartate receptor encephalitis associated with ovarian teratoma. Ann Neurol. 61**,** 25-36.

De Jager, P.L., et al., 2009. Meta-analysis of genome scans and replication identify CD6, IRF8 and TNFRSF1A as new multiple sclerosis susceptibility loci. Nat Genet. 41**,** 776-82.

de Seze, J., 2017. MOG-antibody neuromyelitis optica spectrum disorder: is it a separate disease? Brain. 140**,** 3072-3075.

De Stefano, N., et al., 2014. Clinical relevance of brain volume measures in multiple sclerosis. CNS Drugs. 28**,** 147-56.

Deisenhammer, F., et al., 2019. The Cerebrospinal Fluid in Multiple Sclerosis. Front Immunol. 10**,** 726.

Dendrou, C.A., Fugger, L., 2017. Immunomodulation in multiple sclerosis: promises and pitfalls. Curr Opin Immunol. 49**,** 37-43.

References

Derfuss, T., et al., 2009. Contactin-2/TAG-1-directed autoimmunity is identified in multiple sclerosis patients and mediates gray matter pathology in animals. Proc Natl Acad Sci U S A. 106, 8302-7.

Dhaunchak, A.S., et al., 2012. Implication of perturbed axoglial apparatus in early pediatric multiple sclerosis. Ann Neurol. 71, 601-13.

Diederich, J.M., et al., 2018. Neurofascin and Compact Myelin Antigen-Specific T Cell Response Pattern in Chronic Inflammatory Demyelinating Polyneuropathy Subtypes. Front Neurol. 9, 171.

Doppler, K., et al., 2016. Auto-antibodies to contactin-associated protein 1 (Caspr) in two patients with painful inflammatory neuropathy. Brain. 139, 2617-2630.

Dos Passos, G.R., et al., 2016. Th17 Cells Pathways in Multiple Sclerosis and Neuromyelitis Optica Spectrum Disorders: Pathophysiological and Therapeutic Implications. Mediators Inflamm. 2016, 5314541.

Dou, F., et al., 2009. Temporospatial expression and cellular localization of oligodendrocyte myelin glycoprotein (OMgp) after traumatic spinal cord injury in adult rats. J Neurotrauma. 26, 2299-311.

Durocher, Y., Perret, S., Kamen, A., 2002. High-level and high-throughput recombinant protein production by transient transfection of suspension-growing human 293-EBNA1 cells. Nucleic Acids Res. 30, E9.

Dwyer, J.M., Johnson, C., 1981. The use of concanavalin A to study the immunoregulation of human T cells. Clin Exp Immunol. 46, 237-49.

Ebers, G.C., 1985. Optic neuritis and multiple sclerosis. Arch Neurol. 42, 702-4.

Ehrlich, M., et al., 2017. Rapid and efficient generation of oligodendrocytes from human induced pluripotent stem cells using transcription factors. Proc Natl Acad Sci U S A. 114, E2243-E2252.

Elong Ngono, A., et al., 2012. Frequency of circulating autoreactive T cells committed to myelin determinants in relapsing-remitting multiple sclerosis patients. Clin Immunol. 144, 117-26.

Fairhead, M., Howarth, M., 2015. Site-specific biotinylation of purified proteins using BirA. Methods Mol Biol. 1266, 171-84.

Fang, B., et al., 2016. Autoimmune Glial Fibrillary Acidic Protein Astrocytopathy: A Novel Meningoencephalomyelitis. JAMA Neurol. 73, 1297-1307.

Ferguson, M.A., Williams, A.F., 1988. Cell-surface anchoring of proteins via glycosyl-phosphatidylinositol structures. Annu Rev Biochem. 57, 285-320.

Finelli, P.F., 2011. Autoimmune Limbic Encephalitis With GAD Antibodies. Neurohospitalist. 1, 178-81.

Foroozan, R., et al., 2002. Acute demyelinating optic neuritis. Curr Opin Ophthalmol. 13, 375-80.

Fujihara, K., et al., 2018. Myelin oligodendrocyte glycoprotein immunoglobulin G-associated disease: An overview. Clinical and Experimental Neuroimmunology. 9, 48-55.

Fujinami, R.S., Oldstone, M.B., 1985. Amino acid homology between the encephalitogenic site of myelin basic protein and virus: mechanism for autoimmunity. Science. 230, 1043-5.

Geisse, S., Kocher, H.P., 1999. Protein expression in mammalian and insect cell systems. Methods Enzymol. 306, 19-42.

Gil, V., et al., 2010. Developmental expression of the oligodendrocyte myelin glycoprotein in the mouse telencephalon. Cereb Cortex. 20, 1769-79.

Giovannoni, G., et al., 2016. Brain health: time matters in multiple sclerosis. Mult Scler Relat Disord. 9 Suppl 1, S5-S48.

Gold, R., Linington, C., Lassmann, H., 2006. Understanding pathogenesis and therapy of multiple sclerosis via animal models: 70 years of merits and culprits in experimental autoimmune encephalomyelitis research. Brain. 129, 1953-71.

Goldacre, M.J., et al., 2004. Multiple sclerosis after infectious mononucleosis: record linkage study. J Epidemiol Community Health. 58, 1032-5.

Greer, J.M., McCombe, P.A., 2011. Role of gender in multiple sclerosis: clinical effects and potential molecular mechanisms. J Neuroimmunol. 234, 7-18.

Habib, A.A., et al., 1998. Expression of the oligodendrocyte-myelin glycoprotein by neurons in the mouse central nervous system. J Neurochem. 70, 1704-11.

Hemmer, B., Archelos, J.J., Hartung, H.P., 2002. New concepts in the immunopathogenesis of multiple sclerosis. Nat Rev Neurosci. 3, 291-301.

Hickman, S.J., et al., 2002. Management of acute optic neuritis. Lancet. 360, 1953-62.

Hoffmann, F., Meinl, E., 2014. B cells in multiple sclerosis: good or bad guys?: An article for 28 May 2014 - World MS Day 2014. Eur J Immunol. 44, 1247-50.

Hohlfeld, R., Wekerle, H., 2004. Autoimmune concepts of multiple sclerosis as a basis for selective immunotherapy: from pipe dreams to (therapeutic) pipelines. Proc Natl Acad Sci U S A. 101 Suppl 2, 14599-606.

Hohlfeld, R., et al., 2016a. The search for the target antigens of multiple sclerosis, part 1: autoreactive CD4+ T lymphocytes as pathogenic effectors and therapeutic targets. Lancet Neurol. 15, 198-209.

Hohlfeld, R., et al., 2016b. The search for the target antigens of multiple sclerosis, part 2: CD8+ T cells, B cells, and antibodies in the focus of reverse-translational research. Lancet Neurol. 15, 317-31.

Hollenbach, J.A., Oksenberg, J.R., 2015. The immunogenetics of multiple sclerosis: A comprehensive review. J Autoimmun. 64, 13-25.

Horstmann, L., et al., 2013. Inflammatory demyelination induces glia alterations and ganglion cell loss in the retina of an experimental autoimmune encephalomyelitis model. J Neuroinflammation. 10, 120.

Hurwitz, B.J., 2009. The diagnosis of multiple sclerosis and the clinical subtypes. Ann Indian Acad Neurol. 12, 226-30.

Ineichen, B.V., et al., 2017a. Nogo-A antibodies enhance axonal repair and remyelination in neuro-inflammatory and demyelinating pathology. Acta Neuropathol. 134, 423-440.

Ineichen, B.V., et al., 2017b. Nogo-A Antibodies for Progressive Multiple Sclerosis. CNS Drugs. 31, 187-198.

International Multiple Sclerosis Genetics, C., 2019. Multiple sclerosis genomic map implicates peripheral immune cells and microglia in susceptibility. Science. 365.

Irani, S.R., et al., 2010. Antibodies to Kv1 potassium channel-complex proteins leucine-rich, glioma inactivated 1 protein and contactin-associated protein-2 in limbic encephalitis, Morvan's syndrome and acquired neuromyotonia. Brain. 133, 2734-48.

References

Jarius, S., et al., 2010. Cerebrospinal fluid antibodies to aquaporin-4 in neuromyelitis optica and related disorders: frequency, origin, and diagnostic relevance. J Neuroinflammation. 7, 52.

Jelcic, I., et al., 2018. Memory B Cells Activate Brain-Homing, Autoreactive CD4(+) T Cells in Multiple Sclerosis. Cell. 175, 85-100 e23.

Jersild, C., Svejgaard, A., Fog, T., 1972. HL-A antigens and multiple sclerosis. Lancet. 1, 1240-1.

Jurynczyk, M., et al., 2019. Myelin oligodendrocyte glycoprotein (MOG) antibody-associated disease: practical considerations. Pract Neurol. 19, 187-195.

Kawakami, N., et al., 2004. The activation status of neuroantigen-specific T cells in the target organ determines the clinical outcome of autoimmune encephalomyelitis. J Exp Med. 199, 185-97.

Keegan, M., et al., 2005. Relation between humoral pathological changes in multiple sclerosis and response to therapeutic plasma exchange. Lancet. 366, 579-82.

Kim, J.H., et al., 2011. High cleavage efficiency of a 2A peptide derived from porcine teschovirus-1 in human cell lines, zebrafish and mice. PLoS One. 6, e18556.

Knochelmann, H.M., et al., 2018. When worlds collide: Th17 and Treg cells in cancer and autoimmunity. Cell Mol Immunol. 15, 458-469.

Kontermann, R., Dübel, S., 2010. Antibody engineering, Vol., Springer, Heidelburg.

Kottis, V., et al., 2002. Oligodendrocyte-myelin glycoprotein (OMgp) is an inhibitor of neurite outgrowth. J Neurochem. 82, 1566-9.

Krumbholz, M., et al., 2008. Natalizumab disproportionately increases circulating pre-B and B cells in multiple sclerosis. Neurology. 71, 1350-4.

Krumbholz, M., et al., 2012. B cells and antibodies in multiple sclerosis pathogenesis and therapy. Nat Rev Neurol. 8, 613-23.

Krumbholz, M., Meinl, E., 2014. B cells in MS and NMO: pathogenesis and therapy. Semin Immunopathol. 36, 339-50.

Krupp, L.B., et al., 2013. International Pediatric Multiple Sclerosis Study Group criteria for pediatric multiple sclerosis and immune-mediated central nervous system demyelinating disorders: revisions to the 2007 definitions. Mult Scler. 19, 1261-7.

Kuhle, J., et al., 2015. Fingolimod and CSF neurofilament light chain levels in relapsing-remitting multiple sclerosis. Neurology. 84, 1639-43.

Kunemund, V., et al., 1988. The L2/HNK-1 carbohydrate of neural cell adhesion molecules is involved in cell interactions. J Cell Biol. 106, 213-23.

Kurtzke, J.F., 1983. Rating neurologic impairment in multiple sclerosis: an expanded disability status scale (EDSS). Neurology. 33, 1444-52.

Kutzelnigg, A., et al., 2005. Cortical demyelination and diffuse white matter injury in multiple sclerosis. Brain. 128, 2705-12.

Langer-Gould, A., et al., 2014. The incidence of clinically isolated syndrome in a multi-ethnic cohort. J Neurol. 261, 1349-55.

Lassmann, H., van Horssen, J., 2011. The molecular basis of neurodegeneration in multiple sclerosis. FEBS Lett. 585, 3715-23.

Lassmann, H., 2014. Mechanisms of white matter damage in multiple sclerosis. Glia. 62, 1816-30.

Lee, E.K., et al., 1998. Morvan's fibrillary chorea: a paraneoplastic manifestation of thymoma. J Neurol Neurosurg Psychiatry. 65, 857-62.

Lee, J.K., et al., 2010. Assessing spinal axon regeneration and sprouting in Nogo-, MAG-, and OMgp-deficient mice. Neuron. 66, 663-70.

Lee, J.Y., Petratos, S., 2013. Multiple sclerosis: does Nogo play a role? Neuroscientist. 19, 394-408.

Lee, X., et al., 2011. Oligodendrocyte differentiation and myelination defects in OMgp null mice. Mol Cell Neurosci. 46, 752-61.

Lennon, V.A., et al., 2004. A serum autoantibody marker of neuromyelitis optica: distinction from multiple sclerosis. Lancet. 364, 2106-12.

Lennon, V.A., et al., 2005. IgG marker of optic-spinal multiple sclerosis binds to the aquaporin-4 water channel. J Exp Med. 202, 473-7.

Liang, J., Kong, Q., 2012. alpha-Cleavage of cellular prion protein. Prion. 6, 453-60.

Liao, X.X., et al., 2011. The expression patterns of Nogo-A, myelin associated glycoprotein and oligodendrocyte myelin glycoprotein in the retina after ocular hypertension: the expression of myelin proteins in the retina in glaucoma. Neurochem Res. 36, 1955-61.

Linington, C., et al., 1988. Augmentation of demyelination in rat acute allergic encephalomyelitis by circulating mouse monoclonal antibodies directed against a myelin/oligodendrocyte glycoprotein. Am J Pathol. 130, 443-54.

Lodygin, D., et al., 2019. beta-Synuclein-reactive T cells induce autoimmune CNS grey matter degeneration. Nature. 566, 503-508.

Loov, C., et al., 2012. Neutralization of LINGO-1 during in vitro differentiation of neural stem cells results in proliferation of immature neurons. PLoS One. 7, e29771.

Lowenthal, A., Karcher, D., Van Sande, M., 1959. Electrophophoretic studies of central nervous system proteins. Exp Neurol. 1, 233-47.

Lucchinetti, C., et al., 2000. Heterogeneity of multiple sclerosis lesions: implications for the pathogenesis of demyelination. Ann Neurol. 47, 707-17.

Lutterotti, A., et al., 2013. Antigen-specific tolerance by autologous myelin peptide-coupled cells: a phase 1 trial in multiple sclerosis. Sci Transl Med. 5, 188ra75.

Lutterotti, A., Martin, R., 2014. Antigen-specific tolerization approaches in multiple sclerosis. Expert Opin Investig Drugs. 23, 9-20.

Lyons, A.B., Parish, C.R., 1994. Determination of lymphocyte division by flow cytometry. J Immunol Methods. 171, 131-7.

Mader, S., et al., 2010. Patterns of antibody binding to aquaporin-4 isoforms in neuromyelitis optica. PLoS One. 5, e10455.

Mader, S., et al., 2011. Complement activating antibodies to myelin oligodendrocyte glycoprotein in neuromyelitis optica and related disorders. J Neuroinflammation. 8, 184.

Marrack, P., Kappler, J., Kotzin, B.L., 2001. Autoimmune disease: why and where it occurs. Nat Med. 7, 899-905.

Mathey, E.K., et al., 2007. Neurofascin as a novel target for autoantibody-mediated axonal injury. J Exp Med. 204, 2363-72.

Mayer, M.C., Meinl, E., 2012. Glycoproteins as targets of autoantibodies in CNS inflammation: MOG and more. Ther Adv Neurol Disord. 5, 147-59.

References

Mayer, M.C., et al., 2013. Distinction and temporal stability of conformational epitopes on myelin oligodendrocyte glycoprotein recognized by patients with different inflammatory central nervous system diseases. J Immunol. 191, 3594-604.

McDonald, A.J., Millhauser, G.L., 2014. PrP overdrive: does inhibition of alpha-cleavage contribute to PrP(C) toxicity and prion disease? Prion. 8.

McLaughlin, K.A., et al., 2009. Age-dependent B cell autoimmunity to a myelin surface antigen in pediatric multiple sclerosis. J Immunol. 183, 4067-76.

McLean, B.N., Luxton, R.W., Thompson, E.J., 1990. A study of immunoglobulin G in the cerebrospinal fluid of 1007 patients with suspected neurological disease using isoelectric focusing and the Log IgG-Index. A comparison and diagnostic applications. Brain. 113 (Pt 5), 1269-89.

Menge, T., et al., 2005. Acute disseminated encephalomyelitis: an update. Arch Neurol. 62, 1673-80.

Mikol, D.D., Stefansson, K., 1988. A phosphatidylinositol-linked peanut agglutinin-binding glycoprotein in central nervous system myelin and on oligodendrocytes. J Cell Biol. 106, 1273-9.

Mikol, D.D., Szuchet, S., Stefansson, K., 1988. A peanut agglutinin binding glycoprotein in CNS myelin and oligodendrocytes. Ann N Y Acad Sci. 540, 409-12.

Mikol, D.D., et al., 1990a. Structure and chromosomal localization of the gene for the oligodendrocyte-myelin glycoprotein. J Cell Biol. 111, 2673-9.

Mikol, D.D., Gulcher, J.R., Stefansson, K., 1990b. The oligodendrocyte-myelin glycoprotein belongs to a distinct family of proteins and contains the HNK-1 carbohydrate. J Cell Biol. 110, 471-9.

Misu, T., et al., 2013. Presence of six different lesion types suggests diverse mechanisms of tissue injury in neuromyelitis optica. Acta Neuropathol. 125, 815-27.

Ng, J.K., et al., 2012. Neurofascin as a target for autoantibodies in peripheral neuropathies. Neurology. 79, 2241-8.

Nielsen, T.R., et al., 2007. Multiple sclerosis after infectious mononucleosis. Arch Neurol. 64, 72-5.

Noseworthy, J.H., et al., 2000. Multiple sclerosis. N Engl J Med. 343, 938-52.

O'Connor, K.C., et al., 2007. Self-antigen tetramers discriminate between myelin autoantibodies to native or denatured protein. Nat Med. 13, 211-7.

Obermeier, B., et al., 2008. Matching of oligoclonal immunoglobulin transcriptomes and proteomes of cerebrospinal fluid in multiple sclerosis. Nat Med. 14, 688-93.

Ogawa, R., et al., 2017. MOG antibody-positive, benign, unilateral, cerebral cortical encephalitis with epilepsy. Neurol Neuroimmunol Neuroinflamm. 4, e322.

Olerup, O., Hillert, J., 1991. HLA class II-associated genetic susceptibility in multiple sclerosis: a critical evaluation. Tissue Antigens. 38, 1-15.

Ota, K., et al., 1990. T-cell recognition of an immunodominant myelin basic protein epitope in multiple sclerosis. Nature. 346, 183-7.

Parker Harp, C.R., et al., 2015. B Cell Antigen Presentation Is Sufficient To Drive Neuroinflammation in an Animal Model of Multiple Sclerosis. The Journal of Immunology. 194, 5077-5084.

Peng, Y., et al., 2018. Diagnostic implications of MOG/AQP4 antibodies in recurrent optic neuritis. Exp Ther Med. 16, 950-958.

Perera, N.C., et al., 2013. NSP4 is stored in azurophil granules and released by activated neutrophils as active endoprotease with restricted specificity. J Immunol. 191, 2700-7.

Pette, M., et al., 1990. Myelin basic protein-specific T lymphocyte lines from MS patients and healthy individuals. Neurology. 40, 1770-6.

Picelli, S., et al., 2014. Full-length RNA-seq from single cells using Smart-seq2. Nat Protoc. 9, 171-81.

Pinna, D., et al., 2009. Clonal dissection of the human memory B-cell repertoire following infection and vaccination. Eur J Immunol. 39, 1260-70.

Planas, R., et al., 2018. GDP-l-fucose synthase is a CD4(+) T cell-specific autoantigen in DRB3*02:02 patients with multiple sclerosis. Sci Transl Med. 10.

Probstel, A.K., et al., 2011. Antibodies to MOG are transient in childhood acute disseminated encephalomyelitis. Neurology. 77, 580-8.

Pruss, H., et al., 2010. Retrospective analysis of NMDA receptor antibodies in encephalitis of unknown origin. Neurology. 75, 1735-9.

Quesada, A., et al., 2011. Myelin oligodendrocyte-specific protein is expressed in Muller cells of myelinated vertebrate retinas. J Neurosci Res. 89, 674-88.

Raiker, S.J., et al., 2010. Oligodendrocyte-myelin glycoprotein and Nogo negatively regulate activity-dependent synaptic plasticity. J Neurosci. 30, 12432-45.

Ramanathan, S., et al., 2016. Radiological differentiation of optic neuritis with myelin oligodendrocyte glycoprotein antibodies, aquaporin-4 antibodies, and multiple sclerosis. Mult Scler. 22, 470-82.

Reich, D.S., Lucchinetti, C.F., Calabresi, P.A., 2018. Multiple Sclerosis. New England Journal of Medicine. 378, 169-180.

Reindl, M., et al., 2017. Myelin oligodendrocyte glycoprotein antibodies: How clinically useful are they? Curr Opin Neurol. 30, 295-301.

Renner, M., et al., 2017. Optic Nerve Degeneration after Retinal Ischemia/Reperfusion in a Rodent Model. Front Cell Neurosci. 11, 254.

Renoux, C., et al., 2007. Natural history of multiple sclerosis with childhood onset. N Engl J Med. 356, 2603-13.

Richert, J.R., et al., 1983. Expansion of antigen-specific T cells from cerebrospinal fluid of patients with multiple sclerosis. J Neuroimmunol. 5, 317-24.

Rodriguez, M., et al., 1995. Optic neuritis: a population-based study in Olmsted County, Minnesota. Neurology. 45, 244-50.

Roemer, S.F., et al., 2007. Pattern-specific loss of aquaporin-4 immunoreactivity distinguishes neuromyelitis optica from multiple sclerosis. Brain. 130, 1194-205.

Rosenblum, M.D., Remedios, K.A., Abbas, A.K., 2015. Mechanisms of human autoimmunity. J Clin Invest. 125, 2228-33.

Rostasy, K., et al., 2012. Anti-myelin oligodendrocyte glycoprotein antibodies in pediatric patients with optic neuritis. Arch Neurol. 69, 752-6.

Saadoun, S., et al., 2014. Neuromyelitis optica MOG-IgG causes reversible lesions in mouse brain. Acta Neuropathol Commun. 2, 35.

Sato, D.K., et al., 2014. Distinction between MOG antibody-positive and AQP4 antibody-positive NMO spectrum disorders. Neurology. 82, 474-81.

Schmidt, T., et al., 2014. Comparative analysis of assays for detection of cell-mediated immunity toward cytomegalovirus and M. tuberculosis in samples from deceased organ donors. Am J Transplant. 14, 2159-67.

Schuh, E., et al., 2016. Features of Human CD3+CD20+ T Cells. J Immunol. 197, 1111-7.

Sellebjerg, F., Blinkenberg, M., Sorensen, P.S., 2020. Anti-CD20 Monoclonal Antibodies for Relapsing and Progressive Multiple Sclerosis. CNS Drugs.

Sherman, D.L., et al., 2005. Neurofascins are required to establish axonal domains for saltatory conduction. Neuron. 48, 737-42.

Soltys, J., et al., 2019. Membrane assembly of aquaporin-4 autoantibodies regulates classical complement activation in neuromyelitis optica. J Clin Invest. 129, 2000-2013.

Sormani, M.P., Arnold, D.L., De Stefano, N., 2014. Treatment effect on brain atrophy correlates with treatment effect on disability in multiple sclerosis. Ann Neurol. 75, 43-9.

Sospedra, M., Martin, R., 2005a. Antigen-specific therapies in multiple sclerosis. Int Rev Immunol. 24, 393-413.

Sospedra, M., Martin, R., 2005b. Immunology of multiple sclerosis. Annu Rev Immunol. 23, 683-747.

Spadaro, M., et al., 2016. Autoantibodies to MOG in a distinct subgroup of adult multiple sclerosis. Neurol Neuroimmunol Neuroinflamm. 3, e257.

Spadaro, M., Meinl, E., 2016. Detection of Autoantibodies Against Myelin Oligodendrocyte Glycoprotein in Multiple Sclerosis and Related Diseases. Methods Mol Biol. 1304, 99-104.

Spadaro, M., 2017. Autoantibodies to myelin oligodendrocyte glycoprotein (MOG) in patients with demyelinating diseases of the central nervous system (CNS): investigation of the clinical spectrum and pathological potential. PhD Thesis.

Spadaro, M., et al., 2018. Pathogenicity of human antibodies against myelin oligodendrocyte glycoprotein. Ann Neurol. 84, 315-328.

Steinman, L., et al., 2019. Antigen-specific tolerance to self-antigens in protein replacement therapy, gene therapy and autoimmunity. Curr Opin Immunol. 61, 46-53.

Sundstrom, P., et al., 2004. An altered immune response to Epstein-Barr virus in multiple sclerosis: a prospective study. Neurology. 62, 2277-82.

Tay, C.H., Welsh, R.M., 1997. Distinct organ-dependent mechanisms for the control of murine cytomegalovirus infection by natural killer cells. J Virol. 71, 267-75.

Tengvall, K., et al., 2019. Molecular mimicry between Anoctamin 2 and Epstein-Barr virus nuclear antigen 1 associates with multiple sclerosis risk. Proc Natl Acad Sci U S A. 116, 16955-16960.

Thaler, F.S., et al., 2019. Abundant glutamic acid decarboxylase (GAD)-reactive B cells in gad-antibody-associated neurological disorders. Ann Neurol. 85, 448-454.

Theofilopoulos, A.N., Kono, D.H., Baccala, R., 2017. The multiple pathways to autoimmunity. Nat Immunol. 18, 716-724.

Thompson, A.J., et al., 2018. Diagnosis of multiple sclerosis: 2017 revisions of the McDonald criteria. Lancet Neurol. 17, 162-173.

Titulaer, M.J., et al., 2014. Overlapping demyelinating syndromes and anti-N-methyl-D-aspartate receptor encephalitis. Ann Neurol. 75, 411-28.

Tohid, H., 2016. Anti-glutamic acid decarboxylase antibody positive neurological syndromes. Neurosciences (Riyadh). 21, 215-22.

Torisu, H., et al., 2010. Clinical study of childhood acute disseminated encephalomyelitis, multiple sclerosis, and acute transverse myelitis in Fukuoka Prefecture, Japan. Brain Dev. 32, 454-62.

Trapp, B.D., et al., 2018. Cortical neuronal densities and cerebral white matter demyelination in multiple sclerosis: a retrospective study. Lancet Neurol. 17, 870-884.

Trotter, J.L., et al., 1991. Peripheral blood mononuclear cells from multiple sclerosis patients recognize myelin proteolipid protein and selected peptides. J Neuroimmunol. 33, 55-62.

Tuzun, E., Dalmau, J., 2007. Limbic encephalitis and variants: classification, diagnosis and treatment. Neurologist. 13, 261-71.

van Sonderen, A., et al., 2016. The clinical spectrum of Caspr2 antibody-associated disease. Neurology. 87, 521-8.

Varrin-Doyer, M., et al., 2012. Aquaporin 4-specific T cells in neuromyelitis optica exhibit a Th17 bias and recognize Clostridium ABC transporter. Ann Neurol. 72, 53-64.

Viskochil, D., et al., 1991. The gene encoding the oligodendrocyte-myelin glycoprotein is embedded within the neurofibromatosis type 1 gene. Mol Cell Biol. 11, 906-12.

von Budingen, H.C., et al., 2010. Clonally expanded plasma cells in the cerebrospinal fluid of patients with central nervous system autoimmune demyelination produce "oligoclonal bands". J Neuroimmunol. 218, 134-9.

von Budingen, H.C., et al., 2015. Update on the autoimmune pathology of multiple sclerosis: B-cells as disease-drivers and therapeutic targets. Eur Neurol. 73, 238-46.

Vural, A., Doppler, K., Meinl, E., 2018. Autoantibodies Against the Node of Ranvier in Seropositive Chronic Inflammatory Demyelinating Polyneuropathy: Diagnostic, Pathogenic, and Therapeutic Relevance. Front Immunol. 9, 1029.

Wallin, M.T., et al., 2019. The prevalence of MS in the United States: A population-based estimate using health claims data. Neurology. 92, e1029-e1040.

Wang, K.C., et al., 2002a. P75 interacts with the Nogo receptor as a co-receptor for Nogo, MAG and OMgp. Nature. 420, 74-8.

Wang, K.C., et al., 2002b. Oligodendrocyte-myelin glycoprotein is a Nogo receptor ligand that inhibits neurite outgrowth. Nature. 417, 941-4.

Wang, L., et al., 2019. Encephalitis is an important clinical component of myelin oligodendrocyte glycoprotein antibody associated demyelination: a single-center cohort study in Shanghai, China. Eur J Neurol. 26, 168-174.

Waters, P., Vincent, A., 2008. Detection of anti-aquaporin-4 antibodies in neuromyelitis optica: current status of the assays. Int MS J. 15, 99-105.

Waters, P., et al., 2015. MOG cell-based assay detects non-MS patients with inflammatory neurologic disease. Neurol Neuroimmunol Neuroinflamm. 2, e89.

Wijnands, J.M.A., et al., 2017. Health-care use before a first demyelinating event suggestive of a multiple sclerosis prodrome: a matched cohort study. Lancet Neurol. 16, 445-451.

Wingerchuk, D.M., et al., 2007. The spectrum of neuromyelitis optica. Lancet Neurol. 6, 805-15.

References

Wingerchuk, D.M., et al., 2015. International consensus diagnostic criteria for neuromyelitis optica spectrum disorders. Neurology. 85**,** 177-89.

Winklmeier, S., et al., 2019. Identification of circulating MOG-specific B cells in patients with MOG antibodies. Neurol Neuroimmunol Neuroinflamm. 6**,** 625.

Wynford-Thomas, R., Jacob, A., Tomassini, V., 2019. Neurological update: MOG antibody disease. J Neurol. 266**,** 1280-1286.

Xiao, B.G., Linington, C., Link, H., 1991. Antibodies to myelin-oligodendrocyte glycoprotein in cerebrospinal fluid from patients with multiple sclerosis and controls. J Neuroimmunol. 31**,** 91-6.

Yamamoto, S., et al., 2002. Mice deficient in nervous system-specific carbohydrate epitope HNK-1 exhibit impaired synaptic plasticity and spatial learning. J Biol Chem. 277**,** 27227-31.

Yamout, B., Al Khawajah, M., 2017. Radiologically isolated syndrome and multiple sclerosis. Mult Scler Relat Disord. 17**,** 234-237.

Yeh, E.A., Nakashima, I., 2019. Live-cell based assays are the gold standard for anti-MOG-Ab testing. Neurology. 92**,** 501-502.

Zabad, R.K., Stewart, R., Healey, K.M., 2017. Pattern Recognition of the Multiple Sclerosis Syndrome. Brain Sci. 7.

Zamvil, S.S., Steinman, L., 1990. The T lymphocyte in experimental allergic encephalomyelitis. Annu Rev Immunol. 8**,** 579-621.

9. PUBLICATIONS

Autoimmunity to oligodendrocyte myelin glycoprotein (OMGP) mediates cortical meningitis and gray matter pathology in the spinal cord

Gerhards R, Pfeffer LK, Lorenz J, Starost L, Thaler FS, Schlüter M, Rübsamen H, Macrini C, Winklmeier S, Mader S, Bronge M, Grönlund H, Feederle R, Hsia HE, Lichtenthaler SF, Merl-Pham J, Kuhlmann T, Bauer IJ, Gerdes LA, Meinl I, Beltrán E, Mezydlo A, Bar-Or A, Banwell B, Khademi M, Olsson T, Hohlfeld R, Lassmann H, Kümpfel T, Kawakami N*, Meinl E*.

Submitted. 2020

Identification of circulating MOG-specific B cells in patients with MOG antibodies

Winklmeier S, Schlüter M, Spadaro M, Thaler FS, Vural A, Gerhards R, Macrini C, Mader S, Kurne A, Inan B, Karabudak R, Özbay FG, Esendagli G, Hohlfeld R, Kümpfel T, Meinl E.

Neurol. Neuroimmunol. Neuroinflamm. 2019, 6(6):625. DOI: 10.1212/NXI.0000000000000625

Abundant glutamic acid decarboxylase (GAD)-reactive B cells in gad-antibody-associated neurological disorders

Thaler FS, Thaller AL, Biljecki M, Schuh E, Winklmeier S, Mahler CF, Gerhards R, Völk S, Schnorfeil F, Subklewe M, Hohlfeld R, Kümpfel T, Meinl E.

Ann Neurol. 2019, 85(3):448-454. DOI: 10.1002/ana.25414

Pathogenicity of human antibodies against myelin oligodendrocyte glycoprotein

Spadaro M, Winklmeier S, Beltrán E, Macrini C, Höftberger R, Schuh E, Thaler FS, Gerdes LA, Laurent S, Gerhards R, Brändle S, Dornmair K, Breithaupt C, Krumbholz M, Moser M, Krishnamoorthy G, Kamp F, Jenne D, Hohlfeld R, Kümpfel T, Lassmann H, Kawakami N*, Meinl E*.

Ann Neurol. 2018, 84(2):315-328. DOI: 10.1002/ana.25291

10. CONTRIBUTIONS OF COLLABORATORS

Samples and clinical data of patients from MS outpatient clinic of the Institute of Clinical Neuroimmunology, LMU were provided by Prof. Dr. Tania Kümpfel. Additionally, samples from Prof. Dr. Tomas Olsson and Dr. Mohsen Khademi from the Karolinska institute in Stockholm and the Canadian Pediatric Study Group (Prof. Dr. Amit Bar-Or and Prof. Dr. Brenda Banwell) were received.

Monoclonal Abs against OMGP were generated by Dr. Elisabeth Kremmer and Dr. Regina Feederle (Helmholtz Centrum Munich), whereas the evaluation was carried out in our institute by Lena Kristina Pfeffer as part of her MD thesis. Therefore, we collaborated with Laura Starost and Prof. Dr. Tanja Kuhlmann from the neuropathology department of Westfälischen Wilhelms-Universität Münster.

Hippocampal and cortical neurons for IF staining were obtained from Dr. Hung-En Hsia (AG Prof. Dr. Stefan Lichtenthaler, DZNE, Munich). Spinal cord sections and tissue staining was carried out in collaboration with Aleksandra Mezydlo (AG Prof. Dr. Martin Kerschensteiner, Institute of Clinical Neuroimmunology, LMU).

All rat transfer experiments were conducted by Dr. Naoto Kawakami (NK at Institute of Clinical Neuroimmunology, LMU) and subsequent histological analysis by Prof. Dr. Hans Lassmann (HL at Center for Brain Research, Medizinische Universität Vienna).

Bead-based T cell stimulation assays and FluoroSpot analysis were carried out by myself at the Karolinska Institute in Stockholm with help of Mattias Bronge and Prof. Dr. Hans Grönlund.

11. CURRICULUM VITAE

- **Persönliches**

Geburtsdatum	04.01.1989
Geburtsort	Augsburg
Nationalität	deutsch

- **Ausbildung**

10/2016 – heute	**Studium der Humanmedizin an der LMU München** 8. Fachsemester (4. Klinisches Semester) I. Staatsexamen August 2018
10/2014 – 07/2020	**Promotion zum Dr. rer. nat. am Institut für Klinische Neuroimmunologie der LMU** Prof. Martin Kerschensteiner, Arbeitsgruppe Prof. Edgar Meinl „Autoimmunity against Oligodendrocyte Myelin Glycoprotein (OMGP)"
10/2012 – 09/2014	**Master Studium der Biologie an der TUM** Master Thesis bei Biotechnologiefirma Roche Diagnostics GmbH „Molecular and biochemical characterization of new enzymes for selective protein ligation"
10/2009 – 07/2012	**Bachelor Studium der Biologie an der LMU** Bachelor Thesis am Max-Planck-Institut für Neurobiologie „Characterization of the potential phosphorylation site S678 in *Drosophila* Psidin"
02/2010 – 02/2014	Wissenschaftliche Hilfskraft am Max-Planck-Institut für Neurobiologie
10/2008 – 09/2009	Studium der Lebensmittelchemie an der TUM
10/1999 – 06/2008	Peutinger Gymnasium Augsburg

- **Forschungsaufenthalte**

09/2019	Forschungsaufenthalt am Karolinska Institut in Stockholm (Prof. Hans Grönlund, Therapeutic Immune Design)
08/2012 – 09/2012	Forschungspraktikum in Genetik am IBDM in Marseille (Prof. Nicolas Gompel & Prof. Benjamin Prud'homme)

- **Stipendien & Preise**

08/2019	SFB Young Investigator Reisestipendium für den Forschungsaufenthalt am Karolinska Institut und den Besuch der ECTRIMS Konferenz
07/2019	NEUROCAMP AWARD 2019 „Outstanding Scientific Mentor" für die Betreuung eines zweiwöchigen Schülerpraktikums
06/2015	„European School of Neuroimmunology" Reisestipendium für die ESNI in Prag
07/2012	Auslandsstipendium PROSA^{LMU} für das Forschungspraktikum am IBDE in Marseille

- **Kenntnisse und Fähigkeiten**

Microsoft Office, Endnote, Adobe Photoshop, Adobe Illustrator, Graphpad Prism

Sprachen: deutsch (Muttersprache), englisch (verhandlungssicher)